Construction of Engineered Nanoparticles with Tailored Densities of Self-Antigen for the Study of B-cell Activation

by

Zhilin Chen

A dissertation submitted in partial fulfillment
of the requirements for the degree of
Doctoral of Philosophy
(Pharmaceutical Sciences)
in the University of Michigan
2019

Doctoral Committee:

Associate Professor Wei Cheng, Chair
Assistant Professor Irina Grigorova
Associate Professor James Moon
Professor Akira Ono
Professor Duxin Sun

Zhilin Chen

zhilinch@umich.edu

ORCID: 0000-0002-1738-0332

To my family, my partner and friends

for their love and support

Acknowledgements

For the completion of this dissertation, I have many people to thank, for their generous help and great support. First and foremost, I would like to thank my academic advisor, Dr. Wei Cheng. As the chair of my dissertation committee, he input tremendous amount of time and efforts in guiding me through many challenges during my PhD work. His persistent pursuit in scientific truth and detail-driven precision in daily lab work have deeply influenced me since my first day in lab. He taught me to have my own rational judgements and not to believe in the authorities blindly; He encouraged me to pursue my true passion for career and not to follow the ordinary path. Dr. Cheng shaped my way of thinking in both conducting scientific research and making life choices; to that, I am extremely grateful.

I would also like to thank all my committee members: Dr. Irina Grigorova, Dr. James Moon, Dr. Akira Ono and Dr. Duxin Sun, for their active engagement in my thesis project development. They offered valuable insights in all project meetings as well as generous assistance to my lab work in terms of instruments and technical experience.

This dissertation is, by no means, an individual person's work. During this journey, I have collaborated with members from Cheng lab and a few other labs. I would like to thank the past and current members in Cheng Lab: Dr. Jin H. Kim, Dr. Yuanjie Pang, Dr. Michael C. DeSantis, Dr. Abhay Kotnala, Dr. Hanna Song, Dr. Kristin Schimert, Dr. Ziah Dean, Chunjuan Tian, Tai-Wei Li for all the great discussions at lab meetings and the good times in and outside

of the lab. I would also thank all the graduate/undergraduate students that I mentored at Cheng lab: Amir Hobson, Amanda Ames, Richard Schutzman, James Wang, and Manuel J Quinones Perez for their excellent work in various projects. Moreover, I want to thank our collaborating labs: Dr. James Moon lab, Dr. Anna Schwendeman lab, Dr. Irina Grigorova lab, as well as the following collaborators: Alireza Hassani Najafabadi, Dr. Jackson Turner, Wenmin Yuan, Minzhi Yu, Dr. Allison Schafer, and Dr. Mingsheng Chen, for their assistance. Additionally, many thanks to the wonderful community at the College of Pharmacy, where I made many great friends and built a great professional network.

Last but not the least, I want to thank my family for their love and support. My parents have been the biggest supporter of me throughout my entire life. Without them, I would not become who I am today. My brother, sister-in-law and my 18-month niece Yanxi have brought so much joy and excitement to our family. My special thanks go to my partner, Claudio Vilas Boas Favero: all the moments we have spent together are precious to me; you have given me so much strength when faced with difficulties in life; I look forward to building a new chapter of our lives in Boston. Thanks to all the love and support from my dear family and friends, my journey of obtaining PhD degree has been filled with happiness.

Table of Contents

List of Tables

List of Figures

List of Abbreviations

Ab	Antibody
Ag	Antigen
BCA	Bicinchoninic Acid
BCR	B-Cell Receptor
CA	Capsid
CpG	C/G Oligodeoxynucleotides
DMPC	1,2-Dimyristoyl-sn-Glycero-3-Phosphocholine
dNTP	Nucleoside Triphosphate
DSPE-PEG$_{2000}$-m	1,2-Distearoyl-sn-Glycero-3-Phosphoethanolamine-N- [Maleimide (Polyethylene Glycol)-2000])
ELISA	Enzyme-Linked Immunosorbent Assay
Gag	HIV-1 Polyprotein (MA-CA-NC)
HIV	Human Immunodeficiency Virus
ICP-OES	Inductively Coupled Plasma - Optical Emission Spectrometry
IgM	Immunoglobulin M
IgG	Immunoglobulin G
IPTG	Isopropyl β-D-1-Thiogalactopyranoside
LC-MS	Liquid Chromatography – Mass Spectrometry
MA	Matrix
mAb	monoclonal Antibody

MHC II	Major Histocompatibility Complex II
mTFP	monomeric Teal Fluorescent Protein
NC	Nucleocapsid
Ni-NTA	Ni- Nitrilotriacetic Acid
Ni-NTA-DGS	1,2-Dioleoyl-sn-Glycero-3-[(N-(5-Amino-1-Carboxypentyl) Iminodiacetic Acid) Succinyl] (Nickel Salt)
PBS	Phosphate Buffered Saline
PC	Phosphocellulose
PCR	Polymerase Chain Reaction
PEI	Polyethylenimine
PMSF	Phenylmethane Sulfonyl Fluoride
rPG	recombinant Protein G
RA	Rheumatoid Arthritis
RSV	Rous Sarcoma Virus
SDS-PAGE	Sodium Dodecyl Sulfate - Polyacrylamide Gel Electrophoresis
TCR	T-Cell Receptor
TEM	Transmission Electron Microscopy
TLR	Toll-Like Receptor
TNF-α	Tumor Necrosis Factor alpha
TT	Tetanus Toxin Peptide
VLP	Virus Like Particle
VSV-G	Vesicular Stomatitis Virus G Protein

Abstract

Epitope density appears to be a critical factor in pathogens that can elicit effective immune responses. All the viruses that have efficacious FDA-approved target vaccines have high surface densities of antigens. HIV, on the other hand, has limited number of envelope glycoproteins present on individual virions on average, a characteristic with which HIV can evade from human immunity. To investigate how immune cells, particularly B cells, recognize and differentiate surface antigen density, we aim to build nanoparticles with different densities of antigens on the surface. Liposomes are chosen as antigen carriers for their clinical safety and engineering versatility. Both ensemble biochemistry assay and single-molecule biophysical techniques are developed to determine the spatial density of two model proteins on liposomal surface. Our results showed the initial density of protein conjugated on Ni-chelating liposomes could be finely controlled but decreased overtime. In comparison, maleimide-liposomes performed well in both protein density control and conjugation stability. Through maleimide-cysteine reaction, we successfully constructed liposomes with varied surface density levels of TNF-α peptide, a model self-antigen that is critical in the pathogenesis of rheumatoid arthritis. Immunization of mice using liposomes that display TNF-α peptide at high density consistently elicited both IgM and class-switched IgG antibodies that are reactive towards self-antigen TNF-α protein. In transgenic mice lacking either functional T-cell receptors or MHC II on B cells, the liposomal particles elicited similar levels of IgM and IgG responses, implying that this is a T-independent process. Addition of CpG or T-cell epitope tetanus toxin peptide improved antibody

responses elicited by liposomal particles but not by soluble antigen peptide. Furthermore, the Ab titer elicited can be increased by 1000-fold upon replacement of liposomes by bacteriophage Qβ virus-like particles of similar epitope densities. Remarkably, this enhancement of Ab titer is almost lost entirely in transgenic mice lacking TCR or MHC II, which uncovers T cell help as the dominant mechanism behind this enhancement. In conclusion, high epitope density alone can trigger antibody class switching in B cells, and the cognate T-cell help recruited by components in VLPs can further boost antibody response by promoting affinity maturation. As an exploratory work to build on this mechanism of immunogenicity, we attempted next to build HIV VLP using the recombinant HIV Gag protein, which is known to contain many well-defined human T cell epitopes. If successful, the display of HIV envelope glyproteins on the surface of this VLP at high density may afford an attractive lead for HIV vaccine development. HIV Gag protein can self-assemble in vitro to HIV virus-like particles, however, the quantitative aspects and in particular, the yield of this process are poorly characterized. Our results revealed that purified Gag proteins assembled into aggregates as large as micron-sized particles that are visible under light microscope. This self-assembly is induced by addition of nucleic acids and interestingly, it is reversible with addition of excess nucleic acids. Thus, further engineering of this process is required to in order to make it useful for production of HIV VLPs. In summary, our study overall has answered a fundamental question in immunology regarding B-cell activation by particulate antigens, offering insights to the process of pathogen recognition. These findings will help guide future design of therapeutic vaccines for chronic conditions including cancer and Alzheimer's disease, as well as prophylactic vaccine for infectious agents like HIV.

Chapter 1

Introduction

1.1.   Background

HIV and Its Low Surface Envelope Protein Density

Since human immunodeficiency virus type 1 (HIV-1) was identified as the causative agent of acquired immunodeficiency syndrome (AIDS), almost 78 million people have been infected with the HIV virus and about 39 million people have died of AIDS[1]. HIV/AIDS has become the biggest burden among infectious diseases all over the world. In last thirty years, a lot of efforts have been put into the research of HIV vaccine development, but only until recently, the first vaccine candidate to exhibit evidence for protection against infection was reported after RV144 trial, showing 31.2% vaccine efficacy in a group of 16,395 subjects, yet the extent and mode of protection are still under debate[2].

HIV has multiple ways to evade the human immune system, including rapid mutation of the two glycoproteins that comprise the envelope trimer, gp120 and gp41, and structural features

that enables the trimer to hide conserved epitopes from antibodies, such as a shield of host-derived carbohydrates, conformational masking, steric occlusion and so on[3]. Besides all the features above, HIV also has a very low surface envelope protein density, compared to other virions of the similar size such as influenza, measles, papillomavirus and hepatitis B viruses (Figure 1.1). For example, influenza type A virus incorporates ~450 trimers per virus particle spaced at intervals less than 10 nm[4], while cryo-EM studies revealed that virions of wild-type HIV had ~14 envelope trimers per particles, with some clustering of HIV trimers and most spikes are separated by distances that far exceed the 15 nm reach of the two Fab arms of an IgG[5,6]. This low number of envelope trimers on HIV virion surface may be a potential reason that human immunity fails to develop neutralizing antibodies specific to HIV virions promptly.

Low Surface Antigen Density May Help HIV Evade Human Immunity

In a review written by Dr. Rolf Zinkernagel in 1996, various virus parameters and their capacity to induce T-cell-independent (TI) IgM responses were listed and compared. All viruses that induce TI antibodies exhibit highly organized surface antigens, while those lacking a highly organized surface structure do not induce TI antibodies[7]. Although TI antibody responses are usually short-lived and mostly IgM, the initial TI B-cell response can lead to a rapid expansion of specific B cells without the need of prior Th cell induction, thus greatly enhancing the chance for a cognate T-B-cell interaction for a more rapid and rigorous IgG response[8]. The low number of trimers and the large distance between each trimer on the HIV surface can lead to no or little TI response, and thus a substantial delay in specific antibody production compared to other viruses.

Besides the potential lack of TI response, the small number of envelope trimers can also attribute to their low binding affinities with specific antibodies. The Fabs region of an IgG antibody are linked to the Fc region by a flexible hinge, which typically allows a 10-15 nm center-to-center separation between the antigen-binding sites of two Fabs for IgGs[9]. However, the majority of nearest neighbor distances of HIV envelope trimers falls outsides the range of 10-15 nm, leaving only a minority of HIV envelope trimers available for cross-linking by a bivalent antibody[5], which limits the ability of the humoral immune response to recognize and neutralize the viruses present in body fluids.

Additionally, the low density of envelope trimers on HIV may also be the reason that HIV virus have a very low infectivity of less than 0.1% in plasma or culture media[10]. Envelope protein contents have been correlated with the infectivity of the virions. The infectivity of simian immunodeficiency virus (SIV) were increased for more than 100 folds when a mutation was made to increase the amount of envelope to be incorporated onto the virion[11]. Clinical studies have shown that transmitted founder HIV viruses are enriched for higher envelope protein content, enhanced cell-free infectivity, improved dendritic cell interaction, and relative IFN-α resistance[12]. Although it seems unlikely that HIV evolved the feature of low density of envelope protein to limit its infectivity and thus transmission efficiency, low density of envelope protein may prevent HIV virion from being cross-linked with neutralizing antibodies and delay the induction of a broad spectrum antibody response through lack of TI response, which generate a lot of evolutional advantages that overcome the disadvantage of low infectivity.

Surface Antigenic Density and B Cell Response

The induction of efficient B cell responses requires two sets of signals: the first is mediated by the BCR, while the second is usually provided by T cells. Antigens that stimulate antibody production in the absence of MHC class II-restricted T cell help are classified as T cell-independent (TI) antigens[13]. Traditionally, TI responses have been categorized according to whether they can be elicited in CBA/N mice, which have an X-linked immunological defect caused by deficiency in the kinase Btk[14]: antigens that do not elicit responses in CBA/N mice are designated 'TI type 2' (TI-2), whereas those that do elicit antibody responses in the absence of Btk are designated 'TI type 1' (TI-1). TI-1 antigens provide a second signal via Toll-like receptors (TLRs) specific for microbial products such as lipopeptides, lipopolysaccharide (LPS), microbial CpG DNA, viral RNA and certain viral coat proteins[15]; while TI-2 are typically multivalent antigens and they are believed to extensively crosslink BCRs and deliver a prolonged and persistent signal to the B cell, transmitted via Btk. Typical TI-2 antigens are bacterial capsular polysaccharides, such as those found in *Streptococcus pneumoniae, Haemophilus influenzae* type b and *Neisseria meningitidis*, but TI-2 responses can also develop in response to the highly repetitive motifs found in viral capsids[16].

Many studies have revealed that *in vivo* antibody response to viral, bacterial and fungi infections consist of both T-dependent and T-independent components, depending on epitopes being studies and the infectivity of the organism[13]. For example, in the response to infection with Trypanosoma brucei, a T cell-independent antibody response to the exposed surface glycoprotein was observed. In contrast to the response seen after active infection, immunization of mice with purified glycoprotein or paraformaldehyde-fixed parasites elicited only a T-dependent response to the glycoprotein[17]. Hepatitis B virus infection is a vigorous TI IgM anti-hepatitis core (HBc) antibody production during the early acute stage of infection and a later switch to TD production

of IgG anti-hepatitis core antigen[18]. Similarly, influenza virus can induce specific TI IgG in mice lacking CD40 or CD4 T cells, and those mice can recover from influenza infection in a manner similar to that of normal mice[19]. However, whether the TD or TI nature of the response reflects the density of the exposed glycoprotein epitopes on the organisms or whether it reflects differences in the ability of different organisms to recruit certain cytokines or cells into the response, remains to be determined. To study the relationship between surface antigen density and TI B cell response, many researchers have conducted remarkable studies using various models: early studies showed that the repetitive structure of the polymerized flagellin is able to induce B cell response, whereas monomeric flagellin cannot induce B cell response[20]; Haptenated polymers with a minimum number of 12-16 antigenic determinants spaced approximately 10nm apart are able to activate B cells in the absence of T cell help[21]… These results showed that B cell responses against highly organized antigens requires none or less T cell help than poorly organized or monomeric antigens.

High Surface Density Can Be A Signal of Foreignness for Immune System

Furthermore, it has been proposed that the density of surface antigen may be an important marker of foreignness for B cell to recognize. Surfaces of viruses, bacteria, and parasites tend to be repetitive, quasi-crystalline in nature, while cell surface molecules almost never form stable clusters such as those found on viral surfaces but remain laterally mobile, rendering them less able to activate B cells[22]. In vesicular stomatitis virus glycoprotein (VSV-G) transgenic mice, where VSV-G was encoded as a self-antigen, B cells were unresponsive to the soluble VSV-G or poorly organized VSV-G but responded promptly to the same antigen presented in the highly organized form on inactivated VSV[23]. Corroborating results were found when tolerant hen egg

lysozyme (HEL) -specific B cells were activated by membrane-bound organized form of HEL but not the soluble HEL[24]. A recent study showed that when immunized with virus-like particle (VLP) conjugated with self-antigen TNF-α, mice will produce higher titers of TNF-α-specific IgG antibodies to those VLPs with high density of TNF-α rather than low density of TNF-α, even though the total amount of TNF-α was the same[25]. Collectively, these results suggest that B cell can be directly activated by antigens displayed in a highly-repetitive, organized manner. In effect, the immune system is largely unable to distinguish between self and foreign proteins based on antigenic epitopes but does so based on antigenic organization.

In healthy individuals, immune cells are evolved to mount effective immune response against foreign antigens but remain unresponsive to various self-antigens through mechanisms of tolerance. Both B cells and T cells developed immune tolerance in both central (bone marrow, thymus) and peripheral (spleen, lymph nodes) through various processes including clonal deletion, involving apoptosis, receptor editing, anergy and ignorance[26,27]. Anergy refers to a state in which self-reactive B cells exist in the periphery but are quiescent and unresponsive to antigen stimulation. Anergic B cells typically have reduced lifespan, altered migration and anatomical localization, inability to interact productively with T cells, and downmodulation of surface IgM compared to normal mature B cells[26]. It was found out that as many as 50% of newly produced B cells are destined to become anergic, making anergy the primary mechanism by which autoreactive B cells are silenced[28].

B cell tolerance, particularly B cell anergy, can be overcome experimentally. High density display of self-antigen was shown to break B cell tolerance. In a study led by John Schiller, multivalent virus-like particle (VLP)- based immunogen could induce autoantibody responses in

transgenic mice that express soluble form of hen egg lysozyme tolerated by B cells through anergy. Adoptive transfer model study showed the immunization with VLP, but not trivalent form of hen egg lysozyme reversed B cell anergy *in vivo*[29]. However, the mechanism under which highly dense, multivalent antigens can activate B cells still remains unclear. One theory is that extensive crosslinking of BCR by high density of antigen display induces the association of the BCR with detergent-insoluble lipid rafts that are associated with long-term stable activation of tyrosine phosphorylation[30,31]. Still, the role of T-cell help or Toll-like receptor signal is yet to be understood.

Our design of engineered particles aims to answer several fundamental immunology questions: Does human B cell directly recognize highly-repetitive antigen displayed on pathogens? Is the recognition process dependent on help from T cells or other cells? What are the recognition mechanism and activation pathways involved? The answers to these questions will not only expand our knowledge of human immunity, but also give indications to future vaccine design. Current vaccine development mainly focuses on the arm of TD B cell response, due to the common belief that TI antigens will not elicit germinal center (GC) formation and memory B cell differentiation. Recent studies have revealed that some TI antigens are capable to induce long-lived TI memory B cells that originate from B-1b cells, which provided rapid IgM specific antibody protection upon the second challenge[32], and two independent studies have demonstrated that the prototypic TI antigen NP-Ficoll induces GCs in nude mice[33,34]. More importantly, TI antigens may serve as a rapid stimulus to specific B cells and induce their clonal expansion, thus leading to an easier recognition of cognate T cells and a stronger TD response[7]. Our study may help to reveal the surface antigen density that is optimal for T-independent B cell activation, which would greatly facilitate future vaccine design strategy.

1.2. Significance

Understanding of Surface Density Factor in Immunology

Our study aims to answer several fundamental immunology questions: Does B cell directly recognize the density of antigens as a signal? Does B cell have different density threshold requirement for self-antigens and foreign antigens? What is the recognition mechanism and activation pathways? Is this activation process independent on T cells or other cells? The answers to these questions will not only expand our current knowledge of human immunity, but also give indications to future vaccine design, especially to pathogens with no existing effective vaccine like HIV.

One approach for HIV vaccine is to develop high-density virus-like display of HIV antigen to induce broadly neutralizing antibody. A study showed HIV virus-like particles with increased density of envelope glycoprotein (Env) have superior activation of Env-specific B cells[35]. Nanoparticle presentation of HIV Env on carriers like liposomes or ferritin particles have also been explored: high density of Env display more efficiently activates Env-specific B cells *ex vivo* and enhances the generation of germinal center B cells *in vivo*[36,37]. These studies utilizing high density display of HIV antigens represent a promising lead towards development of an effective HIV vaccine.

Another implication in understanding surface density factor is to employ high-density display of self-antigen to break B-cell tolerance and elicit auto-reactive antibodies. Monoclonal antibody specific for host proteins have proven to be highly effective in the treatment of

autoimmune diseases, such as rheumatoid arthritis and Crohn's disease. More antibody drugs against self-antigens are under development for the treatment of many chronic conditions including cancer, hypertension and Alzheimer's disease[38,39].

Clinical Use of Therapeutic Antibody Against Self-Antigen in Autoimmune Diseases

A number of antibody drugs specific for pro-inflammatory cytokine tumor necrosis factor alpha (TNF-α) have been developed and achieved success in both clinical use and the market place. The mechanism of action is that anti-TNF-α monoclonal antibody drugs can specifically neutralize TNF-α in patients with active rheumatoid arthritis, psoriatic arthritis and ankylosing spondylitis to relieve symptoms caused by elevated levels of TNF-α [40–42].

Among these antibody drugs, Adalimumab is the first fully human, high-affinity, recombinant immunoglobulin G_1 anti- TNF-α monoclonal antibody for the treatment of rheumatoid arthritis[43]. For patients who do not respond to traditional disease-modifying antirheumatic drugs (DMARD) (e.g., methotrexate, leflunomide), 32 percent of patients will experience a major clinical response when adalimumab is substituted[44]. When combined with methotrexate, the remission rates reaches to 43 percent and response rate nearly doubles (62 percent)[45]. Adalimumab requires subcutaneous self-injection every other week; more than 10% of patients have reported inconvenient or unable to self-inject due to disease condition[46]. The cost of Adalimumab is approximately $1662 per month, more than 20 folds of the cost of methotrexate ($13 to $85 per month)[47], making it the top per-person drug spending in 2016[48]. The high cost and frequent administration limited the use of adalimumab in resource-limited communities and developing countries.

Given the success of passive vaccination with therapeutic monoclonal antibodies, a better strategy to actively induce the same therapeutic antibodies in situ is envisioned. In mouse models, active vaccination against TNF-α elicited effective production of anti- TNF-α neutralizing antibodies, sufficient in controlling the symptoms of arthritis[49]. One study led by John Schiller using papillomavirus VLPs with TNF-α peptides conjugated to the surface for mouse immunization revealed that VLP attached TNF-α induced 1000 folds higher autoantibody production compared to soluble TNF-α. Vaccination with conjugated particles also inhibited development of type II collagen-induced arthritis in mouse model[50].

Potential of Therapeutic Vaccines Against Self-Antigens in Chronic Diseases

Beyond rheumatoid arthritis, therapeutic vaccines against self-antigens are applicable to many other chronic diseases. Today, many therapeutic vaccines are under development for conditions including cancer, Alzheimer's disease, diabetes, hypertension and obesity. One vaccine candidate for prostate cancer, D17DT, consisting of the GnRH (gonadotrophin releasing hormone) was shown to elicit significant anti-GnRH antibody titer in volunteers and almost half of patients vaccinated achieved castrate level of testosterone, proving great potential in controlling prostate cancer[51]. Similarly, G17DT, a vaccine candidate for pancreatic cancer, is also acting towards a self-antigen gastrin (growth factor for pancreatic cancer). In phase II trials of G17DT, 20 of 30 patients produced an antibody response; Antibody responders demonstrate significantly greater survival than antibody non-responders[52]. For treatment of hypertension, a novel vaccine based on angiotensin II- derived peptide conjugated VLP Qβ demonstrated high efficacy in reducing systolic blood pressure in spontaneously hypertensive rats. The followed

clinical trial in human showed good tolerance and 100% response rate in production of anti-angiotensin antibody[53].

The Alzheimer's disease vaccines also rely on self-antigens. Alzheimer's disease is a chronic condition of neurodegeneration allegedly caused by deposition of amyloid β-peptide (Aβ) in plaques in brain tissue[54]. The goal of the vaccine is to immunize patients against Aβ so that the accumulation of plaque in brain will stop and cognitive functions will be restored. Vaccination towards Aβ-peptide in mouse disease model resulted in reduced plaque mass and improved their mental performance[55,56]. Despite of good tolerance and no side effect in vaccination to mice, anti-Aβ vaccines caused symptoms of acute meningoencephalitis in 6% of vaccinated patients in phase I trial[57]. Nevertheless, a phase II study revealed a substantial delay of cognitive decline in patients that produced anti-Aβ antibodies[58]. Besides chronic diseases like cancer and hypertension, this vaccination strategy has also applied to contraception use. A vaccine toward human chorionic gonadotropin (hCG) was developed and put to clinical trials: a heterospecies dimer of the beta subunit of human chorionic gonadotropin (hCG) associated noncovalently with the alpha subunit of ovine luteinizing hormone and conjugated to tetanus and diphtheria toxoids as carriers effectively elicited anti-hCG antibody and only 1 pregnancy was recorded for vaccinated fertile women over 1224 cycles[59,60].

Overall, understanding of high-density display in breaking B cell tolerance will guide the development of therapeutic vaccines towards various self-antigen targets. Our study aims to reveal the role of antigen density in B cell activation quantitatively through construction of a novel nanoparticle platform with controlled densities of antigens. The results will further our current understandings in antigen surface density and offer insights to our future vaccine design.

1.3. Hypothesis and Specific Aims

Specific Aim 1:

Construction of Nanoparticles with Tailored Densities of Surface Antigens

We hypothesize antigen density is a key factor in eliciting B cell response, and it has different requirements of density threshold for B cells to activate upon self-antigens or foreign antigens. As illustrated in Figure 1.2, the density threshold for foreign antigens is low, as many in soluble monomeric forms still activates B cells effectively, while self-antigens under their density threshold will be tolerated by B cells. Once self-antigen density exceeds the threshold, B-cell tolerance breaks and B cells are activated. When both antigens have very high density, B cell activation may be lowered and B cell tolerance may be restored[61].

To validate this hypothesis, we aim to construct nanoparticles with tailored densities of antigens on the surface. HIV VLP is the first particle platform we attempt to use. Previous studies showed HIV matrix protein Gag assembled into virus-like particles *in vitro*[62–64]. Without the using of cells, these VLPs will not carry any additional proteins other than target antigens[65]. An additional benefit of HIV VLP is that it contains the Gag protein as potent T-cell epitopes, soliciting T-cell help for B cell activation. By fusion of HIV Gag protein with target antigens, we can build VLP with target antigens presented on the surface with a fixed orientation. We hope to control the surface density of antigens on VLPs by manipulating the ratio of Gag-fusion protein and unmodified Gag protein during their assembly *in vitro*.

A second choice of nanoparticle platform is liposome. Liposomes are well documented drug delivery systems with a safe record of clinical applications[66,67]. As antigen carrier, liposomes have multiple advantages including safety, low immunogenicity, versatility in engineering and production. Here, we aim to construct liposomes, similar to HIV VLP in size and shape, with various densities of surface antigens. To conjugate target antigens on liposomes, we plan to explore different conjugation methods reported by literature. For example, Ni-NTA-his-tag binding was used in a recent study conjugating HIV Env protein on the surface of liposomes[37]; Chemical conjugation such as maleimide reaction has also been used in peptide conjugation on liposomes[68].

Specific Aim 2:

Characterization of Engineered Nanoparticles and Their Surface Antigen Densities

Following the construction of nanoparticles with antigens on the surface, we aim to characterize the nanoparticles in terms of size, surface charge, homogeneity in size and antigen densities. Among these parameters, the surface density of antigens is the key factor to be determined. We have designed two methods for antigen density quantitation: bulk biochemical assay and single-molecule fluorescence assay. The bulk assay aims to use the Stewart Assay to quantitate lipid amount and use SDS-PAGE (SDS- polyacrylamide gel electrophoresis) to quantitate protein amount. The molar amounts of both combined gives rise to the average antigen density on the nanoparticles.

To determine the heterogeneity of peptide density among individual nanoparticle, we resort to fluorescence labeling of peptide on the surface of nanoparticles. By labeling all the peptide molecules specifically on the particle surface and observing under fluorescence microscopy and optical tweezers, we are capable to quantitate the number of molecules on individual particles. Through this method, the heterogeneity of peptide densities on nanoparticles can be observed and evaluated. We aim to achieve a homogeneous distribution of antigen density among nanoparticles, so particles with low antigen density do not contain some high-density particles that influence the immune response outcomes.

Moreover, the stability of antigen conjugation on nanoparticles are critical to our study. We aim to construct engineered nanoparticles with stable conjugation with antigens in the presence of serum. Upon inoculation in mice subcutaneously or intravenously, nanoparticles are expected to transit through blood vessel, tissues, lymph vessels and lymph nodes. Nanoparticles require a stable conjugation with antigens so that the antigen density level does not change drastically before entering lymph nodes and exposure to naïve B cells. For this purpose, we plan to evaluate the kinetics of antigen association/ dissociation on liposomal surface by quantitating the number of antigens on individual liposomes during days of incubation in serum.

Besides antigen density, characterization of nanoparticles in size, surface charge, and size homogeneity will be carried out by dynamic light scattering and electron microscopy. The physical stability of nanoparticles with antigens in serum will be tested to ensure no aggregation or precipitation occurs upon interaction with serum proteins.

14

Specific Aim 3:

Study of B cell Activation by Engineered Nanoparticles *In vivo* and *In vitro*

To determine the effects of surface antigen density, we aim to use nanoparticles with self-antigens of different densities for study of B cell activation (Figure. 1.3). As described previously, we hypothesize that B cell activation requires a higher threshold of antigen density for self-antigen compared to foreign antigens. Thereby, we will use engineered nanoparticles with different levels of self-antigen density to directly immunize wild-type mice and study if B cell tolerance of self-antigen can break. Through ELISA and flow cytometry, we can estimate the level of specific autoantibody production and the amount of specifically activated B cells in mice. Furthermore, we are interested in the role of T cells and Toll-like receptors (TLR) in B-cell recognition of surface antigen density: addition of T-cell epitopes and TLR ligands to engineered nanoparticles for mice immunization can show the effects of T-cell or TLR help for antigen density recognition. Moreover, we aim to use transgenic micein v lacking T-cell receptors and MHC class II for immunization of engineered nanoparticles to determine the role of T-cell help in breaking B-cell tolerance.

In addition to *in vivo* study, we aim to study B cell activation *in vitro* as well. As the number of specific B cells for one antigen is very low, use of BCR transgenic mice recognizing one specific antigen is necessary to obtain large amount of specific B cells. We plan to use HEL-BCR specific mice to isolate HEL-specific B cells and study the activation of B cells *in vitro* upon stimulation with nanoparticles of different antigen densities. B cells surface activation markers, cytokine production, antibody production and life span will be evaluated as indicators of activation and compared between nanoparticles with different antigen densities.

1.4. Figures
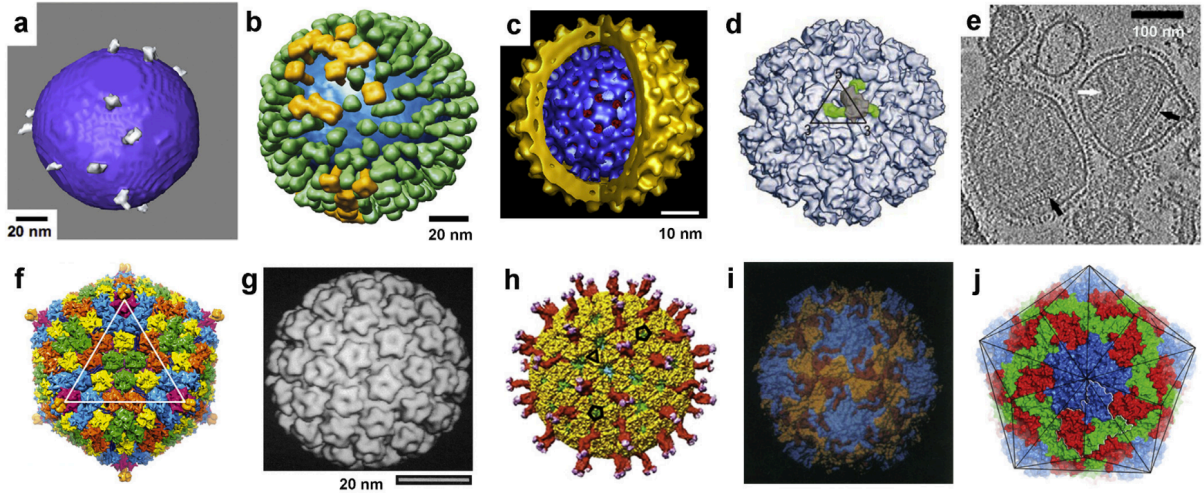
Figure 1.1. Comparison of protein densities on virion particle.

(a) HIV-1. (b) Influenza virus. (c) Hepatitis B virus. (d) Yellow fever virus. (e) Measles virus. (f) Human adenovirus. (g) Human papillomavirus. (h) Rotavirus. (i) Poliovirus. (j) Hepatitis A virus. Models for a-e, g, and h are from cryoelectron microscopy, and models for f, i, and j are from crystal structures. Whereas a-e and j are enveloped viruses, f-i are considered as nonenveloped viruses. All these viruses have licensed vaccines available except HIV-1.[69-78]
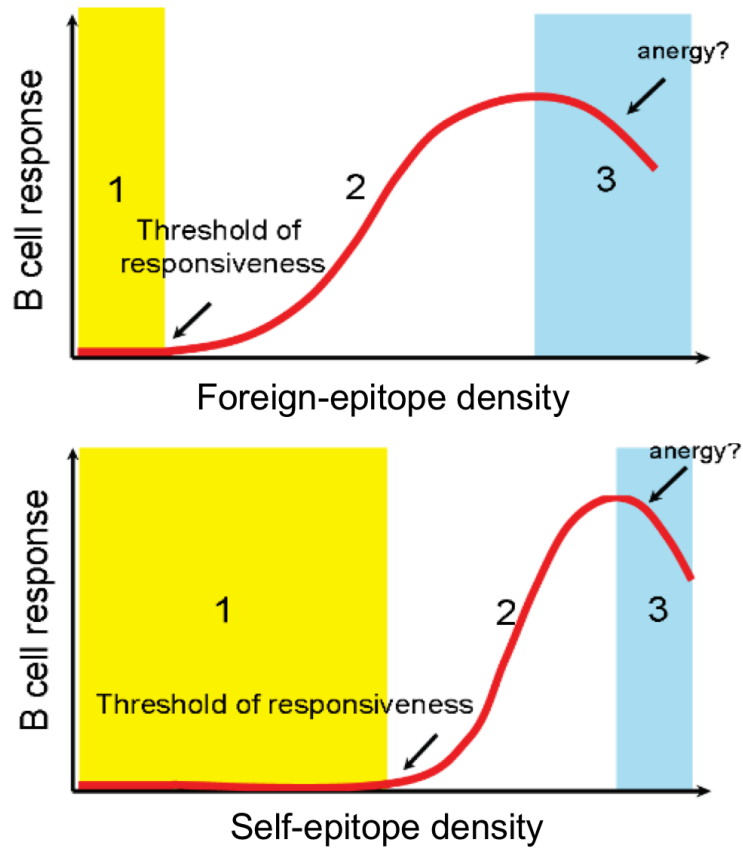
Figure 1.2. Hypothetical model of B cell responses to foreign-epitope and self-epitope densities.

For one particular antigen, the epitope density serves as a direct signal to B cells. Only when the epitope density is higher than a threshold of responsiveness, will B cells start to be activated. This threshold of density is higher for self-epitope than for foreign-epitope.
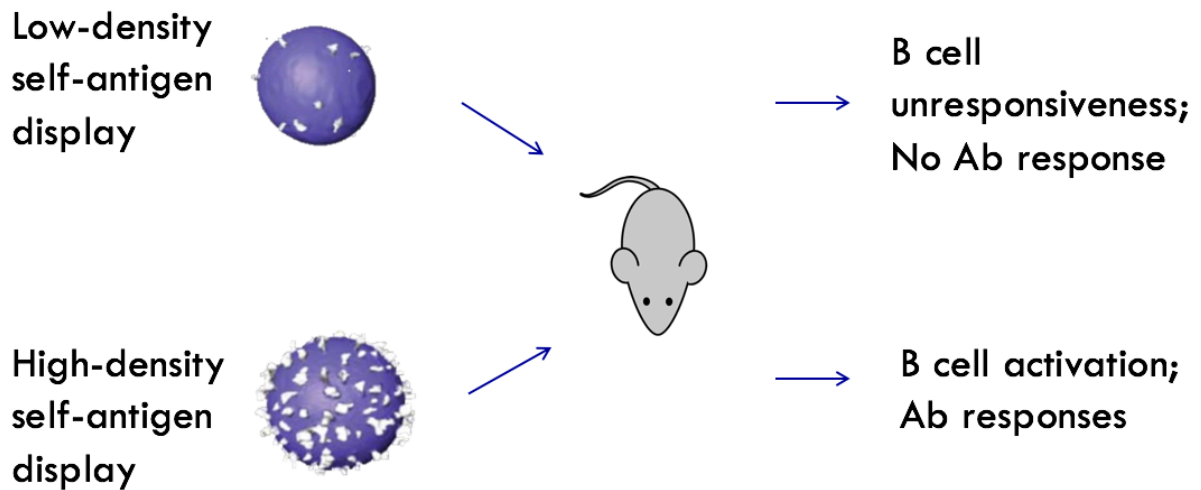
Figure 1.3. Schematic figure of experimental design.

High- or low-density level of self-antigen on nanoparticles (antigen amount in total is controlled) are inoculated to mice for study of B cell activation *in vivo*. Antibody production and activated B cell quantitation will determine if B-cell tolerance towards specific self-antigen has been broken.

1.5.   References

1.   HIV/AIDS: Global situation and trend. *Glob Heal Obs data*. 2013. http://www.who.int/gho/hiv/en/.
2.   Intelli- E, Intelli- E, Development C, et al. New England Journal. 2009:2209-2220. doi:10.1056/NEJMoa1404595.
3.   Haynes BF, Kelsoe G, Harrison SC, Kepler TB. B-cell–lineage immunogen design in vaccine development with HIV-1 as a case study. *Nat Biotechnol*. 2012;30(5):423-433. doi:10.1038/nbt.2197.
4.   Yamaguchi M, Danev R, Nishiyama K, Sugawara K, Nagayama K. Zernike phase contrast electron microscopy of ice-embedded influenza A virus. *J Struct Biol*. 2008;162(2):271-276. doi:10.1016/j.jsb.2008.01.009.
5.   Klein JS, Bjorkman PJ. Few and far between: how HIV may be evading antibody avidity. *PLoS Pathog*. 2010;6(5):e1000908. doi:10.1371/journal.ppat.1000908.
6.   Zhu P, Liu J, Bess J, et al. Distribution and three-dimensional structure of AIDS virus envelope spikes. *Nature*. 2006;441(7095):847-852. doi:10.1038/nature04817.
7.   Bachmann MF, Zinkernagel RM. The influence of virus structure on antibody responses and virus serotype formation. *Immunol Today*. 1996;17(12):553-558. doi:10.1016/S0167-5699(96)10066-9.
8.   Bachmann MF, Zinkernagel RM. Neutralizing antiviral B cell responses. *Annu Rev Immunol*. 1997;(15):235-270.
9.   Saphire EO, Parren PWHI, Pantophlet R, et al. Crystal Structure of a Neutralizing Human IgG Against HIV-1: A Template for Vaccine Design. *Sci* . 2001;293(5532):1155-1159. doi:10.1126/science.1061692.
10.   Thomas JA, Ott DE, Gorelick RJ. Efficiency of Human Immunodeficiency Virus Type 1 Postentry Infection Processes: Evidence against Disproportionate Numbers of Defective Virions . *J Virol*. 2007;81(8):4367-4370. doi:10.1128/JVI.02357-06.
11.   Kuwata T, Kaori T, Enomoto I, Yoshimura K, Matsushita S. Increased infectivity in human cells and resistance to antibody-mediated neutralization by truncation of the SIV gp41 cytoplasmic tail. *Front Microbiol*. 2013;4(May):117. doi:10.3389/fmicb.2013.00117.
12.   Parrish NF, Gao F, Li H, et al. Phenotypic properties of transmitted founder HIV-1. *Proc Natl Acad Sci U S A*. 2013;110(17):6626-6633. doi:10.1073/pnas.1304288110.
13.   Mond JJ, Lees A, Snapper CM. T CELL-INDEPENDENT. 1995.
14.   Mosier DE, Mond JJ, Goldings EA. The ontogeny of thymic independent antibody responses *in vitro* in normal mice and mice with an X-linked B cell defect. *J Immunol*. 1977;119(6):1874-1878. http://www.ncbi.nlm.nih.gov/pubmed/334975. Accessed August 17, 2015.
15.   Bekeredjian-Ding I, Jego G. Toll-like receptors--sentries in the B-cell response. *Immunology*. 2009;128(3):311-323. doi:10.1111/j.1365-2567.2009.03173.x.
16.   García de Vinuesa C, O'Leary P, Sze DM, Toellner KM, MacLennan IC. T-independent type 2 antigens induce B cell proliferation in multiple splenic sites, but exponential growth is confined to extrafollicular foci. *Eur J Immunol*. 1999;29(4):1314-1323. doi:10.1002/(SICI)1521-4141(199904)29:04<1314::AID-IMMU1314>3.0.CO;2-4.
17.   Reinitz DM, Mansfield JM. T-cell-independent and T-cell-dependent B-cell responses to exposed variant surface glycoprotein epitopes in trypanosome-infected mice. *Infect Immun*. 1990;58(7):2337-2342.

http://www.pubmedcentral.nih.gov/articlerender.fcgi?artid=258817&tool=pmcentrez&ren dertype=abstract. Accessed August 17, 2015.

18.   Milich DR, McLachlan A. The nucleocapsid of hepatitis B virus is both a T-cell-independent and a T-cell-dependent antigen. *Science*. 1986;234(4782):1398-1401. http://www.ncbi.nlm.nih.gov/pubmed/3491425. Accessed August 17, 2015.

19.   Lee BO, Rangel-Moreno J, Moyron-Quiroz JE, et al. CD4 T Cell-Independent Antibody Response Promotes Resolution of Primary Influenza Infection and Helps to Prevent Reinfection. *J Immunol*. 2005;175(9):5827-5838. doi:10.4049/jimmunol.175.9.5827.

20.   Feldmann M. THE RELATIONSHIP BETWEEN ANTIGENIC STRUCTURE AND THE REQUIREMENT FOR THYMUS-DERIVED CELLS IN THE IMMUNE RESPONSE. *J Exp Med*. 1971;134(1):103-119. doi:10.1084/jem.134.1.103.

21.   Dintzis HM, Dintzis RZ, Vogelstein B. Molecular determinants of immunogenicity: the immunon model of immune response. *Proc Natl Acad Sci U S A*. 1976;73(10):3671-3675. doi:10.1073/pnas.73.10.3671.

22.   Hinton HJ, Jegerlehner a., Bachmann MF. Pattern recognition by B cells: The role of antigen repetitiveness versus toll-like receptors. *Curr Top Microbiol Immunol*. 2008;319:1-15. doi:10.1007/978-3-540-73900-5_1.

23.   Bachmann MF, Rohrer UH, Kündig TM, Bürki K, Hengartner H, Zinkernagel RM. The influence of antigen organization on B cell responsiveness. *Science*. 1993;262(5138):1448-1451. doi:10.1126/science.8248784.

24.   Cooke MP. Immunoglobulin signal transduction guides the specificity of B cell-T cell interactions and is blocked in tolerant self-reactive B cells. *J Exp Med*. 1994;179(2):425-438. doi:10.1084/jem.179.2.425.

25.   Chackerian B, Lenz P, Lowy DR, Schiller JT. Determinants of autoantibody induction by conjugated papillomavirus virus-like particles. *J Immunol*. 2002;169(11):6120-6126. doi:10.4049/jimmunol.169.11.6120.

26.   Bluestone JA. Mechanisms of tolerance. *Immunol Rev*. 2011;241(1):5-19. doi:10.1111/j.1600-065X.2011.01019.x.

27.   Nemazee D. Mechanisms of central tolerance for B cells. *Nat Rev Immunol*. 2017;17(5):281-294. doi:10.1038/nri.2017.19.

28.   Merrell KT, Benschop RJ, Gauld SB, et al. Identification of Anergic B Cells within a Wild-Type Repertoire. *Immunity*. 2006;25(6):953-962. doi:10.1016/J.IMMUNI.2006.10.017.

29.   Chackerian B, Durfee MR, Schiller JT. Virus-like display of a neo-self antigen reverses B cell anergy in a B cell receptor transgenic mouse model. *J Immunol*. 2008;180(9):5816-5825. doi:10.4049/JIMMUNOL.180.9.5816.

30.   Thyagarajan R, Arunkumar N, Song W. Polyvalent antigens stabilize B cell antigen receptor surface signaling microdomains. *J Immunol*. 2003;170(12):6099-6106. http://www.ncbi.nlm.nih.gov/pubmed/12794139. Accessed November 13, 2018.

31.   Pierce SK. Lipid rafts and B-cell activation. *Nat Rev Immunol*. 2002;2(2):96-105. doi:10.1038/nri726.

32.   Alugupalli KR, Leong JM, Woodland RT, Muramatsu M, Honjo T, Gerstein RM. B1b lymphocytes confer T cell-independent long-lasting immunity. *Immunity*. 2004;21(3):379-390. doi:10.1016/j.immuni.2004.06.019.

33.   Lentz VM, Manser T. Cutting edge: germinal centers can be induced in the absence of T cells. *J Immunol*. 2001;167(1):15-20. http://www.ncbi.nlm.nih.gov/pubmed/11418626. Accessed August 13, 2015.

34.   de Vinuesa CG, Cook MC, Ball J, et al. Germinal Centers without T Cells. *J Exp Med*.

2000;191(3):485-494. http://jem.rupress.org/content/191/3/485. Accessed August 13, 2015.

35. Schiller J, Chackerian B. Why HIV Virions Have Low Numbers of Envelope Spikes: Implications for Vaccine Development. *PLoS Pathog*. 2014;10(8):e1004254. doi:10.1371/journal.ppat.1004254.

36. Sliepen K, Ozorowski G, Burger JA, et al. Presenting native-like HIV-1 envelope trimers on ferritin nanoparticles improves their immunogenicity. *Retrovirology*. 2015;12(1):82. doi:10.1186/s12977-015-0210-4.

37. Ingale J, Stano A, Guenaga J, et al. High-Density Array of Well-Ordered HIV-1 Spikes on Synthetic Liposomal Nanoparticles Efficiently Activate B Cells. *Cell Rep*. 2016;15(9):1986-1999. doi:10.1016/j.celrep.2016.04.078.

38. Cummings J, Lee G, Ritter A, Zhong K. Alzheimer's disease drug development pipeline: 2018. *Alzheimer's Dement (New York, N Y)*. 2018;4:195-214. doi:10.1016/j.trci.2018.03.009.

39. Lambert JM, Berkenblit A. Antibody–Drug Conjugates for Cancer Treatment. *Annu Rev Med*. 2018;69(1):191-207. doi:10.1146/annurev-med-061516-121357.

40. Braun J, Bollow M, Neure L, et al. Use of immunohistologic and in situ hybridization techniques in the examination of sacroiliac joint biopsy specimens from patients with ankylosing spondylitis. *Arthritis Rheum*. 1995;38(4):499-505. http://www.ncbi.nlm.nih.gov/pubmed/7718003. Accessed November 16, 2018.

41. Partsch G, Steiner G, Leeb BF, Dunky A, Bröll H, Smolen JS. Highly increased levels of tumor necrosis factor-alpha and other proinflammatory cytokines in psoriatic arthritis synovial fluid. *J Rheumatol*. 1997;24(3):518-523. http://www.ncbi.nlm.nih.gov/pubmed/9058659. Accessed November 16, 2018.

42. Saxne T, Palladino MA, Heinegård D, Talal N, Wollheim FA. Detection of tumor necrosis factor alpha but not tumor necrosis factor beta in rheumatoid arthritis synovial fluid and serum. *Arthritis Rheum*. 1988;31(8):1041-1045. http://www.ncbi.nlm.nih.gov/pubmed/3136775. Accessed November 16, 2018.

43. Mease PJ. Adalimumab in the treatment of arthritis. *Ther Clin Risk Manag*. 2007;3(1):133-148. http://www.ncbi.nlm.nih.gov/pubmed/18360621. Accessed November 15, 2018.

44. Burmester GR, Mariette X, Montecucco C, et al. Adalimumab alone and in combination with disease-modifying antirheumatic drugs for the treatment of rheumatoid arthritis in clinical practice: the Research in Active Rheumatoid Arthritis (ReAct) trial. *Ann Rheum Dis*. 2007;66(6):732-739. doi:10.1136/ard.2006.066761.

45. Breedveld FC, Weisman MH, Kavanaugh AF, et al. The PREMIER study: A multicenter, randomized, double-blind clinical trial of combination therapy with adalimumab plus methotrexate versus methotrexate alone or adalimumab alone in patients with early, aggressive rheumatoid arthritis who had not had previous methotrexate treatment. *Arthritis Rheum*. 2006;54(1):26-37. doi:10.1002/art.21519.

46. AbbVie. EValuation of HumIRA® in Patients With Active Rheumatoid Arthritis, Psoriatic Arthritis and Ankylosing Spondylitis in EASTern European Countries - Full Text View - ClinicalTrials.gov. https://clinicaltrials.gov/ct2/show/NCT01078402. Accessed November 16, 2018.

47. BETH WELCH. Adalimumab (Humira) for the Treatment of Rheumatoid Arthritis. *Am Fam Physician*. 1970;78(12):1406. https://www.aafp.org/afp/2008/1215/p1406.html. Accessed November 16, 2018.

48. Richard Franki. Humira Pen topped per-person drug spending in 2016 | Rheumatology

News. https://www.mdedge.com/rheumatologynews/article/132370/rheumatoid-arthritis/humira-pen-topped-person-drug-spending-2016. Accessed November 16, 2018.

49. Dalum I, Butler DM, Jensen MR, et al. Therapeutic antibodies elicited by immunization against TNF-α. *Nat Biotechnol*. 1999;17(7):666-669. doi:10.1038/10878.

50. Chackerian B, Lowy DR, Schiller JT. Conjugation of a self-antigen to papillomavirus-like particles allows for efficient induction of protective autoantibodies. *J Clin Invest*. 2001;108(3):415-423. doi:10.1172/JCI200111849.

51. Simms MS, Scholfield DP, Jacobs E, et al. Anti-GnRH antibodies can induce castrate levels of testosterone in patients with advanced prostate cancer. *Br J Cancer*. 2000;83(4):443-446. doi:10.1054/bjoc.2000.1315.

52. Brett BT, Smith SC, Bouvier C V., et al. Phase II Study of Anti–Gastrin-17 Antibodies, Raised to G17DT, in Advanced Pancreatic Cancer. *J Clin Oncol*. 2002;20(20):4225-4231. doi:10.1200/JCO.2002.11.151.

53. Ambühl PM, Tissot AC, Fulurija A, et al. *A Vaccine for Hypertension Based on Virus-like Particles: Preclinical Efficacy and Phase I Safety and Immunogenicity*. Lippincott Williams & Wilkins; 2007. https://insights.ovid.com/pubmed?pmid=17143175. Accessed October 15, 2018.

54. Hardy J, Selkoe DJ. The amyloid hypothesis of Alzheimer's disease: progress and problems on the road to therapeutics. *Science*. 2002;297(5580):353-356. doi:10.1126/science.1072994.

55. Morgan D, Diamond DM, Gottschall PE, et al. Aβ peptide vaccination prevents memory loss in an animal model of Alzheimer's disease. *Nature*. 2000;408(6815):982-985. doi:10.1038/35050116.

56. Schenk D, Barbour R, Dunn W, et al. Immunization with amyloid-β attenuates Alzheimer-disease-like pathology in the PDAPP mouse. *Nature*. 1999;400(6740):173-177. doi:10.1038/22124.

57. Wisniewski T, Konietzko U. Amyloid-beta immunisation for Alzheimer's disease. *Lancet Neurol*. 2008;7(9):805-811. doi:10.1016/S1474-4422(08)70170-4.

58. Hock C, Konietzko U, Streffer JR, et al. Antibodies against beta-amyloid slow cognitive decline in Alzheimer's disease. *Neuron*. 2003;38(4):547-554. http://www.ncbi.nlm.nih.gov/pubmed/12765607. Accessed November 16, 2018.

59. Talwar GP, Singh OM, Gupta SK, et al. The HSD-hCG vaccine prevents pregnancy in women: feasibility study of a reversible safe contraceptive vaccine. *Am J Reprod Immunol*. 1997;37(2):153-160. http://www.ncbi.nlm.nih.gov/pubmed/9083611. Accessed November 16, 2018.

60. Talwar GP, Singh O, Pal R, et al. A vaccine that prevents pregnancy in women. *Proc Natl Acad Sci U S A*. 1994;91(18):8532-8536. http://www.ncbi.nlm.nih.gov/pubmed/8078917. Accessed November 16, 2018.

61. Hanson MC, Abraham W, Crespo MP, et al. Liposomal vaccines incorporating molecular adjuvants and intrastructural T-cell help promote the immunogenicity of HIV membrane-proximal external region peptides. *Vaccine*. 2015;33(7):861-868. doi:10.1016/j.vaccine.2014.12.045.

62. Campbell S, Rein A. *In vitro* Assembly Properties of Human Immunodeficiency Virus Type 1 Gag Protein Lacking the p6 Domain *In vitro* Assembly Properties of Human Immunodeficiency Virus Type 1 Gag Protein Lacking the p6 Domain. 1999;73(3).

63. Datta S a K, Curtis JE, Ratcliff W, et al. Conformation of the HIV-1 Gag Protein in Solution. *J Mol Biol*. 2007;365(3):812-824. doi:10.1016/j.jmb.2006.10.073.

64. Datta SAK, Rein A. Preparation of recombinant HIV-1 gag protein and assembly of virus-

like particles *in vitro*. *Methods Mol Biol*. 2009;485:197-208. doi:10.1007/978-1-59745-170-3_14.

65. Tagliamonte M, Visciano ML, Tornesello ML, De Stradis a, Buonaguro FM, Buonaguro L. HIV-Gag VLPs presenting trimeric HIV-1 gp140 spikes constitutively expressed in stable double transfected insect cell line. *Vaccine*. 2011;29(31):4913-4922. doi:10.1016/j.vaccine.2011.05.004.

66. Allen TM, Cullis PR. Drug Delivery Systems: Entering the Mainstream. *Science (80-)*. 2004;303(5665):1818-1822. doi:10.1126/science.1095833.

67. Allen TM, Cullis PR. Liposomal drug delivery systems: From concept to clinical applications. *Adv Drug Deliv Rev*. 2013;65(1):36-48. doi:10.1016/j.addr.2012.09.037.

68. Kirpotin D, Park JW, Hong K, et al. Sterically stabilized anti-HER2 immunoliposomes: design and targeting to human breast cancer cells *in vitro*. *Biochemistry*. 1997;36(1):66-75. doi:10.1021/bi962148u.

69. Cheng W. The Density Code for the Development of a Vaccine? *J Pharm Sci*. 2016;105(11):3223-3232. doi:10.1016/j.xphs.2016.07.020.

70. Yoder JD, Dormitzer PR, Baker T, et al. Alternative intermolecular contacts underlie the rotavirus VP5* two- to three-fold rearrangement. EMBO J. 2006;25(7):1559-1568. doi:10.1038/sj.emboj.7601034

71. Hogle J, Chow M, Filman D. Three-dimensional structure of poliovirus at 2.9 A resolution. Science (80-). 1985;229(4720):1358-1365. doi:10.1126/science.2994218

72. Baker TS, Newcomb WW, Olson NH, Cowsert LM, Olson C, Brown JC. Structures of bovine and human papillomaviruses. Analysis by cryoelectron microscopy and three-dimensional image reconstruction. Biophys J. 1991;60(6):1445-1456. doi:10.1016/S0006-3495(91)82181-6

73. Reddy VS, Natchiar SK, Stewart PL, Nemerow GR. Crystal structure of human adenovirus at 3.5 A resolution. Science. 2010;329(5995):1071-1075. doi:10.1126/science.1187292

74. Heggeness MH, Smith PR, Choppin PW, Wong T, Butcher SJ. *In vitro* assembly of the nonglycosylated membrane protein (M) of Sendai virus. Proc Natl Acad Sci. 1982;79(20):6232-6236. doi:10.1073/pnas.79.20.6232

75. Zhang Y, Corver J, Chipman PR, et al. Structures of immature flavivirus particles. EMBO J. 2003;22(11):2604-2613. doi:10.1093/emboj/cdg270

76. Dryden KA, Wieland SF, Whitten-Bauer C, Gerin JL, Chisari F V., Yeager M. Native Hepatitis B Virions and Capsids Visualized by Electron Cryomicroscopy. Mol Cell. 2006;22(6):843-850. doi:10.1016/J.MOLCEL.2006.04.025

77. Harris A, Cardone G, Winkler DC, et al. Influenza virus pleiomorphy characterized by cryoelectron tomography. Proc Natl Acad Sci U S A. 2006;103(50):19123-19127. doi:10.1073/pnas.0607614103

78. Zhu P, Liu J, Bess J, et al. Distribution and three-dimensional structure of AIDS virus envelope spikes. Nature. 2006;441(7095):847-852. doi:10.1038/nature04817

Chapter 2

Construction and Characterization of Liposomes Conjugated with Proteins for Controlled Density of Surface Epitopes

2.1. Abstract

Liposomes have been widely used as antigen carriers due to its safety and flexibility. However, one key question remained to be answered is how to stably conjugate antigens on liposomes and quantitate the surface antigen density. Ni-chelating liposomes have been widely used as protein carriers in experimental studies of vaccine delivery, owing to the convenience and versatility of this conjugation chemistry. However, the epitope number per particle as well as the stability of protein conjugation on liposomes remain far less characterized. Here we have developed quantitative methods to measure the average spatial density of proteins on liposomes using both ensemble and single-molecule techniques and demonstrated their utility using liposomes conjugated with native proteins of two different sizes. These studies revealed that the initial density of protein conjugation on Ni-chelating liposomes can be finely controlled, but the density can decrease over time upon dilution due to the noncovalent nature of Ni-chelation chemistry. In comparison, peptide conjugated on liposomes through maleimide-cysteine

conjugation is much more stable over time. Our study suggests maleimide covalent conjugation is a better strategy to precisely regulate the epitope density on liposomes for B-cell antigen delivery.

2.2. Introduction

Vaccination is a concept that can be broadly applied to the prevention and treatment of human diseases, including but not limited to infectious diseases, cancer and neurodegenerative diseases. Currently, there are more than 90 vaccine products that are licensed for immunization and distribution in the US. The mechanisms of protection in the majority of these licensed vaccines are correlated with antibodies[1]. As a result, how to optimally activate antigen-specific B cells for the production of memory B cells is likely to be the key to the success of these vaccines.

There are extensive and well controlled studies in the literature that document the impact of epitope density on B-cell responses. Quantitative differences in epitope density can easily produce quantitative or qualitative differences in antibody responses in mouse models of immunization [2-5]. Indeed, the variation of the spatial density of a protein on a particulate antigen, e.g., vaccine candidate, has a direct impact on the antibody response in animals [6,7]. These studies revealed that the spatial density of epitopes on particulate antigens is a critical feature that one needs to consider for the delivery of B-cell based vaccines. However, the application of this fundamental principle to vaccine delivery remains incompletely developed for two reasons: (1) a robust antigen-delivery system is yet to be developed that allows the delivery of antigens, especially protein antigens with well-defined spatial densities, and (2) the techniques that are

necessary to precisely quantitate the spatial density of epitopes on particulate antigens remain lagging behind.

Varieties of nanomaterials have been developed over the past decade for the experimental delivery of various immunogens [8,9]. A simple and yet versatile approach is the protein-conjugated liposomes. Liposomes are well documented drug delivery systems with a safe record of clinical applications [10,11]. Liposome and liposome-derived nanovesicles have become important platforms for carrying antigens and immune-stimulatory molecules for vaccine development.[12] A variety of different parameters including the lipid composition, size, charge, and antigen conjugation can be manipulated for various applications.[13] At least two lipid-related vaccine products have been approved: Inflexal V[14] and Epaxal[15], targeting influenza and hepatitis A respectively, and more liposome-based vaccines are at different stages of clinical trials.

A potential advantage of liposome for vaccine delivery is that a purified protein can be attached to the particle surface through chemical conjugation, during which the density of the protein averaged over a single particle may be controlled. This strategy, if it works, may allow a fine control over the spatial density of epitopes per particle to optimize the B-cell antibody response. For anchoring epitope of interests on the surface of liposomes, a variety of conjugation methods have been developed[16]. Among them, Ni-NTA-his-tag conjugation has been a widely-accepted choice due to the convenience of its operation. Chelator-lipids were first synthesized and characterized for immobilization of engineered proteins at self-assembled lipid interface in 1994[17]. Since then, many groups have used liposomes containing metal-ion-chelating lipid to attach histidine-tagged protein of interest, which led to an elevated level of immune

response compared to traditional forms of antigen.[18-21] However, the spatial density of the proteins attached on these liposomes was often not reported in these studies.

In this paper, we explore the feasibility to fine control the surface density of epitopes attached to unilamellar liposomes and develop quantitative methods to characterize the spatial density of epitopes averaged over a single particle. It is worth noting that proteins attached onto the outer surface of liposomes, either covalently or non-covalently, may still be capable of two-dimensional diffusion on the liposome surface, which may allow formation of protein clusters with high local spatial density. Whether this phenomenon may occur during B-cell recognition of the particulate antigens is a subject of future research. Specifically, herein, the term 'spatial density' is referred to as the spatial density of proteins that is averaged over a single particle. Our results revealed that the initial density of proteins conjugated on liposomes via Ni-chelation chemistry can be fine controlled, but the density will decay with time upon dilution. In contrast, the epitope density is more stable upon dilution for epitopes conjugated onto the liposome surface via thiol-maleimide chemistry. These results support thiol-maleimide reaction instead of Ni-chelation chemistry for conjugation of B-cell epitopes onto liposomes and also suggest a strategy to regulate the average spatial density of proteins on liposomes for optimization of antibody responses.

2.3. Materials and Methods

Preparation of Ni-Chelating Liposomes

All liposomes used in this study were prepared using oil-in-water microemulsion precursor followed by membrane extrusion as originally described in literature.[22-24] Two different lipids at designated molar ratios were used in the synthesis of liposomes: DMPC (1,2-dimyristoyl-sn-glycero-3-phosphocholine) and Ni-NTA-DGS (1,2-dioleoyl-sn-glycero-3-[(N-(5-amino-1-carboxypentyl) iminodiacetic acid) succinyl] (nickel salt)) (Avanti Lipids). Briefly, various amount of Ni-NTA-DGS lipid was added into 5 mg DMPC in a round-bottom bottle to reach the indicated molar percentage for the Ni-NTA-DGS lipids. The lipid mixture in chloroform was then vacuum desiccated to allow thin film formation at the bottom of the bottle. One mL PBS buffer was then added to the bottle to hydrate the lipid film through gentle rocking at 37°C overnight. The next morning, the content was retrieved and extruded through polycarbonate membrane of 1000 nm and 100 nm sequentially, each for ten times. The resulting liposomes were then stored at 4°C for all experiments.

Preparation of TNF-α Peptide Conjugated Liposomes via Maleimide-Thiol Addition and Alexa-594 Fluorophore Labeling

Liposomes containing maleimide functionalized lipids were prepared using the same extrusion method as described above for Ni-chelating liposomes with minor modifications. Briefly, DMPC (1,2-dimyristoyl-sn-glycero-3-phosphocholine), cholesterol, and DSPE-PEG$_{2000}$-maleimide (1,2-distearoyl-sn-glycero-3-phosphoethanolamine-N- [maleimide (polyethylene

glycol)-2000]) (Avanti lipids) were included at a molar ratio of 5:3:2 (total lipid amount in moles was kept the same as that of Ni-chelating liposomes). To avoid maleimide hydrolysis during lipid film hydration, we adopted vigorous vortex instead of overnight incubation. After the lipid film was hydrated in HEPES buffer (100 mM HEPES, 150 mM NaCl, pH 6.9 at 20°C), the lipid film resuspension was extruded using polycarbonate membrane with pore sizes of 1000 nm and 100 nm sequentially for ten times each. Synthesized liposomes were incubated with TNF-α peptide (CSSQNSSDKPVAHVVANHQVE, 95% purity, Biomatik Scientific) at molar ratio of maleimide to peptide as 3:1. After overnight incubation at room temperature, the liposome peptide mixture was applied to Sepharose CL-4B gel filtration column to separate TNF-α conjugated liposomes from unconjugated free peptide. For labeling of Alexa-594 fluorophore through free amines, the pH of the peptide conjugated liposomes was first adjusted using one tenth volume of 1 M sodium bicarbonate solution. A stock solution of Alexa Fluor ® 594 succinimidyl ester (Invitrogen CAT#A37572) was then added to reach a molar ratio of 600:1 between the fluorophore and the liposome. The mixture was incubated in dark at 20°C for 15 min, and the reaction was then quenched by addition of 1 M Tris pH 7.0 to reach a molar ratio of 500:1 between Tris and the fluorophore. The labeled liposomes were then passed through 100 kD molecular weight cut off membrane (Sartorious) at 15 kg for three times to remove free fluorophores and stored at 4ºC.

Purification of Hexahistidine-Tagged Proteins

We have used two recombinant proteins of different sizes in this study: the B1 domain of streptococcal protein G and the monomeric teal fluorescent protein (mTFP)[25]. The B1 domain of protein G has a molecular weight of 7.7 kD while the mTFP has a molecular weight of 28 kD,

which provides a reasonable size difference for testing conjugation onto liposomes. Both proteins carry a hexahistidine tag at the C-terminus of the respective proteins for attachment onto liposomes through Ni-NTA coordination chemistry. Both proteins were house expressed in E. coli BL21(DE3) pLysS strain and purified to greater than 95% purity using nickel-nitrilotriacetic acid (Ni-NTA) agarose technology, as judged by intensity comparisons on an acrylamide gel loaded with different amounts of final purified proteins. The native B1 domain of protein G does not carry any cysteine residues[26]. To site-specifically label a single Alexa-594 fluorophore onto the protein for single-molecule studies, we have engineered a single cysteine at position 2, after the N-terminal methionine. We have developed a protocol to label the single cysteine on the B1 domain with high efficiency. Briefly, the purified B1 domain was treated with fivefold molar excess of TCEP at 4°C for 18 hours. The excess TCEP was removed by passing the protein through a desalting column. The Alexa-594 maleimide (ThermoFisher) freshly dissolved in water was then added to the protein at a tenfold molar excess. The crosslinking reaction was incubated at 20°C for 8 hours. The reaction was stopped by adding 2-mercaptoethanol to a final concentration of 20 mM. After additional 30 min incubation at 20°C, the labeled protein was extensively dialyzed at 4°C using a 3kD molecular weight cut-off membrane against the storage buffer containing 50 mM HEPES, 150 mM NaCl pH 7.0 at 22°C in order to remove excess dye molecules. The concentration of the labeled protein was measured by absorbance at 280 nm (corrected for dye absorbance at this wavelength) using an extinction coefficient of 9530 $M^{-1}cm^{-1}$, and the concentration of the conjugated Alexa-594 was quantified simultaneously by absorbance at 590 nm with an extinction coefficient of 9.00×10^4 $M^{-1}cm^{-1}$. The efficiency of dye labeling was thus calculated to be 96%. The status of single fluorophore labeling was also confirmed by positive ion electrospray mass spectrometry. This fluorescently labeled B1 domain of the streptococcal protein G is referred as rPG throughout this manuscript.

Attachment of Proteins to Liposomes and Size Exclusion Chromatography

For attachment of purified proteins onto liposome surface, the purified proteins were incubated with synthesized liposomes at 37°C for 1 hour at the indicated molar ratio between the proteins and the Ni-NTA group, which is sufficient to reach equilibrium as indicated by a comparison with the result from an overnight incubation at the same temperature. The mixture at 400 µl volume was then directly applied to the top of a 10-ml Sepharose CL-4B (GE Life Sciences) gel filtration column that was already equilibrated in PBS in order to remove excess free proteins not bound to liposomes. The column was run by gravity at 4°C and again PBS was used as the elution buffer. 20 fractions were collected after the sample application and each fraction contained 0.5 ml eluate. To identify fractions containing liposomes, dynamic light scattering measurement was conducted for samples from each fraction and the fractions with most of the liposomes were pooled and further stored at 4°C. For each coupling of proteins to liposomes reported in this work, the coupling efficiencies of proteins were calculated as the ratio between the amount of proteins on liposomes after the size-exclusion column and the initial input protein and reported as percentages in Table 2.2. The yield of lipid recovery was also calculated as the ratio between the amount of lipids present in liposomes after the size-exclusion column and the initial input lipids and reported as percentages in Table 2.2.

Stewart Assay to Measure Lipid Content

We have used the established Stewart assay[27] to determine the phospholipid content in the purified liposomes, based on which the molarity of the liposomes can be further estimated. It is

worth noting, however, that under Steward assay conditions, Ni-NTA-DGS alone can also give rise to non-negligible absorbance at 470 nm that is in linear proportion to the molarity of this specific lipid. Thus, throughout our studies, the phospholipid content measured has been corrected based on the percentage of Ni-NTA-DGS in the liposome sample, although this correction was minor for most cases. Purified liposomes bound with fluorescence labelled B1 domain of the streptococcal protein G or mTFP were both examined using Stewart assay for phospholipid quantitation. Briefly, 100 μL liposome samples were added to 1mL chloroform in a clean glass tube, and then 1mL ferrothiocynate solution containing 0.1 M ferric chloride hexahydrate and 0.4 M ammonium thiocyanate was added. The mixture was vigorously vortexed for 1 min and further kept at 22°C in the dark for at least one hour or until its full separation into two layers. The lower aqueous layer was then taken for absorption measurement at 470 nm. The phospholipid content was then calculated based on the comparison with a standard curve of DMPC lipids measured under identical conditions.

Estimation of Liposome Molarity Based on Geometric Considerations

To further estimate the molarity of the liposome based on the phospholipid content, we used geometric considerations of liposomes. Briefly, we calculated the number of lipid molecules N per liposome using the following equation:

$$N = \frac{\left[4\pi\left(\frac{D}{2}\right)^2 + 4\pi\left(\frac{D}{2}-h\right)^2\right]}{a} \quad (1)$$

Where D is the diameter of the liposome, h is the thickness of the bilayer, and a is the area of the lipid molecule head group. In our calculation for liposomes prepared using DMPC as the major lipids, the bilayer thickness h was taken as 4.6 nm based on previous experimental measurement on DMPC bilayers[28]. The area of DMPC lipid head group was taken as 0.657 nm^2

based on X-ray scattering measurement on DMPC lipid vesicles[29]. The average diameters of the

liposomes were measured using dynamic light scattering for each liposomal sample using

Malvern Zetasizer Nano ZS at 20ºC. The molarity of the liposomes was then calculated based on

the measured phospholipid content.

Fluorescence Plate Reader to Measure rPG Content in Liposomes

To measure the rPG protein content in the purified liposome samples, we employed

fluorescence plate reader (Synergy HT, Biotek). Briefly, the fluorescence of Alexa-594 was

recorded using an excitation filter of 590 nm with 20 nm bandwidth, and an emission filter of

645 nm with 40 nm bandwidth. Comparison with a standard curve prepared and measured using

known quantities of corresponding rPG free in PBS solution (0 to 3 ng/µL) yields an estimate of

protein content in liposome samples. The corresponding liposome samples without proteins

contributed negligibly to the fluorescence reading at the above settings.

Epifluorescence Imaging of Liposome Samples

To use single-molecule fluorescence to quantitate the spatial density of rPG on individual

liposomes, we have employed epifluorescence imaging approach. Liposome samples after gel

filtration was diluted 1000 folds and immediately applied onto poly-L-lysine coated coverslips

for epifluorescence imaging under an IX71 Olympus Advanced Research Fluorescence

microscope. Alexa-594 was excited using a 592 nm fiber laser and its emission monitored using

a 630 nm filter with 40 nm bandwidth. To record fluorescence with single-molecule sensitivity,

a laser power of 100 mW, EM gain of 100 and an exposure time of 20 ms were used throughout

so that the recorded fluorescence intensity can be directly compared across experiments. All the imaging experiments were conducted at 20ºC. The irradiance of the incident laser on the sample was estimated to be 87 mW/cm^2 or less, and the heating of the sample by laser irradiation was negligible under these conditions.

Inductively Coupled Plasma- Optical Emission Spectrometry (ICP-OES)

We have used ICP-OES (Optima 2000 DV, Perkin-Elmer) to quantitatively measure the amount of nickel ions in mTFP-conjugated liposomes collected through a gel filtration column. The atomic emission of Ni was detected at both wavelengths of 221 nm and 231 nm. To quantitate the amount of Ni in the liposome samples, a series of reference Ni samples from 100 ppb to 1000 ppb were prepared and standard curves were constructed. The final concentration of Ni in each sample was determined based on the standard curve and the average values from both 221 and 231 nm wavelengths was used as the final concentration of the Ni. Throughout our studies, reference Yttrium samples served as internal controls for the instrument by measuring their emissions at 371nm.

2.4. Results and Discussion

Characterization of the Spatial Density of rPG on Liposomal Surface

To facilitate the quantitation of the spatial density of proteins conjugated onto liposomes, we have chosen to use a fluorescent labeled protein, rPG, for attachment onto liposomes via the Ni-NTA coordination chemistry. The site-specific labeling of Alexa-594 fluorophore on this protein allows us to quantitate the spatial density of protein attached on liposomes using both ensemble and single-molecule fluorescence approaches. We prepared liposomes by the lipid thin film hydration method, followed by membrane extrusion.[22-24] For conjugation of proteins onto liposome surface, a minor percentage of Ni-NTA-DGS lipid was doped into DMPC during liposome preparation. Extrusion through polycarbonate membrane of 100 nm pore size allowed liposome formation with a relatively uniform size. As shown in Table 2.1A, these synthesized Ni-chelating liposomes had an average diameter of 97 ± 1 nm (mean $\pm$ standard error) with a mean polydispersity index of 0.04 ± 0.02 (mean $\pm$ standard error). The average diameter of these liposomes does not change significantly with the increase in the molar percentage of Ni-NTA-DGS lipids in the range of 0-20% that we have investigated.

To quantitate the spatial density of rPG on liposomes, we started out by focusing on liposomes that carried 1% of Ni-NTA-DGS. After liposome synthesis, a designated amount of rPG was incubated with liposomes for 1 hour at 37ºC, followed by purification through gel filtration. This experiment was then repeated using the same amount of liposomes (0.44 μmol DMPC) but with increasing concentrations of rPG. As shown in Table 2.1B, these liposomes after rPG association had a measurable increase in their diameters compared to that of the

liposome alone before rPG binding, consistent with protein binding on the surface of the liposomes. To determine the average number of rPG molecules per liposome, we first used fluorescent plate reader to measure the fluorescence intensity from the purified liposome samples. Comparison with a standard curve that was constructed using free rPG protein at various concentrations in PBS buffer under the same instrument conditions (Fig. 2.5a) allowed us to estimate the concentration of rPG in liposome samples. Control experiments showed that incubation of liposomes with rPG did not cause any change in the fluorescence signal for Alexa-594, suggesting that the quantum yield of Alexa-594 was not significantly perturbed by rPG attachment onto liposomes. Based on the molarity of liposomes calculated using Eq. 1, we can thus calculate the average number of rPG molecules per liposome. This result is shown in Fig. 2.1a. As the quantity of rPG increased from 2.5 to 80 µg, the average number of rPG per liposome also increased gradually and showed a trend to reaching a plateau, resembling a typical binding isotherm. It is worth noting that at 80 µg rPG, the molar ratio between Ni and rPG is 1: 1.6, suggesting that the trend of approaching plateau is a result of saturation of all the available Ni-NTA binding sites on liposomes, instead of surface crowding, i.e., saturation as a result of the crowding of proteins on liposome surface.

To provide further proof for this point, we have thus compared liposomes containing 1%, 3% and 5% Ni-NTA-DGS (all in molar percentage) for their protein surface densities, as shown in Fig. 2.1b. These liposomes were prepared by incubating the same moles of liposomes (0.44 µmol DMPC for liposomes with 1% Ni-NTA-DGS) with 30 µg rPG, followed by gel filtration. The average number of rPG molecules per liposome increased in a linear fashion with the percentage of Ni-NTA-DGS in the liposomes, as indicated by the solid line from a linear regression analysis. The average number of rPG per liposome observed from liposomes

containing 5% Ni-NTA is threefold higher than the plateau in Fig. 2.1a, which clearly

demonstrates that the trend of saturation observed in Fig. 2.1a is not due to surface crowding.

Rather, it is due to the limited number of Ni-NTA sites per liposome. These results also suggest

that one potential strategy to regulate the spatial densities of proteins on these liposome surfaces

is to adjust the percentage of Ni-NTA-DGS lipids incorporated into liposomes.

The above approach to estimate the average number of proteins on liposomes is an

ensemble-based measurement, where we assume each liposome has an average number of lipid

molecules, based on which to calculate liposome molarity and thus the number of rPG molecules

per liposome. Moreover, for the above approach to work, the fluorescence intensity of Alexa-

594 fluorophore should not change significantly upon conjugation onto liposomes through

protein G, i.e., rPG free in solution and rPG conjugated on the surface of a liposome should have

similar fluorescence intensity, otherwise any change in fluorophore quantum yield has to be

taken into account when doing estimations using this approach, which is not trivial. To provide

an alternative and yet direct measurement for the spatial densities of rPG on individual

liposomes, we have resorted to single-molecule fluorescence approach.

As shown in Fig. 2.2a, we deposited purified rPG-conjugated liposomes on poly-L-lysine

coated coverslips, and use epi-fluorescence imaging to directly visualize individual liposomes

through excitation of the Alexa-594 fluorophore by a 592-nm laser. Individual liposomes

showed up in a dark background as bright spots. These liposomes were prepared by incubating

2.5 µg rPG with liposomes containing 1% Ni-NTA-DGS (0.44 µmol DMPC), followed by gel

filtration. Neither liposome samples alone nor free rPG alone at the same concentrations yielded

these bright spots under the microscope. Moreover, no fluorescent spots were visible when rPG

was incubated with liposomes without Ni-NTA-DGS, suggesting that these fluorescent spots were liposomes conjugated with rPG through Ni-NTA but not protein aggregates. In order to determine the number of rPG molecules per liposome, we selected to work at a laser power of 100 mW. This illumination condition allowed us to collect the initial fluorescence intensity from individual spots, and the constant illumination of the sample under this condition also allowed us to observe the photobleaching of individual fluorophores with time. As shown in Fig. 2.2b, these photobleaching events display a hallmark feature of 'steps', where the fluorescence persists for a finite time followed by a sudden decrease in fluorescence intensity. These steps correspond to the photobleaching of individual molecules. We have used a step-detection algorithm that we developed previously [30] to identify steps from these real-time fluorescence traces. Measurement of this 'step' size yields the fluorescence intensity of a single Alexa-594 fluorophore, which can be used as an internal reference to convert the initial fluorescence intensity of individual liposomes to the number of Alexa-594 fluorophores, as we have done recently for individual HIV-1 virions using the same quantitation methodology[31]. As shown in Fig. 2.2c, the histogram of the individual photobleaching step sizes for Alexa-594 molecules (N=163) could be well described by the sum of two Gaussians (black curve), one centered at 649 ± 136 analog-to-digital units (a.u., mean $\pm$ standard deviation) and the other centered at 1164 ± 235 a.u. Under a statistical significance level of 5%, Pearson's Chi-square test [32] selected the double-Gaussian distribution (P-value=0.84) and rejected the single-Gaussian distribution (P-value=0.02) as the model to describe the data. The difference in peak values is close to twofold. As we have observed previously, the secondary peak may result from the photobleaching of two Alexa-594 molecules that occurred almost simultaneously, which could not be resolved by either the finite camera exposure time or the step-finding algorithm [33,34]. The fluorescence intensity of a single Alexa-594 fluorophore can then be used to calculate the total number of Alexa-594 molecules

per liposome based on a ratio comparison [35,36] with the initial fluorescence intensity of Alexa-594 associated with individual liposomes. Fig. 2.2d shows the distribution for the number of rPG molecules per liposome gathered from this analysis. It is very clear that the individual liposomes are heterogeneous in the number of rPG molecules per liposome, ranging from a value below 20 to a value above 100. Under a typical statistical significance level of 5%, Pearson's Chi-square test [32] selected a single-Gaussian distribution (p-value = 0.2249, shown in black curve) and strongly rejected Poisson distribution (p-value < 0.0001) as the model to describe the data. The arithmetic mean value is 53, which is very close to the value of 57 ± 3 rPG molecules per liposome estimated using the ensemble approach as described above (Fig. 2.1a). Therefore, the results from the single-molecule fluorescence measurements further support the use of the ensemble approach to estimate the average spatial density of proteins under our current experimental conditions.

Characterization of the Average Spatial Density of mTFP on Liposomal Surface

The B1 domain of the streptococcal protein G is a very small protein: even after the site-specific labeling of the Alexa-594 fluorophore, the molecular weight is still less than 9kD. To test if the above results for protein G may also be relevant to larger protein antigens, we have overexpressed and purified a green fluorescent protein variant, mTFP[25], which carries a hexahistidine tag for attachment onto liposomes through Ni-NTA coordination chemistry. This protein adopts a 'β-can'[25] structure that is typical of Green Fluorescent Proteins and the hexahistidine-tagged version of the protein has a molecular weight of 28 kD.

We prepared liposomes containing varied percentages of Ni-NTA-DGS, and incubated the purified mTFP proteins with various liposomes followed by gel filtration to remove free proteins. To develop an approach that is more applicable to generic protein antigens, we also decided to use the silver staining method instead of fluorescence to quantitate the amount of proteins present in the purified liposome samples. This method entails a standard curve based on band intensities quantitated from a silver-stained polyacrylamide gel using the proteins of interest at various quantities. The linear dependence between the band intensity and the quantity of mTFP protein (Fig. 2.5b) allows us to estimate the amount of mTFP proteins present in the purified liposome samples, by running the purified liposome sample on the same gel.

As shown in Fig. 2.3a, the average number of mTFP molecules per liposome determined in this way shows a linear dependence on the percentage of Ni-NTA-DGS contained in the liposomes, consistent with the trend observed for rPG on liposomes (Fig. 2.1b). With 20% Ni-NTA-DGS, on average, over 600 molecules of mTFP can be conjugated per liposome. It is worth noting that for 20% Ni-NTA-DGS in a liposome of 100 nm diameter, theoretically there are more than 17,000 Ni-NTA groups per liposome available for binding with hexahistidine-tagged proteins. Therefore, 600 molecules may not have reached the limit that one can conjugate on individual liposomes. To obtain more insight on the capacity of individual liposomes for conjugation of mTFP, we have thus decided to carry out the following experiment: we prepared liposomes containing 20% Ni-NTA-DGS lipids, and then incubated these liposomes with increasing quantities of mTFP proteins. After gel filtration to remove excess free proteins, we carried out three separate measurements on these purified liposomes: (1) run polyacrylamide gel to quantitate the amount of mTFP proteins based on silver staining (Fig. 2.5b); and (2) using Steward assay to determine phospholipid content and thus derive the moles of liposome based on

the average diameter measured from dynamic light scattering, and (3) using inductively coupled plasma optical emission spectrometry (ICP-OES) to directly measure Ni content for each purified liposome sample in order to verify the amount of Ni-NTA-DGS.

As shown in Fig. 2.3b, the amount of mTFP conjugated on liposomes increased with increasing quantities of mTFP initially incubated with liposomes (filled circles), showing a trend of reaching a plateau. Meanwhile, the percentage of Ni-NTA-DGS that we experimentally measured for these purified samples using ICP-OES (open circles) yielded an excellent agreement with theoretical expectations, with a mean and standard deviation of 20.3 ± 0.7 % among these samples. It is worth noting that under these conditions, even for the highest quantities of mTFP we tried, the amount of Ni-NTA was still in excess, with a molar ratio of 3:1 between Ni-NTA-DGS and the mTFP protein. This result thus indicates that there were more Ni-NTA binding sites on liposomes than the amount of free mTFP available, and this trend of plateau is unlikely to be a result of limiting Ni-NTA-DGS quantity in liposomes. More likely, it is due to the crowding of mTFP molecules on the liposomal surface. The radius of gyration for a globular protein of 28 kD is close to 2 nm[37]. For a liposome of 100 nm diameter, the upper limit on the number of mTFP molecules per liposome is thus estimated to be 2,500 with the assumption that the entire surface of the liposome can be fully occupied by arrays of mTFP molecules without significant vacancies in between. This estimation thus supports our interpretation on the mechanism behind the trend of plateau observed in Fig. 2.3b (filled circles) and indicates that the epitope density on these liposomes can be fine controlled by adjusting the percentage of Ni-chelating lipids.

Stability of the Ni-NTA Noncovalent Conjugation Chemistry

Although the use of Ni-NTA coordination chemistry is of great convenience considering

the varieties of recombinant proteins that can be purified using hexahistidine technology, the

noncovalent nature of this coordination chemistry may give rise to undesired drawbacks. The

binding affinity between hexahistidine-tagged proteins and Ni-NTA-modified surface has been

reported to be 0.1-1 μM.[38,39] In particular, Groves and coworkers have revealed that there is a

great degree of heterogeneity in the Ni-NTA coordination complex formed between the

hexahistidine tag and the nickel ions, which depends on the initial binding conditions and results

in different off rates observed for proteins attached to supported lipid bilayer through this non-

covalent chemistry and a changing protein density with time.[40]

To examine the stability of proteins conjugated onto liposome surface through this

noncovalent chemistry, we have thus measured the dissociation of proteins from liposomes by

direct observation using fluorescence microscopy. This experiment was done by using the rPG-

conjugated liposomes, the same preparation of liposomes that we used in Fig. 2.2 for quantitation

of the number of rPG molecules per liposome using the single-molecule fluorescence approach.

The starting sample has 53 rPG molecules per liposome on average (Fig. 2.2d). To monitor the

kinetics of dissociation, the liposome sample was diluted 1,000 fold into PBS buffer on Day 0.

The diluted sample was stored in dark in a polypropylene test tube for designated time at 22ºC

and then aliquots were taken out for measurement of the protein density using the single-

molecule fluorescence approach as illustrated above, and also the size using dynamic light

scattering. Although the size of liposomes does not change over a two-week period (Fig. 2.5c),

as shown in Fig. 2.4, the average number of rPG molecules per liposome dropped with

increasing days after the initial dilution (black circles). The average number of rPG per liposome

decreased from 53 ± 4 (Mean ± standard error) on Day 0 to 27 ± 3 after a week, and 13 ± 1 after

two weeks. In contrast, the liposome sample without dilution still had similar number of rPG

molecules per liposome bound after two weeks (data not shown). For comparison, we also

prepared liposomes whose surface was conjugated with a peptide epitope using covalent

maleimide-thiol conjugation chemistry (Materials and Methods) and used the same epi-

fluorescence imaging approach to quantitate the number of fluorophores per liposome. After

dilution of the liposome sample to the same concentration as that for rPG liposomes, no apparent

decrease of the fluorophore number per liposome was observed over the same time period of two

weeks (Fig. 2.4 open squares), suggesting that the epitopes are stably conjugated on the liposome

surface.

Discussion

In this study, we have developed quantitative methods to measure the average spatial

density of proteins on the surface of liposomes after conjugation. Our method of ensemble

estimation is supported by direct single-molecule measurement of protein densities on individual

liposomes (Fig. 2.2). Proximity of fluorophores is less an issue for our current quantitation using

fluorescence, because even for the highest spatial density we have, 500 rPG per liposome (Fig.

2.1b) the average distance between rPG molecules will be 8 nm, which is still large enough to

prohibit quenching through energy transfer or complex formation. Based on our studies, the

spatial density of a protein that one can attach onto liposome surface is limited by the percentage

of Ni-NTA-DGS under saturating protein conditions (Fig. 2.1a). On the other hand, as the

percentage of Ni-NTA-DGS increases, the spatial density of proteins will be eventually limited

by the surface crowding effect (Fig. 2.3b), i.e., the available liposomal surface will be fully occupied by the attached proteins. These methods of density quantitation are not protein-specific and thus can be applied to protein-conjugated liposomes in general.

Moreover, these quantitative studies revealed that the density of protein conjugation on liposomes can be fine controlled, and suggest a potential strategy for regulating the spatial density of epitopes on liposomes as particulate antigens, which is an important parameter for B cell antibody response and vaccination[1]. This strategy entails the following important steps: (1) purification of target proteins containing specific tags or active groups for chemical conjugation; (2) liposome synthesis using a mixture of lipids, in which a small percentage of lipids carry specific and reactive head groups; (3) after liposome synthesis, use excess protein for conjugation to the outer surface of the liposome via the specific conjugation chemistry; (4) gel filtration to purify protein-conjugated liposomes away from excess proteins. Compared to other alternative procedures, this strategy has the following advantages: (1) conjugation of protein post liposome synthesis helps to keep proteins in their native states and avoid their exposure to organic solvents used for liposome synthesis; (2) because of excess proteins used for conjugation, variation of the percentage of the specific lipid head-groups will thus allow the regulation of protein density. Systematic enumeration of the specific lipid percentage may allow formation of liposomes with surface epitopes at discrete densities, which would be very important tools for antibody-based vaccine development.

As we mentioned in the introduction, our current quantitation of protein density is an average over a single particle. These proteins attached onto liposome surface may still undergo two-dimensional diffusion, which may allow formation of protein clusters and a high local

surface density. Whether this may occur as a result of B cell recognition remains to be investigated in the future.

In this study, we have compared two different methods of epitope conjugation onto the outer surface of liposomes: Ni-chelation chemistry versus Michael addition of a thiol group to a maleimide. As we showed for Ni-NTA coordination chemistry, due to its noncovalent nature, the spatial density of proteins is not stable but decreases upon dilution (Fig. 2.4). This is not desired for the long-term storage of this formulation nor *in vivo* vaccination, because the time-dependent change of epitope density will confound the interpretation of the immunogenicity data based on liposome particles that use this noncovalent chemistry. Second, it is worth noting that substantial studies in literature have documented the adverse biological effects of nickel ions *in vivo*, which include tissue inflammation that is correlated with their distributions [41], allergy [42], toxicity and carcinogenicity [43-45]. Third, the hexahistidine tags might also be immunogenic *in vivo,* whose safety profile remains to be demonstrated. As a result, Ni-chelating liposomes may encounter significant safety challenges towards a final clinical product. In contrast, the alternative approach using maleimide-thiol reaction to conjugate epitopes onto liposome surface will yield a spatial density that is stable over time *in vitro* (Fig. 2.4). Moreover, the maleimide-thiol conjugation is less likely to be a regulatory concern because several FDA approved drug products contain maleimide-thiol conjugates [46-48]. Also, this chemistry has been widely used in the conjugation of drugs to macromolecules. There is a wide interest in the pharmaceutical and biotech industry to further optimize the chemistry of this conjugation to improve drug products [49,50]. We thus expect synergistic efforts towards the use of this conjugation chemistry.

Lastly, we emphasize that our strategy presented above to regulate the spatial density of surface epitopes on liposomes should also be applicable to the maleimide-thiol reaction chemistry, where maleimide-containing lipids can be doped into liposomes at varied percentages during synthesis, and conjugation with excess proteins that contain specific and accessible thiol groups will thus allow formation of liposomes bearing varied densities of epitopes. Based on the stability comparison for the protein conjugation (Fig. 2.4), and the safety issues that we have outlined above, we argue that the Michael addition of thiol to maleimide is a superior strategy than Ni-NTA coordination chemistry to conjugate epitopes onto liposomes for elicitation of antibody responses. Future experiments should explore maleimide-thiol reaction chemistry to conjugate epitopes at regulated spatial density on liposome surface and test these liposomal particles in animals for optimal B-cell antibody response.

2.5. Acknowledgements

2.6. Tables and Figures

A. Characterization of Ni-chelating liposomes by dynamic light scattering.

	Average diameter (nm)	Count rate (kcps)	Polydispersity index
0% Ni-NP	101.4	11.7	0.008
5% Ni-NP	95.5	9.6	0.024
10% Ni-NP	96.4	10.2	0.027
20% Ni-NP	95.2	9.3	0.094
Average	97.1	10.2	0.038

B. Characterization of Ni-chelating liposomes before and after rPG association by dynamic light scattering.

	Average diameter (nm)	Polydispersity index
1% Ni-NP alone	91.10	0.084
1% Ni-NP with 2.5 μg rPG	100.1	0.016
1% Ni-NP with 5 μg rPG	101.9	0.045
1% Ni-NP with 10 μg rPG	102.9	0.067
1% Ni-NP with 40 μg rPG	100.4	0.091
1% Ni-NP with 80 μg rPG	103.0	0.069

Table 2.1. Characterization of Ni-chelating liposomes of different percentage of Ni-NTA lipid before and after rPG association by dynamic light scattering.

(one representative out of three results).

A. Coupling of rPG at various initial quantities to liposomes of 1% Ni-NTA-DGS.

rPG input (µg)	rPG coupling efficiency (%)	Lipid recovery (%)
2.5	37.6	48.4
5.0	32.5	44.7
10	25.7	44.4
40	7.3	51.4
80	4.5	48.1

B. Coupling of 30 µg rPG with liposomes of various percentages of Ni-NTA-DGS.

Ni-NTA-DGS (%)	rPG coupling efficiency (%)	Lipid recovery (%)
1.0	4.9	41.7
3.0	16.8	34.8
5.0	36.6	47.6

C. Coupling of 40 µg mTFP with liposome of various percentages of Ni-NTA-DGS.

| Ni-NTA-DGS (%)	mTFP coupling efficiency (%)	Lipid recovery (%)
5.0	17.9	46.1
10	26.9	54.8
20	48.5	49.5

D. Coupling of mTFP at various initial quantities to liposomes of 20% Ni-NTA-DGS.

| mTFP input (µg)	mTFP coupling efficiency (%)	Lipid recovery (%)
10	46.7	57.2
40	54.5	60.1
160	39.9	42.0
320	23.8	54.0
640	15.7	58.6

Table 2.2. The coupling efficiency of proteins onto liposomes together with the yield of lipid recovery after size-exclusion chromatography for each protein coupling reported in this work.

The subpanels (A-D) are from experiments reported in Fig. 2.1a, Fig. 2.1b, Fig. 2.3a and Fig. 2.3b, respectively.
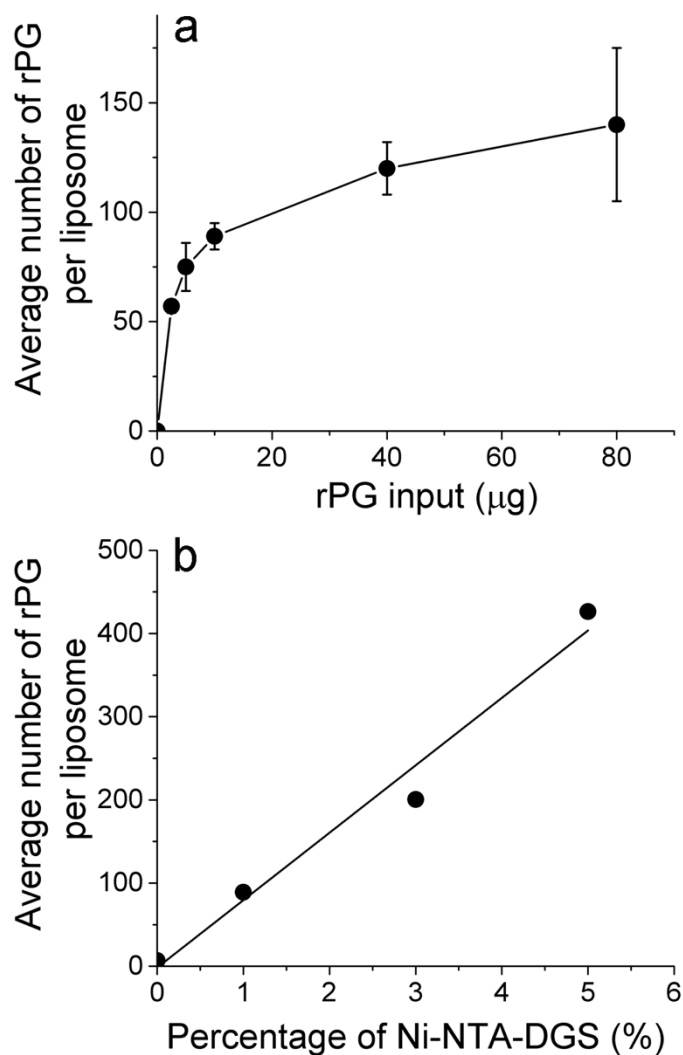
Figure 2.1. Characterization of rPG-conjugated liposomes using ensemble approach.

(a) The average number of rPG per liposome as a function of the initial input quantity of rPG during incubation with liposomes that contain 1% Ni-NTA-DGS. The error bars are standard deviations from three independent repeats of the same experiment. The solid line serves as a guide for the eye only. (b) The average number of rPG per liposome as a function of the percentage of the Ni-NTA-DGS incorporated into the liposomes (a representative of two). The solid line is a result of linear regression for the experimental data points.
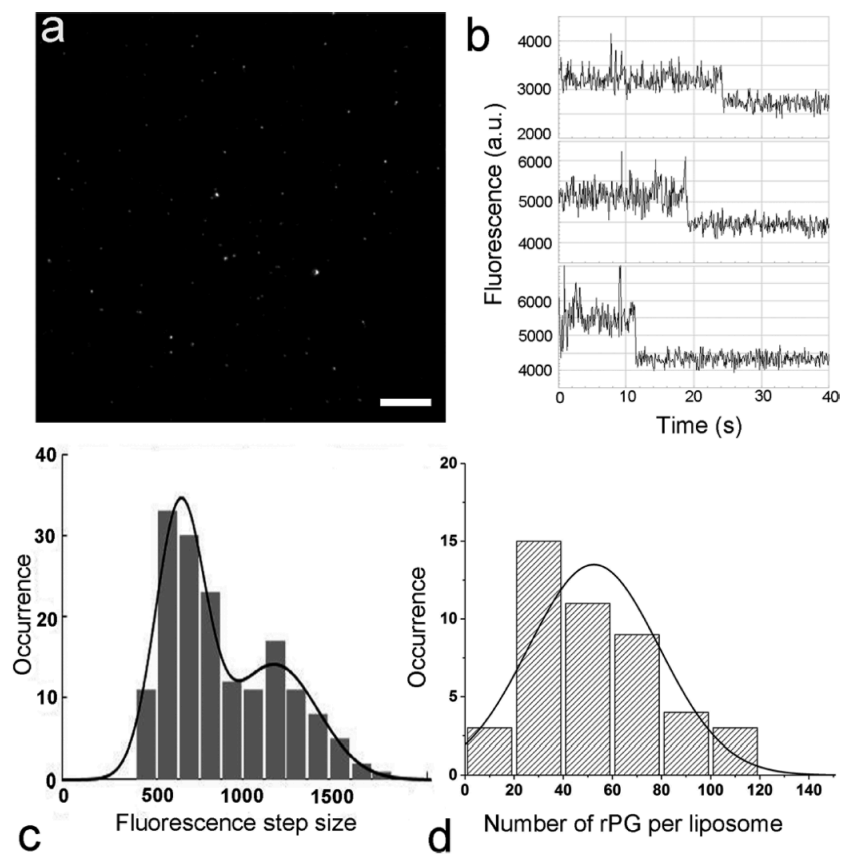
Figure 2.2. Characterization of rPG-conjugated liposomes using a single-molecule fluorescence approach.

These liposomes were prepared by incubating 2.5 μg rPG with liposomes containing 1% Ni-NTA-DGS (0.44 μmol DMPC), followed by gel filtration. Immediately before imaging, the liposome sample was diluted 1000-fold in PBS and deposited onto a coverslip. (a) A snapshot of the epi-fluorescence image of rPG-conjugated liposomes deposited on poly-L-lysine coated coverslip. The scale bar represents 10 μm. (b) Representative time trajectories of single-molecule photobleaching recorded from individual rPG-conjugated liposomes. (c) Histogram of the individual photobleaching step sizes for Alexa-594 molecules identified from the fluorescence time courses (b) using a step-finding algorithm (n = 163), which could be described by the sum of two Gaussians (black curve). (d) Histogram for the number of rPG molecules per liposome based on the initial fluorescence intensity of individual liposomes normalized by the average fluorescence intensity of a single Alexa-594 fluorophore (N = 45). The solid line is a fit to a Gaussian probability density function.
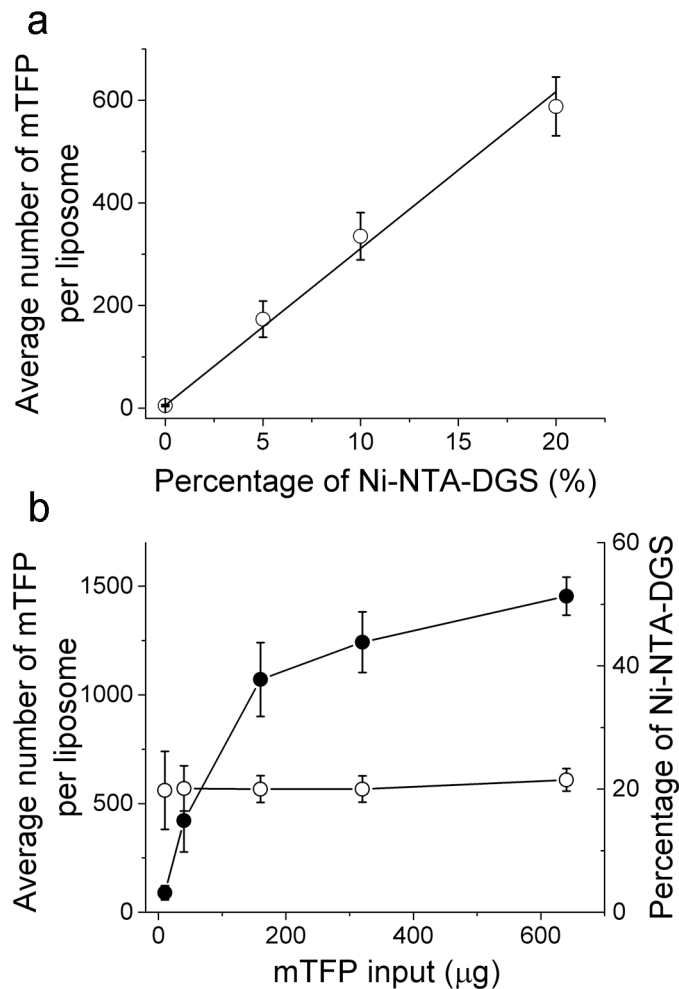
Figure 2.3. Characterization of mTFP-conjugated liposomes.

(a) Average number of mTFP per liposome as a function of the percentage of the Ni-NTA-DGS incorporated into the liposomes. The various liposomes were prepared by incubation of the same moles of liposomes (0.07 μmol DMPC for liposomes with 5% Ni-NTA-DGS) with 40 μg of mTFP, followed by gel filtration to remove free mTFP proteins. (b) Left y-axis: the average number of mTFP molecules per liposome as a function of the initial mTFP input during incubation with liposomes containing 20% Ni-NTA-DGS. The initial amounts of liposomes were all identical among different samples (0.18 μmol DMPC). Right y-axis: the percentage of Ni-NTA-DGS incorporated into liposomes measured by ICP-OES. The error bars are standard deviations from three independent repeats of the same experiment.
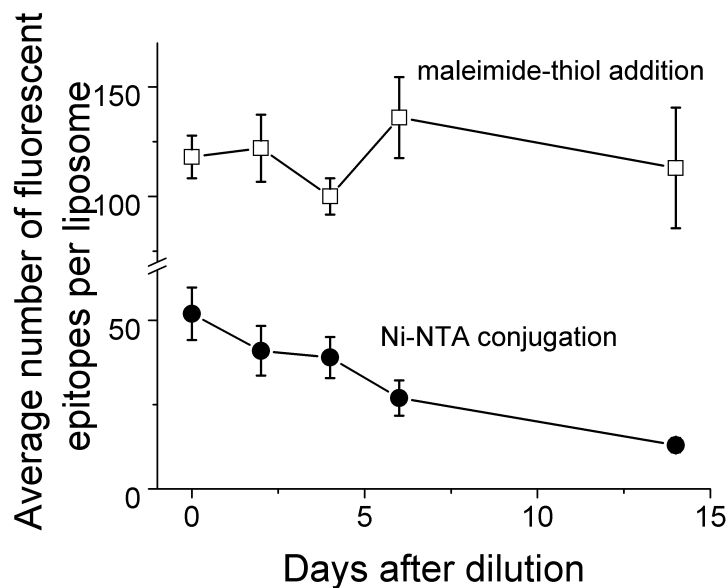
Figure 2.4. The kinetics of epitope dissociation from individual liposomes.

The average number of rPG molecules or fluorescent TNF-α peptides per liposome measured from single-molecule fluorescence approach as a function of the days after the initial dilution of the liposome samples. For each data point, 45 individual liposomes were randomly selected from fluorescence images for each sample and analyzed for the average number of fluorescent epitopes per liposome. The error bars represent 1.96 standard error of the mean.
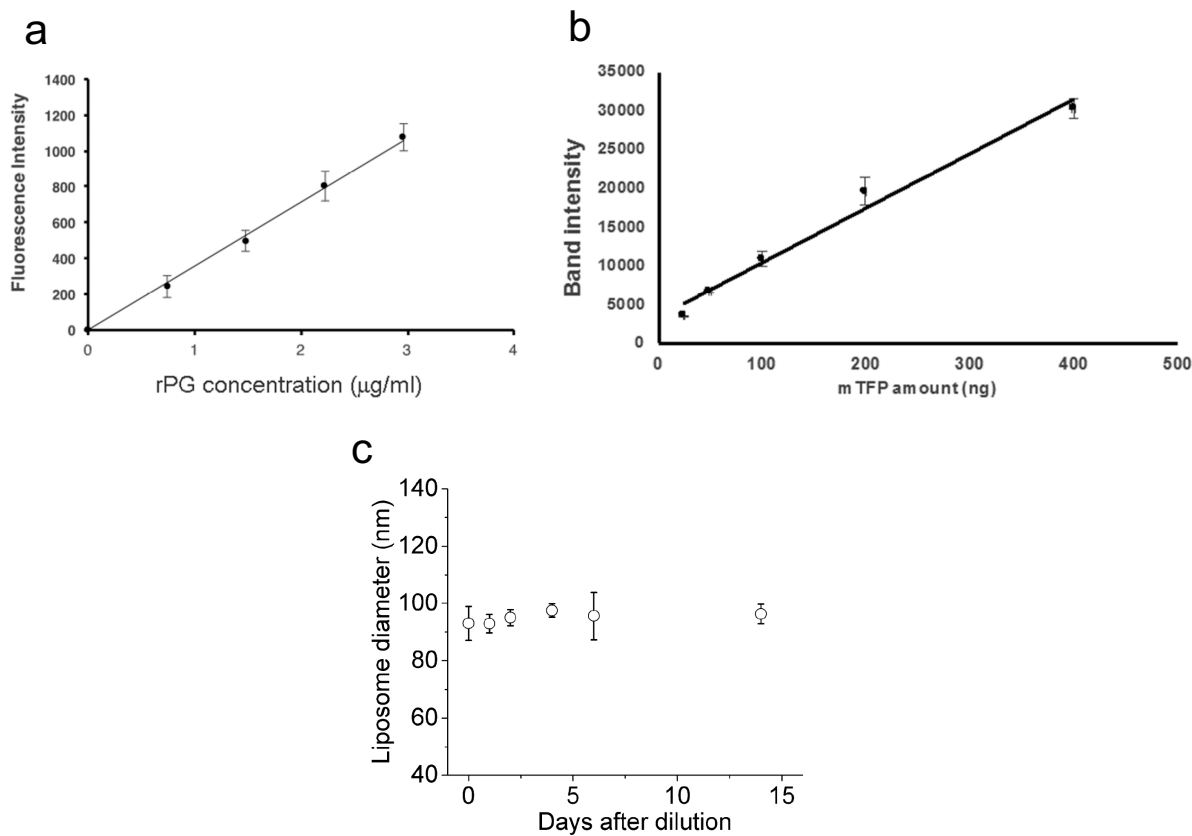
Figure 2.5. Supplementary figures.

a. Standard curve of rPG concentration from 0.74 μg/ml to 2.96 μg/ml. The solid line shows the linear regression analysis performed on the fluorescence intensity of rPG as a function of its concentration, which yields an R-squared value of 0.997. The error bars are standard deviations from three independent repeats of the same experiment. **b.** Standard curve for measurement of mTFP concentration in purified liposome samples with band intensities quantified from a silver-stained SDS-PAGE using ImageJ. The solid line shows the linear regression analysis performed on the band intensity of mTFP as a function of the loaded protein mass, which yields an R-squared value of 0.981. The error bars are standard deviations from three independent repeats of the same experiment. **c.** Size of rPG-conjugated liposomes as a function of time after dilution. The error bars are standard deviations from three independent measurements.

2.7. References

1. Cheng W 2016. The Density Code for the Development of a Vaccine? J Pharm Sci:10.1016/j.xphs.2016.1007.1020.

2. Dintzis HM, Dintzis RZ, Vogelstein B 1976. Molecular determinants of immunogenicity: the immunon model of immune response. Proc Natl Acad Sci U S A 73(10):3671-3675.

3. Bachmann MF, Rohrer UH, Kundig TM, Burki K, Hengartner H, Zinkernagel RM 1993. The influence of antigen organization on B cell responsiveness. Science 262(5138):1448-1451.

4. Chackerian B, Lowy DR, Schiller JT 1999. Induction of autoantibodies to mouse CCR5 with recombinant papillomavirus particles. Proc Natl Acad Sci U S A 96(5):2373-2378.

5. Feldmann M, Easten A 1971. The relationship between antigenic structure and the requirement for thymus-derived cells in the immune response. J Exp Med 134(1):103-119.

6. Hanson MC, Abraham W, Crespo MP, Chen SH, Liu H, Szeto GL, Kim M, Reinherz EL, Irvine DJ 2015. Liposomal vaccines incorporating molecular adjuvants and intrastructural T-cell help promote the immunogenicity of HIV membrane-proximal external region peptides. Vaccine 33(7):861-868.

7. Ingale J, Stano A, Guenaga J, Sharma SK, Nemazee D, Zwick MB, Wyatt RT 2016. High-Density Array of Well-Ordered HIV-1 Spikes on Synthetic Liposomal Nanoparticles Efficiently Activate B Cells. Cell Rep 15(9):1986-1999.

8. Irvine DJ, Hanson MC, Rakhra K, Tokatlian T 2015. Synthetic Nanoparticles for Vaccines and Immunotherapy. Chem Rev 115(19):11109-11146.

9. Hartwell BL, Antunez L, Sullivan BP, Thati S, Sestak JO, Berkland C 2015. Multivalent nanomaterials: learning from vaccines and progressing to antigen-specific immunotherapies. J Pharm Sci 104(2):346-361.

10. Allen TM, Cullis PR 2013. Liposomal drug delivery systems: from concept to clinical applications. Adv Drug Deliv Rev 65(1):36-48.

11. Allen TM, Cullis PR 2004. Drug delivery systems: entering the mainstream. Science 303(5665):1818-1822.

12. Watson DS, Endsley AN, Huang L 2012. Design considerations for liposomal vaccines: influence of formulation parameters on antibody and cell-mediated immune responses to liposome associated antigens. Vaccine 30(13):2256-2272.

13. Schwendener RA 2014. Liposomes as vaccine delivery systems: a review of the recent advances. Ther Adv Vaccines 2(6):159-182.

14. Herzog C, Hartmann K, Kunzi V, Kursteiner O, Mischler R, Lazar H, Gluck R 2009. Eleven years of Inflexal V-a virosomal adjuvanted influenza vaccine. Vaccine 27(33):4381-4387.

15. Bovier PA 2008. Epaxal: a virosomal vaccine to prevent hepatitis A infection. Expert Rev Vaccines 7(8):1141-1150.

16. Marques-Gallego P, de Kroon AI 2014. Ligation strategies for targeting liposomal nanocarriers. Biomed Res Int 2014:129458.

17. Schmitt L, Dietrich C, Tampe R 1994. Synthesis and Characterization of Chelator-Lipids for Reversible Immobilization of Engineered Proteins at Self-Assembled Lipid Interfaces. J Am Chem Soc 116(19):8485-8491.

18. van Broekhoven CL, Parish CR, Demangel C, Britton WJ, Altin JG 2004. Targeting dendritic cells with antigen-containing liposomes: a highly effective procedure for induction of antitumor immunity and for tumor immunotherapy. Cancer Res 64(12):4357-4365.

19. Patel JD, O'Carra R, Jones J, Woodward JG, Mumper RJ 2007. Preparation and characterization of nickel nanoparticles for binding to his-tag proteins and antigens. Pharm Res 24(2):343-352.

20. Watson DS, Platt VM, Cao L, Venditto VJ, Szoka FC, Jr. 2011. Antibody response to polyhistidine-tagged peptide and protein antigens attached to liposomes via lipid-linked nitrilotriacetic acid in mice. Clin Vaccine Immunol 18(2):289-297.

21. Pejawar-Gaddy S, Kovacs JM, Barouch DH, Chen B, Irvine DJ 2014. Design of lipid nanocapsule delivery vehicles for multivalent display of recombinant Env trimers in HIV vaccination. Bioconjug Chem 25(8):1470-1478.

22. Hope MJ, Bally MB, Webb G, Cullis PR 1985. Production of large unilamellar vesicles by a rapid extrusion procedure: characterization of size distribution, trapped volume and ability to maintain a membrane potential. Biochim Biophys Acta 812(1):55-65.

23. Mayer LD, Hope MJ, Cullis PR 1986. Vesicles of variable sizes produced by a rapid extrusion procedure. Biochim Biophys Acta 858(1):161-168.

24. Olson F, Hunt CA, Szoka FC, Vail WJ, Papahadjopoulos D 1979. Preparation of liposomes of defined size distribution by extrusion through polycarbonate membranes. Biochim Biophys Acta 557(1):9-23.

25. Ai HW, Henderson JN, Remington SJ, Campbell RE 2006. Directed evolution of a monomeric, bright and photostable version of Clavularia cyan fluorescent protein: structural characterization and applications in fluorescence imaging. Biochem J 400(3):531-540.

26. Gronenborn AM, Filpula DR, Essig NZ, Achari A, Whitlow M, Wingfield PT, Clore GM 1991. A novel, highly stable fold of the immunoglobulin binding domain of streptococcal protein G. Science 253(5020):657-661.

27. Stewart JC 1980. Colorimetric determination of phospholipids with ammonium ferrothiocyanate. Anal Biochem 104(1):10-14.

28. Johnson SJ, Bayerl TM, McDermott DC, Adam GW, Rennie AR, Thomas RK, Sackmann E 1991. Structure of an adsorbed dimyristoylphosphatidylcholine bilayer measured with specular reflection of neutrons. Biophys J 59(2):289-294.

29. Lewis BA, Engelman DM 1983. Lipid bilayer thickness varies linearly with acyl chain length in fluid phosphatidylcholine vesicles. J Mol Biol 166(2):211-217.

30. Arunajadai SG, Cheng W 2013. Step detection in single-molecule real time trajectories embedded in correlated noise. PLoS One 8(3):e59279.

31. DeSantis MC, Kim JH, Song H, Klasse PJ, Cheng W 2016. Quantitative Correlation between Infectivity and Gp120 Density on HIV-1 Virions Revealed by Optical Trapping Virometry. J Biol Chem 291(25):13088-13097.

32. Evans RD 1969. Chapter 27. The Atomic Nucleus (McGraw-Hill):Chapter 27.

33. Pang Y, Song H, Kim JH, Hou X, Cheng W 2014. Optical trapping of individual human immunodeficiency viruses in culture fluid reveals heterogeneity with single-molecule resolution. Nat Nanotechnol 9(8):624-630.

34. Hou X, Cheng W 2011. Single-molecule detection using continuous wave excitation of two-photon fluorescence. Optics letters 36(16):3185-3187.

35. Coffman VC, Wu JQ 2012. Counting protein molecules using quantitative fluorescence microscopy. Trends Biochem Sci 37(11):499-506.

36. Lawrimore J, Bloom KS, Salmon ED 2011. Point centromeres contain more than a single centromere-specific Cse4 (CENP-A) nucleosome. J Cell Biol 195(4):573-582.

37. Garcia De La Torre J, Huertas ML, Carrasco B 2000. Calculation of hydrodynamic properties of globular proteins from their atomic-level structure. Biophys J 78(2):719-730.

38. Nieba L, Nieba-Axmann SE, Persson A, Hamalainen M, Edebratt F, Hansson A, Lidholm J, Magnusson K, Karlsson AF, Pluckthun A 1997. BIACORE analysis of histidine-tagged proteins using a chelating NTA sensor chip. Anal Biochem 252(2):217-228.

39. Dorn IT, Neumaier KR, Tampe R 1998. Molecular recognition of histidine-tagged molecules by metal-chelating lipids monitored by fluorescence energy transfer and correlation spectroscopy. J Am Chem Soc 120(12):2753-2763.

40. Nye JA, Groves JT 2008. Kinetic control of histidine-tagged protein surface density on supported lipid bilayers. Langmuir 24(8):4145-4149.

41. Wataha JC, O'Dell NL, Singh BB, Ghazi M, Whitford GM, Lockwood PE 2001. Relating nickel-induced tissue inflammation to nickel release *in vivo*. J Biomed Mater Res 58(5):537-544.

42. Saito M, Arakaki R, Yamada A, Tsunematsu T, Kudo Y, Ishimaru N 2016. Molecular Mechanisms of Nickel Allergy. Int J Mol Sci 17(2).

43. Magaye R, Zhao J 2012. Recent progress in studies of metallic nickel and nickel-based nanoparticles' genotoxicity and carcinogenicity. Environ Toxicol Pharmacol 34(3):644-650.

44. Marchetti C 2014. Interaction of metal ions with neurotransmitter receptors and potential role in neurodiseases. Biometals 27(6):1097-1113.

45. Kim HS, Kim YJ, Seo YR 2015. An Overview of Carcinogenic Heavy Metal: Molecular Toxicity Mechanism and Prevention. J Cancer Prev 20(4):232-240.

46. Senter PD, Sievers EL 2012. The discovery and development of brentuximab vedotin for use in relapsed Hodgkin lymphoma and systemic anaplastic large cell lymphoma. Nat Biotechnol 30(7):631-637.

47. Peddi PF, Hurvitz SA 2013. Trastuzumab emtansine: the first targeted chemotherapy for treatment of breast cancer. Future Oncol 9(3):319-326.

48. Lang L 2008. FDA approves Cimzia to treat Crohn's disease. Gastroenterology 134(7):1819.

49. Fontaine SD, Reid R, Robinson L, Ashley GW, Santi DV 2015. Long-term stabilization of maleimide-thiol conjugates. Bioconjug Chem 26(1):145-152.

50. Lyon RP, Setter JR, Bovee TD, Doronina SO, Hunter JH, Anderson ME, Balasubramanian CL, Duniho SM, Leiske CI, Li F, Senter PD 2014. Self-hydrolyzing maleimides improve the stability and pharmacological properties of antibody-drug conjugates. Nat Biotechnol 32(10):1059-1062.

Chapter 3

Self-antigens Displayed on Liposomal Nanoparticles at High Surface Density Elicit Class-switched Autoreactive Antibodies Independent of T-cell Help

3.1. Abstract

Epitope density has a profound impact on B cell responses to particulate antigens, the molecular mechanisms of which remains to be explored. Early studies led by Zinkernagel and Schiller, respectively, have established that multivalent display of antigens on viruses or viral-like particles can overcome B-cell tolerance and elicit potent autoreactive antibodies in a T-cell dependent manner. However, how epitope density drives B cell activation in this process remains largely unknown. To dissect the role of epitope density in this process, we have synthesized a series of liposomal particles, similar to the size of viruses, that display a model self-antigen peptide at defined surface densities. Immunization of mice using these particles consistently elicited both IgM and class-switched IgG antibodies that are reactive towards the

59

self-antigen peptide. However, the IgG response shows no boosting effect upon repeated immunizations, suggesting the lack of T-cell involvement in this process. In transgenic mice lacking either functional T-cell receptors or MHC class II molecules on B cells, the liposomal particles elicited similar levels of IgM and IgG responses, confirming that this is a T-independent process. Remarkably, the titer of the IgG elicited in these experiments can be increased by 1000-fold upon replacement of liposomes by bacteriophage Qβ virus-like particles that display the same self-antigen peptide at comparable epitope densities, and this enhancement is lost almost completely in transgenic mice lacking either T-cell receptors or MHC class II molecules on B cells. In conclusion, high epitope density alone can trigger antibody class switching in B cells, and the extraordinary immunogenicity of viral-like particles relies in large part, on their ability to effectively recruit T cell help.

3.2. Introduction

Often, foreign particulate antigens such as viral particles can effectively prime the immune system for elicitation of protective antibody responses, with a few exceptions. This fact forms the basis for the majority of licensed antiviral vaccines [1]. However, how a particulate antigen such as a viral particle activates the immune system to bring about the protective antibody responses, especially at quantitative and mechanistic level, remains largely uncharacterized. One of the breakthroughs in our understanding of this question was put forward by Bachmann et al. [2], who showed that epitope density has a profound impact on B cell responses to antigens. Remarkably, the envelope glycoprotein displayed on the surface of vesicular stomatitis virus can break the tolerance of B cells in transgenic mice that express the same glycoprotein under the

60

control of *H-2K* promoter [2]. Along a similar vein, studies led by Schiller showed that potent and long-lasting autoreactive IgG antibodies were elicited in mice upon immunization with self-antigens incorporated or conjugated to papillomavirus-like particles [3-5]. These discoveries have led to potentially exciting applications of these techniques in efforts to elicit therapeutic antibodies through vaccination approach [6,7]. However, at fundamental mechanistic level, there remain questions unanswered regarding the extraordinary immunogenicity of these viruses or viral-like particles. Specifically, what are the molecular components or quantitative features in these particles that are required for the potent B cell activation? If collaboration with other immune cells is also required to yield the antibody response, to what extent does the production of these antibodies rely on those cells? Answers to these questions can not only help the design and engineering of vaccines, but also help understand the spectra of host immune responses to viral pathogens.

Among various features shared by the particles listed above, epitope density appears to be a dominant parameter in the quality of the antibody response. Ensemble estimations based on RNA and proteins present in viral particles yielded approximately 500 glycoproteins per vesicular stomatitis viral particle [8], while papillomavirus displays 360 copies of the major capsid protein L1 per particle based on a cryoelectron microscopy study[9]. Although the former is an enveloped virus while the latter is an icosahedral virus, both viruses display high number of viral-specific epitopes per particle, which is in fact a feature shared by most of the human viral pathogens with licensed vaccines [1]. Chackerian et al. showed that reduction of epitope density on papillomavirus-like particles significantly decreased the IgG autoantibody production [3], highlighting the critical role of high epitope density in breaking the B cell tolerance. However, high epitope density alone does not seem to entail the full story. It was known early on that very high density of antigens could *induce* B cell tolerance both *in vitro* and *in vivo* [10,11]. A recent

study of mouse B cells also suggested that too high epitope density in the absence of immediate T-cell help may trigger B-cell death instead of activation [12];

In order to understand quantitatively and mechanistically B cell responses to particulate antigens and define the role of epitope density in this process, we have taken a 'deconstructive' approach, by chemically synthesizing particulate antigens similar to the size of viruses, and use these particles for immunization in mice. We chose liposomes as carriers for the epitope of interest because (1) the nonimmunogenic nature of liposomes by themselves, and (2) the versatility of liposomes in epitope conjugation and engineering [13]. In particular, as we have shown recently [14], the epitope of interest can be conjugated onto the surface of these particles in a controlled fashion which yields particles with varied epitope densities, which would be one of the important tools to unravel the role of epitope density in this process. As we show, these particles alone can elicit IgG autoreactive antibody responses in a manner that depends on epitope density. To the best of our knowledge, this is the first time that an antigen, upon conjugation to liposomes at high epitope density, is shown to induce class-switched antibody responses in the absence of T-cell help. At comparable epitope density, replacement of liposomes with bacteriophage Qβ viral-like particles can dramatically enhance the titer of the IgG response. In comparison to liposomes, the superior immunogenicity of viral-like particles originate almost exclusively from their extraordinary capability to recruit MHC Class II dependent T-cell help after B-cell activation. Our study has thus helped answer a fundamental question in immunology regarding B-cell activation by particulate antigens and offered valuable insights to future vaccine design targeting self-antigens.

3.3. Materials and Methods

Synthesis of liposomes and antigen conjugation

Liposomes were prepared using oil-in-water microemulsion precursor followed by membrane extrusion as described[1–3]. Three different lipids of designated molar ratios were used in the synthesis of liposomes: DMPC (1,2-dimyristoyl-sn-glycero-3-phosphocholine), DSPE-PEG (2000) maleimide (1,2-distearoyl-sn-glycero-3-phosphoethanolamine-N- [maleimide (polyethylene glycol)-2000] (ammonium salt)) and cholesterol (Avanti lipids). Briefly, lipid mixture (7.5 μmol in total) in chloroform were added to a round-bottom bottle and desiccated by vacuum to form a thin film at the bottom. 1mL HEPES buffer (50mM HEPES, 150mM NaCl, pH6.9)[15] was added to hydrate the lipid film through vortex and short bursts of sonication (30s) in water bath. After hydration, the lipid film resuspension was extruded using polycarbonate membrane with pore sizes of 1000 nm and 100 nm sequentially for ten times each. Synthesized liposomes were incubated with a peptide from mouse tumor necrosis factor α (TNF-α peptide, CSSQNSSDKPVAHVVANHQVE, 95% purity, Biomatik Scientific) at a chosen molar ratio between the maleimide and the peptide. The N-terminal cysteine of the peptide was engineered for the purpose of maleimide conjugation. After overnight incubation at room temperature, the liposome peptide mixture was applied to Sepharose CL-4B gel filtration column, as we described previously [14], to separate TNF-α conjugated liposomes from unconjugated free peptide. The peptide-conjugated liposomes were stored at 4°C in PBS.

Quantitation of average peptide density on liposomes

To quantitate the average density of TNF-α peptide covalently conjugated on liposomes, our strategy is to estimate the concentration of liposome and peptide respectively for the liposomes purified through gel filtration column. The ratio between the two concentrations represents the average number of TNF-α peptide per liposome, as we described recently [14]. Briefly, to estimate the concentration of liposomes, we used the established Stewart assay[16] to determine the phospholipid content in the purified liposomes, based on which the molarity of the liposomes can be further estimated as described [14]. For each liposomal sample, 20 µL purified liposomes were added to 500 µL of chloroform in a clean glass tube, and then 500 µL ferrothiocynate solution containing 0.1 M ferric chloride hexahydrate and 0.4 M ammonium thiocyanate was added. The mixture was vigorously vortexed for 20 seconds and then centrifuged for 10 minutes at 1000X g. The lower chloroform layer was then taken for absorption measurement at 470 nm. The phospholipid concentration was then calculated based on standard curves constructed from known quantities of DMPC and m-DSPE-PEG, respectively, taken into account the compositions of the two lipids in the liposome samples. To measure the concentration of TNF-α peptide conjugated on liposomes, we used bicinchoninic acid (BCA) protein assay [17]. Briefly, 100µL of the liposome sample was incubated with 2 mL BCA solution at 60 °C for 30 minutes before absorption measurement at 562nm. 8% SDS was also included in this mixture to minimize the interference of lipid to BCA assay as reported [18]. The TNF-α peptide concentration was calculated based on the comparison with a standard curve constructed from known quantities of TNF-α peptide under the same BCA assay conditions.

Stability of epitope density in serum-containing media

Liposome of 20% maleimide-lipid was synthesized and conjugated with TNF-α peptide as described above. After conjugation, liposome$_{20\%-m}$- TNF-α was added with equal volume of fetal bovine serum for incubation at room temperature. After 1, 3, 5, and 7 days of incubation respectively, a fraction of liposome-serum mixture is taken and loaded to size exclusion column for purification of liposomes. After purification, the liposomes are evaluated by the Stewart Assay for quantitation of lipid concentration. Liposomes of same amount of lipid taken from different timepoints of serum incubation are loaded to Tricine-SDS gel for gel electrophoresis. A Tricine-SDS-PAGE protocol reported was followed here. For optimized bands of proteins and peptides <5 kDa, we used 16% acrylamide separating gel with 1cm of 10% spacer gel and 4% stacking gel. The running setting is 120 V for initial 20 mins and 180 V for approximately 90 minutes till the loading dye runs out of gel. Silver staining was carried out for quantitation of peptides and proteins on the gel.

Mice inoculations

All animal procedures were approved by the University of Michigan Animal Care and Use Committee. Female C57BL/6 mice (≥8 weeks, Jackson Laboratory) were used for inoculations. Prior to inoculation, all injection samples were filtered through 0.45 μm pore size membrane to eliminate potential microbial contamination. 100 μL samples were injected to each mouse subcutaneously, 50 μL on each flank. The immunization was boosted on days 14 and 28 using the same materials. Mouse blood was collected submentally using Microvette serum collection tube (Sarstedt) three days before the first injection, and 11 days after each immunization. The serum was harvested by centrifugation at 10,000 g for 10 minutes and immediately frozen and stored at -20°C.

65

Two strains of transgenic mice were purchased from Jackson Laboratory: Tcrb[tm1Mom]/ Tcrd[tm1Mom] (#002122) and Ciita[tm1Ccum] (#003239). Tcrb[tm1Mom]/ Tcrd[tm1Mom] mice are deficient in alpha beta and gamma delta T-cell receptors [19], while Ciita[tm1Ccum] mice do not have MHC class II molecules on the surface of splenic B cells or dendritic cells [20]. Transgenic mice were housed in germ-free environment and immunization protocol were carried out as described above for C57BL/6 mice.

Enzyme-Linked Immunosorbent Assay (ELISA)

Blood serum was tested for ELISA in order to quantitate B cell antibody responses from various immunizations. 96-well plates (Nunc MaxiSorp, Invitrogen) were coated overnight at 4°C with 5 µg of TNF-α peptide in PBS. After blocking with 1% BSA (Bovine Serum Albumin, Fisher) in PBS, mouse serum of different dilution factors (1: 100, 1: 400 and 1:1600) was added to each well for incubation at 22°C for 2 hours. After three washes using PBS with 0.05% Tween-20, secondary anti-mouse-IgG-HRP antibody (# 616520, Life technologies) or anti-mouse-IgM-HRP antibody (# 626820, Life technologies) was added in blocking buffer at 1:5000 dilution and incubated for 1 hour at 22°C. Following three washes, 100 µL TMB substrate (3,3',5,5'-Tetramethylbenzidine, Thermal Scientific) was added to each well and incubated in dark for 10 minutes. The reaction was stopped by addition of 100 µL 2M sulfuric acid in each well. The optical density of each well at 450nm was measured using a microplate reader (Bio-Tek Synergy HT). All the OD values reported were background subtracted by comparison between two wells that were coated with TNF-α peptide and PBS, respectively. Similarly, for ELISA using TNF-α protein as the bait, 200 ng of recombinant murine TNF-α protein (≥ 98%

purity, #315-01A, PeproTech) was coated in each well and the rest procedures were carried out as described above.

To determine the titers of anti- TNF-α antibodies, we used serial dilution of serum (from 1:100 dilution to 1:1638400 by dilution factor of 4) for ELISA with TNF-α peptide or protein for plate coating. Cutoff values are calculated as reported: Cutoff $= \bar{X} + SD \cdot f$, where $\bar{X}$ and SD is the mean and standard deviation of control well OD reading values, f is standard deviation multiplier corresponding to different confidence levels (Here, $f = 2.631$ when the number of control wells is 4 and confidence level is 95%). The titer value is determined as the highest dilution factor of serum that still yields OD450 reading value higher than cutoff value in ELISA.

3.4. Results and Discussion

Liposome-based particulate antigens that carry epitopes of varying density

To obtain a quantitative and mechanistic understanding of B cell responses to particulate antigens such as viruses, we decided to choose liposomes as our platform for antigen design. The unique advantage of using engineered liposomal particles as opposed to a specific virus is threefold: (1) the use of liposomes by themselves will not elicit an immune response and therefore provide a *baseline* for quantification of immunogenicity; (2) it allows us to use defined components to build a particle that mimic certain features of a natural virus particle and therefore no *ambiguity* on the constituents of the input antigen; and (3) it allows us to use model antigens (such as the TNF-α peptide used in this study) to systematically investigate the individual

contribution of various virus features on B-cell responses, including epitope density, the presence or absence of T-cell epitope and Toll receptor (TLRs) ligands, because these different features can be built into a liposomal nanoparticle in a controllable fashion.

In current study, we have selected DMPC (1,2-dimyristoyl-sn-glycero-3-phosphocholine) as the major lipid for construction of our liposomes, which has a phase transition temperature of 23°C [21] and therefore offers ease in extrusion through polycarbonate membranes. For conjugation of B-cell epitopes onto the surface of liposomes, we chose a sequence of 20 amino acids from mouse tumor necrosis factor α (TNF-α) as our model self-antigen. This sequence, SSQNSSDKPVAHVVANHQVE, corresponds to amino acids 83-102 of mouse TNF-α. Based on crystal structures of the highly homologous human TNF [22,23], the C-terminal half of the above sequence is predicted to be solvent exposed and contain critical residues that are directly involved in binding with TNF receptors[22]. Therefore, antibodies directed against this peptide are expected to bind the TNF-α protein and potentially block TNF-α and receptor interactions. Indeed, Chackerian et al. were able to elicit potent and long-lasting autoreactive TNF-α antibodies in mice using this peptide fused to a truncated form of streptavidin that is conjugated to biotinylated bovine papillomavirus-like particles [5], suggesting the presence of a mouse B-cell epitope in this peptide. The lack of Cysteine in the above peptide sequence allows us to engineer a single Cysteine at the N-terminus of the peptide for conjugation of this peptide to the surface of liposomes using maleimide chemistry in an orientation that exposes its C-terminal residues. For this maleimide chemistry, we have specifically chosen DSPE-PEG(2000) maleimide as the phospholipid for incorporation into liposomes. The presence of polyethylene glycol chain between the lipid head group and the maleimide moiety can increase the residence time of liposomes in the bodily fluid as demonstrated for many liposome systems [24-28].

To check the covalent conjugation of the TNF-α peptide onto the liposomes, we ran **16%** polyacrylamide gel and subjected the gel to silver staining. As shown in Fig. 3.1a, two bands were shown, the peptide itself has a molecular weight of 2kD, and the DSPE-PEG(2000) maleimide lipid has a molecular weight of 2941.605 Dal. Thus this is exactly as expected for a 1:1 conjugation of the peptide onto the lipid. We have also characterized these liposomal particles using dynamic light scattering (DLS). As shown in Fig. 3.1b, the DLS data show a well-defined peak around 153 nm for peptide conjugated particles, which compares with 137 nm for bare liposomes, suggesting that the peptide may form a dense layer on liposomal surface under this set of conditions. Consistent with this notion, quantitation of protein content in the purified liposomes (Materials and Methods) revealed 6,030 molecules of TNF-α peptide per liposome on average, which yields a density of 8.2×10^4 peptides/μm^2 that is even more than twofold higher than the epitope density on papillomavirus-like particles (3.2×10^4 peptides/μm^2)[1].

In order to test the effect of epitope density on B cell responses, it is necessary to prepare liposome particles with varied densities of epitope peptides. To this end, we have systematically changed the mole percentage of the DSPE-PEG(2000) maleimide from 1.1 to 20% that we included during liposome synthesis. After conjugation of the TNF-α peptide, these liposomes were purified through gel-filtration column and the epitope density was measured as described (Materials and Methods). As shown in Fig. 3.1c, the epitope density on these liposomes display a monotonic increase with increasing percentage of the DSPE-PEG(2000) maleimide lipids. This dependence can be well described with a linear dependence (the black line in Fig. 3.1c), yielding R-squared value of 0.9922. Specifically, the epitope density decreased to 357 for

liposomes containing 1.1% maleimide lipids, which is 6.6-fold lower than the epitope density on papillomavirus-like particles.

Because the epitope density is a critical parameter that we will evaluate for B cell responses, we have repeated the synthesis of liposomes with 20% maleimide lipids, in order to check the reproducibility of the resulting epitope density. As shown in Fig. 3.1d, for liposomes synthesized from 4 independent repeats of the same synthesis and conjugation procedure, they all yielded an epitope density around 6,000 TNF-α peptides per liposome on average, 6030.0 ± 428.4, suggesting a very good reproducibility of our procedure.

Lastly, because these liposome particles will be used *in vivo* for mouse immunizations, it is important that the epitope density is relatively stable in biological milieu so that the data can be interpreted with confidence. In presence of 50% fetal bovine serum, liposome size remained constant with slight increase over a week as shown in Fig. 3.1e. The conjugated TNF-α peptide density on liposome also remained at a similar level over time, indicated by SDS-PAGE result in Fig. 3.1f, g.

TNF-α peptides conjugated on liposomal surface elicit autoreactive IgG antibody in wild-type mice

To examine whether TNF-α-peptides conjugated on liposomal surface (p-liposome) can elicit autoreactive antibodies, we immunized mice with p-liposomes prepared with 20% maleimide lipids (p-liposome$_{20\%-m}$), which displayed ~6,000 TNF-α-peptides per liposome on average. Each group of mice received three doses of p-liposome$_{20\%-m}$, each dose containing 4.5

μg TNF-α-peptide. Antibody responses were measured by ELISA using serum collected 11 days after each inoculation. As shown in Fig. 3.2a-b, p-liposome$_{20\%-m}$ elicited both IgM and IgG responses towards the TNF-α-peptides after just one dose. Both responses are significantly higher than either the PBS or bare liposome control, and also significantly higher than those elicited by soluble TNF-α-peptides at the same dose (4.5 μg). In fact, the levels of IgM and IgG responses from the soluble TNF-α-peptides are statistically indistinguishable from those of PBS or bare liposome controls, consistent with the fact that this peptide by itself is a *bona fide* self-antigen and no apparent antibody responses were elicited upon immunization. The results shown in Fig. 3.2a-b also suggest that upon conjugation of the peptide to a liposomal nanoparticle, it becomes immunogenic and can induce class-switched IgG antibody responses, even though the liposomal nanoparticles by themselves are not immunogenic.

To further examine the antibody responses elicited by p-liposome$_{20\%-m}$, we continued to measure both IgM and IgG responses after the second and third immunizations. As shown in Fig. 3.2c, the IgM response from p-liposome$_{20\%-m}$ declined after successive injections, although the levels of responses were still distinguishable from those from soluble peptides. In contrast, the IgG response from p-liposome$_{20\%-m}$ was almost constant after the second and third immunizations, and remained much higher than those from soluble peptides (Fig. 3.2d). The steady level of IgG responses after successive immunizations suggests the lack of apparent antibody affinity maturation or B cell clonal expansion, which is in sharp contrast to the boosting effect typically observed for foreign antigens.

To examine the duration of the above antibody responses elicited by p-liposome$_{20\%-m}$ in the absence of further immunizations, we continued to measure both IgM and IgG responses from

these animals up to 18 weeks after the first immunization. As shown in Fig. 3.2e, the IgM response from immunized animals continued to decline and became indistinguishable from that of the soluble peptide by Week 10. The IgG response also declines, although at a slower pace compared to that of IgM and became indistinguishable from that of the soluble peptide by Week 14 (Fig. 3.2f).

The above results revealed that a self antigen, once conjugated onto the surface of a liposomal nanoparticle, can elicit both IgM and IgG antibody responses that are much higher than those from soluble peptide controls at the same antigen dose. To further examine the dependence of this immunogenicity on epitope density, we immunized C57BL/6 mice using p-liposomes prepared with varied percentages of maleimides. They are p-liposomes prepared with 6.6% maleimides (p-liposome$_{6.6\%-m}$), p-liposomes prepared with 2.2% maleimides (p-liposome$_{2.2\%-m}$), and p-liposomes prepared with 1.1% maleimides (p-liposome$_{1.1\%-m}$), which displayed 2479, 729, 357 TNF-α-peptides per liposome on average (Fig. 3.1c). Together with p-liposome$_{20\%-m}$ and soluble peptide control, a total of five groups of mice were immunized. Throughout these immunizations, the peptide dose was kept the same (4.5 µg TNF-α peptide). Three immunizations were performed for each group, and the antibody responses were measured starting 11 days after the first immunization. As shown in Fig. 3.3a, the IgM response from these various liposomes showed a clear dependence on epitope density: the lower epitope density, the lower IgM response. Although for p-liposome$_{1.1\%-m}$, the IgM response is still statistically higher than that from soluble peptides. Similarly, the IgG response from these liposomes also showed a clear dependence on epitope density: the lower epitope density, the lower IgG response. However, quantitatively, this decrease in IgG response follows a different trend from that of IgM response. In going from p-liposome$_{20\%-m}$ to p-liposome$_{2.2\%-m}$, IgM

response is almost unchanged, but the IgG response has dropped by fivefold (Fig. 3.3b). For p-liposome$_{1.1\%\text{-m}}$, the IgM response remains clearly distinguishable from that from soluble peptides at the same dose, however, the IgG response is indistinguishable from that of soluble peptide. These results reveal that IgG response is more sensitive to the change in epitope density than IgM responses. In particular, *even though a liposome has 357 TNF-α peptide on average, it is incapable of eliciting an autoreactive IgG response*, which clearly shows the dependence of immunogenicity on the epitope density.

All the immunization experiments that we have reported above were conducted in the absence of other immunostimulatory substance. To examine the effect of Toll-like receptor activation on the above processes, we then performed immunizations using the aforementioned liposomes but in the presence of CpG. For each immunization, 20 µg CpG was mixed with p-liposomes and then administered into the animals. The immunization still follows the same schedule as before and blood were collected at designated time for ELISA. As shown in Fig. 3.3c, all four p-liposomes induced very similar levels of IgM response, suggesting that the presence of CpG weakens the sensitivity of IgM response to epitope density. Similarly for IgG, three groups of p-liposomes induced the same levels of IgG response within error (p-liposome$_{20\%\text{-m}}$, p-liposome$_{6.6\%\text{-m}}$, and p-liposome$_{2.2\%\text{-m}}$). The IgG response elicited by p-liposome$_{1.1\%\text{-m}}$ remains the lowest among the four groups of liposomes, but in the presence CpG, this IgG response is clearly significantly higher than that from soluble peptide control, which is in contrast to Fig. 3.3b, where p-liposome$_{1.1\%\text{-m}}$ was incapable of eliciting an IgG response above background. These results suggest that the presence of CpG will likely modulate the sensitivity of B cells to epitope density. Specifically, the presence of CpG will sensitize B cells towards low epitope density, which is true for both IgM and IgG responses. We have continued to

monitor these animals for both IgM and IgG responses for longer time points. As shown in Fig.

3.9, IgG response did not show any boosting effect upon successive immunizations, which is true

for all these liposomal preparations. In addition, both IgM and IgG response drops with time,

consistent with the pattern we observed in Fig. 3.2e-f.

TNF-α peptides conjugated on virus-like particles elicit stronger autoreactive IgG antibody through T-cell help

Even in the presence of CpG, it did not escape our attention that the titers of IgG response

from these liposomes are only on the order of $10^2 \sim 10^3$, which is much lower than the IgG titer

reported for the same peptide but noncovalently conjugated to papillomavirus-like particles[5]. To

examine the mechanisms behind this apparent difference, we have thus conjugated the TNF-α

peptide to bacteriophage Qβ viral-like particles (VLP$_{Qβ}$) using heterobifunctional crosslinker

SMPH. Bacteriophage Qβ has been used as an antigen presentation platform for elicitation of

antibodies against self antigens both in mouse and in limited human clinical trials. The single

available thiol group present in our synthetic TNF-α peptide allows us to conjugate these

peptides to the surface of VLP$_{Qβ}$ that is derivatized by SMPH. The excess free peptide was

removed by passing the reaction mixture through Amicon filtration units 3 times. As shown in

Fig. 3.4a in a silver stained gel to monitor this conjugation reaction, the SMPH-derivatized

VLP$_{Qβ}$ before conjugation with TNF-α peptide showed a major band around 15 kD, which

corresponds to the molecular weight of Qβ major coat protein. Upon crosslinking with TNF-α

peptide, a series of bands were seen on the gel, which matches with the expected molecular

weights for the coat protein conjugated with one TNF-α peptide, two TNF-α peptides, and so on.

Based on silver staining intensity, we estimated that on average there are 260 TNF-α peptides per

VLP$_{Q\beta}$ particle, which yields an epitope density of 132,300 molecules/μm^2. This epitope density is about two thirds of the epitope density on p-liposome$_{20\%\text{-m}}$. We have also characterized these VLP$_{Q\beta}$ particles using DLS. As shown in Fig. 3.4b, the DLS data show a well-defined peak around 42 nm for peptide conjugated particles, which compares with 36 nm for underivatized VLP$_{Q\beta}$ particles, suggesting that the peptide may form a dense layer on VLP$_{Q\beta}$ surface which is also consistent with our estimation for the peptide density on these particles.

We then used these peptide conjugated VLP$_{Q\beta}$ particles (p-VLP$_{Q\beta}$) to immunize C57BL/6 mice. In these experiments, we followed the same immunization schedules as we did for p-liposomes. However, in order to compare the immune responses elicited by p-VLP$_{Q\beta}$ to those previously published in literature using papillomavirus-like particles, we have used p-VLP$_{Q\beta}$ containing 0.5 μg TNF-α peptides for each animal, which was the peptide dose published previously using papillomavirus-like particles. This peptide dose was ninefold lower than those we employed in p-liposomes above, and thus for fair comparison, we also immunized C57BL/6 mice using p-liposome$_{20\%\text{-m}}$ containing 0.5 μg TNF-α peptides for each animal. As shown in Fig. 3.5a, dose decrease for p-liposome$_{20\%\text{-m}}$ elicited a marked lower IgM response compared to that from p-liposome$_{20\%\text{-m}}$ containing 4.5 μg TNF-α peptides. The p-VLP$_{Q\beta}$, on the other hand, elicited much higher IgM responses than p-liposome$_{20\%\text{-m}}$. Remarkably, for IgG responses, under the same dilution of 1:100, the p-VLP$_{Q\beta}$ elicited IgG responses that clearly saturated the OD reading at 450 nm (Fig. 3.5b). Control experiments using a simple admixture of VLP$_{Q\beta}$ and the soluble TNF-α peptide at the same particle and peptide doses did not elicit any IgM or IgG response above the background, clearly revealed that it is the conjugation of the TNF-α peptide onto the VLP$_{Q\beta}$ and presentation of the peptide in the context of these particles that matters.

The saturation in OD450 requires further dilution of the serum in order to obtain meaningful titer values for the IgG antibody responses. By performing a serial dilution of the collected sera and repeat the ELISA measurements (Materials and Methods), we determined that the IgG response elicited by p-VLP$_{Q\beta}$ has a titer between 10^4 and 10^5 (Fig. 3.5b), which occurred 11 days after the first inoculation, and the titer increased to 10^5 11 days after the second inoculation, and thus clearly display a boosting effect. These titer values compare favorably with the titer values previously reported for the same peptide but conjugated to papillomavirus-like particles at the same peptide dose [5]. In contrast, the IgG titer elicited by p-liposome$_{20\%-m}$ was between 10^2 and 10^3 (Fig. 3.5c), which occurred 11 days after the first inoculation, and the titer remains between 10^2 and 10^3 after the second and third inoculation, and no boosting effect was observed. These data clearly suggest that p-VLP$_{Q\beta}$ particles are much more potent than liposomal nanoparticles in eliciting IgG responses.

Previously studies by Chackerian et al. showed that the TNF-α peptide conjugated to papillomavirus-like particles can actually elicit antibodies that can bind the recombinant TNF-α protein. To test whether our construction of the p-VLP$_{Q\beta}$ particles can elicit the same effect, we thus conducted ELISA using a recombinant TNF-α protein coated on the ELISA plate. As shown in Fig. 3.6, the IgG antibody elicited by both p-VLP$_{Q\beta}$ and p-liposome$_{20\%-m}$ can bind to the recombinant TNF-α protein coated on ELISA plates. Similar to TNF-α peptide as coating material, when using TNF-α protein for ELISA, dilution factor of p-VLP$_{Q\beta}$ serum is 1:25600 to reach the same level of ELISA response compared to p-liposome$_{20\%-m}$ serum of 1:100 dilution.

Why are p-VLP$_{Q\beta}$ particles much more potent than the aforementioned liposomal nanoparticles in eliciting IgG responses? Among others, one difference is the size of particles,

while the liposomal particles we have prepared and tested have diameters around 150 nm, the p-VLP$_{Q\beta}$ particles are about threefold smaller in their diameters. To examine the effect of particle size on liposomal immunogenicity, we have thus prepared liposomal particles that are about 75 nm in diameters (see DLS results in Fig. 3.10), again, using 20% maleimide lipids, we conjugated TNF-α peptides to these liposomes at a density of 9.4×10^4 peptides/μm^2 (1721 molecules per liposome), similar to our previous p-liposome$_{20\%-m}$ with peptide density of 8.2×10^4 peptides/μm^2 (6030 molecules per liposome). Follow the same immunization protocol and using the same peptide dose, we immunized C57BL/6 mice. As shown in Fig. 3.7, these smaller particles elicited IgM and IgG responses, although both are very much comparable to those of larger liposomes. Therefore, size of these particles did not apparently explain the huge difference in the immunogenicity between p-VLP$_{Q\beta}$ and p-liposomes.

Because TNF-α peptide is a *bona fide* self antigen, even though this antigen may be internalized and presented by the B cells after their initial recognition by the membrane-bound B cell receptors, it may not find the cognate helper T cells to sustain B-cell proliferation. This is a challenge especially for self-antigens, where T cells that recognize self-antigens may have been eliminated during their maturation [29]. In fact, the lack of boosting effect upon successive immunizations as we observed for the series of p-liposomes (Fig. 3.2 and Fig. 3.9) suggest the lack of T cell help in these IgG responses, which is in contrast to the boosting effect observed for p-VLP$_{Q\beta}$ in this study and also reported previously for the same peptide conjugated on the surface of papillomavirus-like particles[3]. In fact, both the coat protein in bacteriophage Qβ and major capsid protein L1 in papillomavirus are foreign to mice, the inclusion of these proteins in the antigen presentation platforms may have thus inadvertently served this role of foreign

antigens for efficient recruitment of T cell help to sustain B cell activation and germinal center formation.

To test this hypothesis, we have thus utilized two different strains of transgenic mice that are created in C57BL/6 background (Materials and Methods). The first line is deficient in both alpha beta and gamma delta T-cell receptors [19] (denoted as TCR$^{-/-}$), while the second line does not express MHC class II molecules on the surface of splenic B cells or dendritic cells [20] (denoted as MCII$^{-/-}$), and thus both lines are deficient in T-dependent B cell activations. We first immunized these two lines of transgenic mice using p-liposome$_{20\%-m}$, following the same immunization schedule and doses as we did for the wild-type C57BL/6 mice. As shown in Fig. 3.8a, these two lines of transgenic mice produced IgM responses that are identical within error to the wild-type C57BL/6 mice. Similar IgG responses were also observed for these three lines of animals (Fig. 3.8b). In particular, one-way ANOVA test conducted for these data yielded p-values >0.05 for all three groups at Week 2, 4 and 6, suggesting that neither IgM nor IgG responses elicited in these animals are statistically different. Furthermore, no boosting effect of IgG response was observed in either transgenic mice, consistent with the result seen in wild-type mice (Fig. 3.2). These data thus confirm that the IgG response elicited by p-liposomes in wild-type mice is a result of T-independent B cell activation. These data also showed that class-switched antibody responses can be elicited by these p-liposomes in the absence of T cell help.
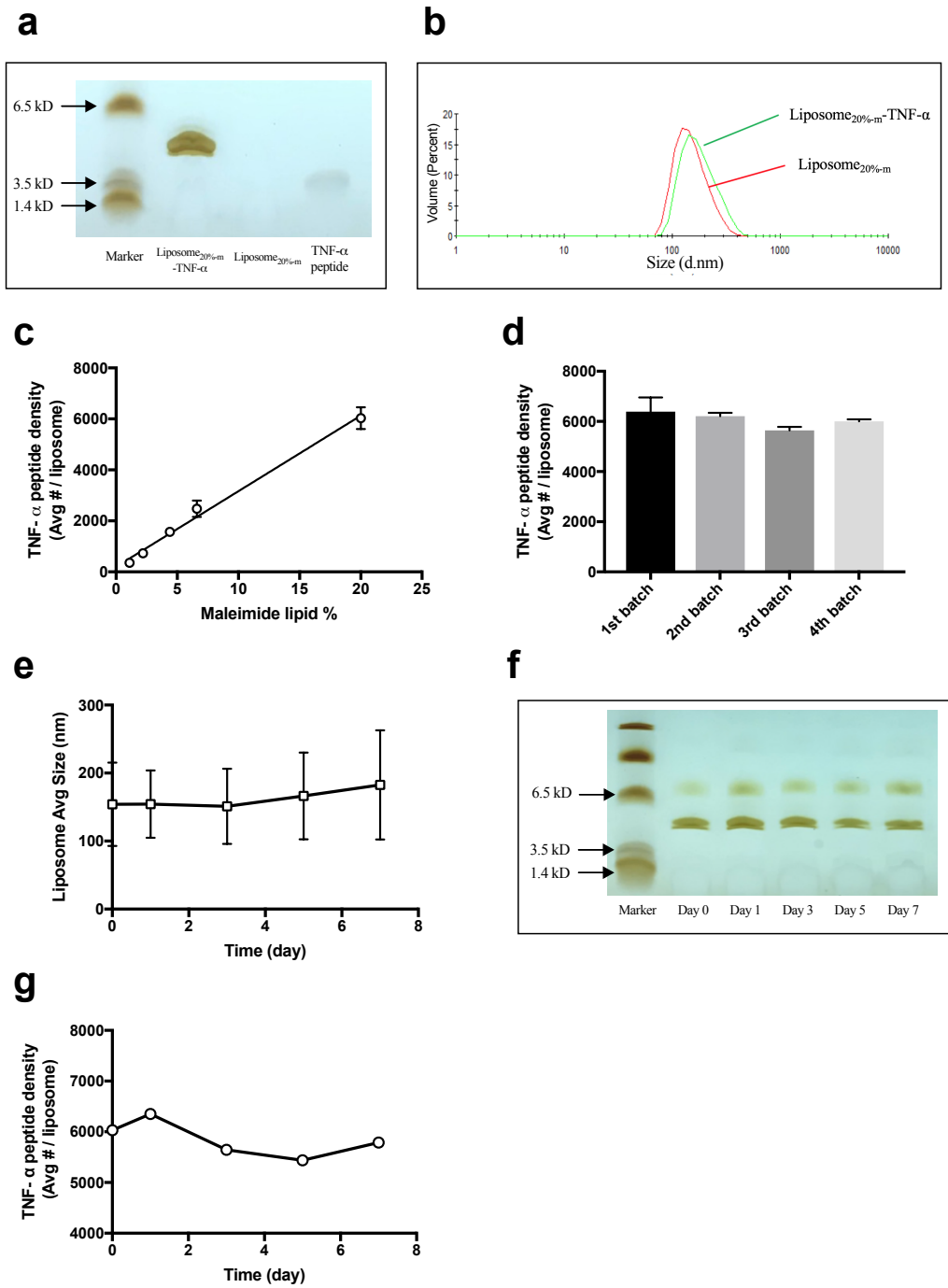
We then used p-VLP$_{Q\beta}$ to immunize the two lines of transgenic mice, following the schedules and doses that we did previously and collected sera at designated time points to measure antibody responses using ELISA. As shown in Fig. 3.8c, the IgG response from these animals has dropped substantially to a level that can be compared to that elicited by p-

liposome$_{20\%\text{-m}}$. This result demonstrates that the extraordinary immunogenicity of p-VLP$_{Q\beta}$ is almost entirely determined by the ability of these particles in recruiting T-cell help. To the best our knowledge, this is the first quantitative description on the molecular origin of the immunogenicity of these viral-like particles.

3.5. Acknowledgements

3.6. Figures:

a

b

c

d

e

f

g

Figure 3.1. Characterization of liposome$_{20\%\text{-m}}$ and liposome$_{20\%\text{-m}}$-TNF-α.

(a) Tricine-SDS-PAGE and silver staining result of samples: lane 1: protein marker (natural polypeptide SDS-PAGE standards, Bio-Rad, # 1610326); lane 2: 0.12 pmol liposome$_{20\%\text{-m}}$-TNF-α; lane 3: 0.12 pmol liposome$_{20\%\text{-m}}$; lane 4: 1 μg TNF- α- peptide. (b) Dynamic light scattering size analysis of liposome$_{20\%\text{-m}}$ and liposome$_{20\%\text{-m}}$-TNF- α. (c) Estimated number of TNF-α peptide per liposome is linearly correlated with maleimide percentage incorporated in liposome. Three independent batches of liposomes with various maleimide percentages 1.1%, 2.2%, 4.4%, 6.6% and 20% were produced and quantitated. (d) Average number of TNF-α peptide molecules per liposome for four batches of liposome$_{20\%\text{-m}}$ is estimated by Stewart lipid quantitation and BCA peptide quantitation. Error bars indicate the standard deviation drawn from two independent measurements for each batch of liposome. (e) Liposomes purified from size exclusion column after incubation with 50% fetal bovine serum for 1, 3, 5, and 7 days are measured for average size in nm by dynamic light scattering. (f) Tricine-SDS-PAGE and silver staining result of samples: lane 1: protein marker (polypeptide standards); lane 2-6: 0.05 pmol liposome$_{20\%\text{-m}}$-TNF- α (before FBS incubation, incubate with 50% FBS for 1 day, 3 days, 5 days and 7 days. (g) Estimated number of TNF-α peptide per liposome over a week of incubation with 50% FBS calculated by the band intensity of TNF-α peptide- lipid from Fig. 3.1f.
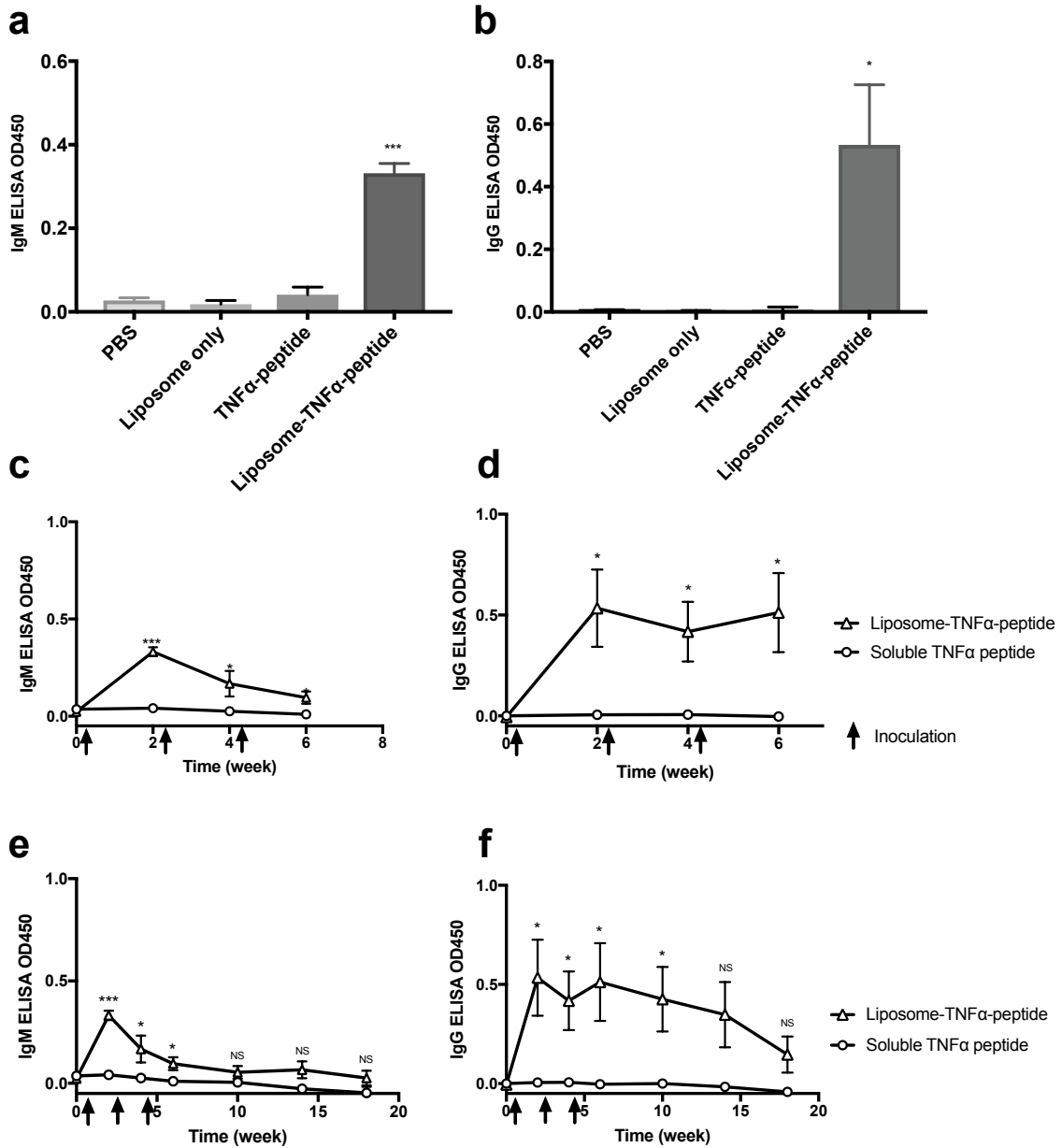
Figure 3.2. Anti-TNF-α-peptide antibody production in immunized mice.

(a-b) ELISA OD values for anti-TNF-α-peptide IgM (a) and IgG (b) antibody in mouse serum (1:100 dilution) after 1st immunization using PBS, liposome$_{20\%-m}$, TNF-α peptide (4.5 µg), and liposome$_{20\%-m}$-TNF-α peptide (4.5 µg peptide). (c-d) ELISA OD values for anti- TNF-α-peptide antibodies in mouse serum (1:100 dilution) during three inoculations using TNF-α peptide and liposome$_{20\%-m}$-TNF-α peptide. Blood serums were collected at week 2, week 4 and week 6, 11

days after each immunization. (e-f) ELISA results for anti-TNF-α-peptide antibodies in mouse serum (1:100 dilution) collected at week 10, week 14 and week 18. Each point presented in the figures represents the mean of OD450 values obtained from four mice of each group. Error bars represents the standard errors. Statistical difference between soluble TNF-α peptide and liposome-TNF-α peptide was determined by Student's T-test (***: p-value < 0.001; **: p-value < 0.01; *: p-value < 0.05; NS (Not Significant): p-value > 0.05).
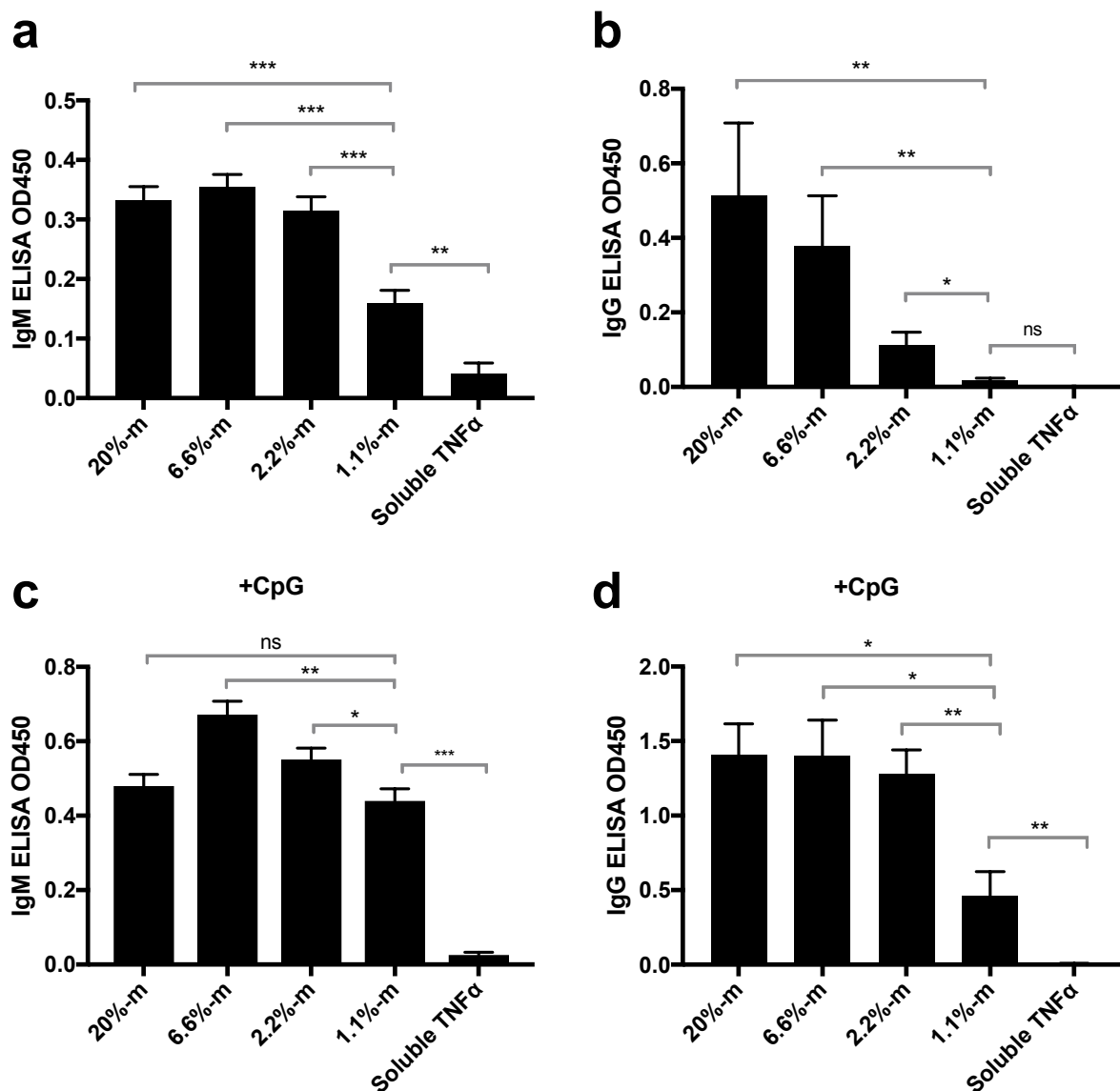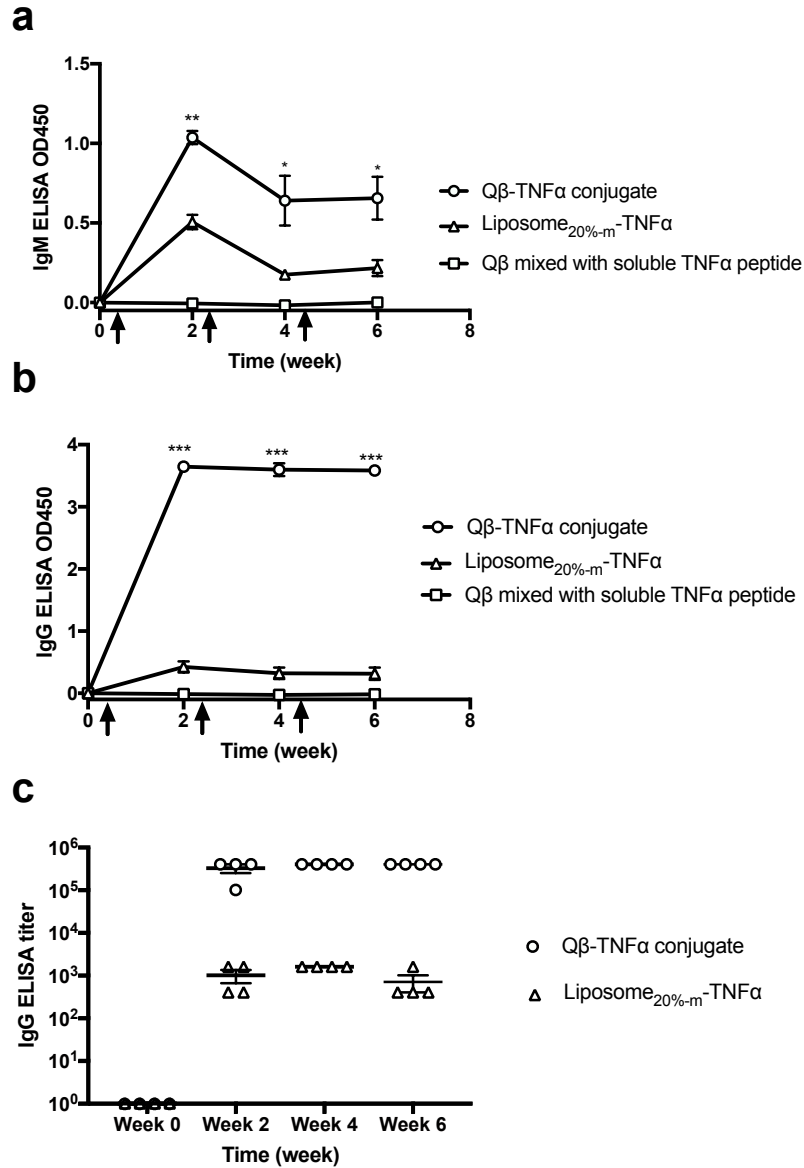
Figure 3.3. Anti-TNF-α-peptide antibody production in wild-type mice immunized with liposome-TNF-α of different peptide density (percentage of maleimide lipid in total lipids is indicated).

(a-b) ELISA OD values for anti-TNF-α-peptide IgM (a) and IgG (b) antibody in mouse serum (1:100 dilution) after 1st immunization using liposome-TNF-α of different TNF-α surface densities (same dose of 4.5 μg TNF-α peptide) and soluble TNF-α peptide. (c-d) ELISA OD values for anti-TNF-α-peptide IgM (a) and IgG (b) antibody in mouse serum (1:100 dilution) after 1st immunization using liposome-TNF-α of different TNF-α surface densities with CpG mixed before inoculation (same dose of 4.5 μg TNF-α peptide, 20 μg CpG) and soluble TNF-α peptide with CpG. In all the figures above, liposome$_{1.1\%-m}$-TNF-α peptide was used as a reference to determine statistical difference by Student's T-test.

a
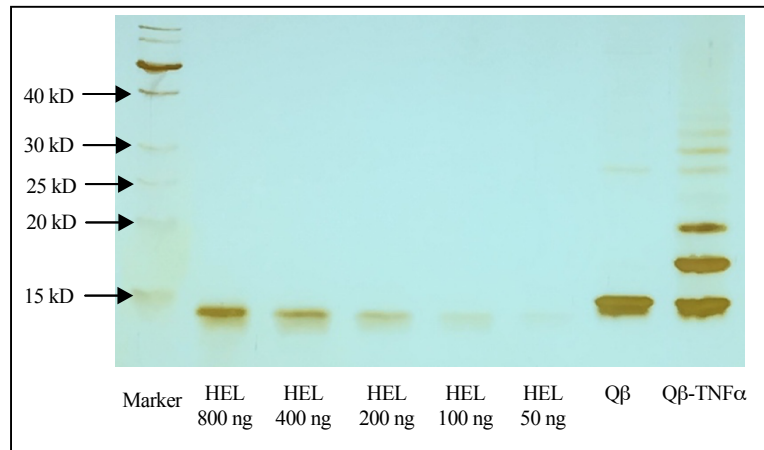
b
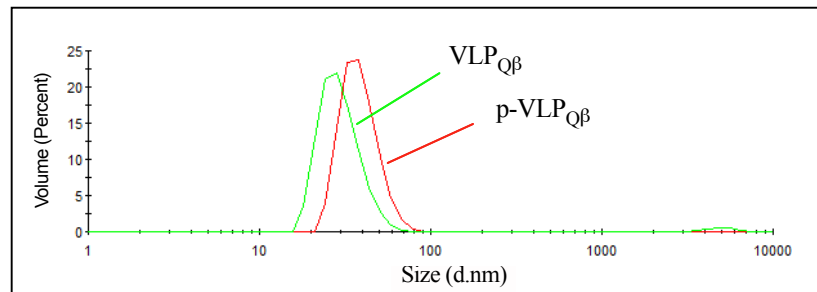

Figure 3.4. Characterization of Qβ and Qβ-TNF-α.

(a) Tricine-SDS-PAGE and silver staining result of samples: lane 1: protein marker (Thermal Scientific, Cat. 26614); lane 2-6: hen egg lysozyme, 14.5 kDa (800ng, 400ng, 200ng, 100ng, 50ng); lane 7: $VLP_{Qβ}$ (2 μg Qβ); lane 8: p-$VLP_{Qβ}$ (4 μg Qβ). (b) Dynamic light scattering size analysis of $VLP_{Qβ}$ and p-$VLP_{Qβ}$.

Figure 3.5. Anti-TNF-α-peptide antibody production in mice immunized with liposome-TNF-α and Qβ-TNF-α.

(a-b) ELISA OD values for anti-TNF-α-peptide IgM (a) and IgG (b) antibody in mouse serum (1:100 dilution) after three repeated inoculations using liposome-TNF-α of 20% maleimide lipid (4.5 μg TNF-α peptide) and Qβ-TNF-α (0.5 μg TNF-α peptide). Student's T-test was done for group Qβ-TNF-α comparing to liposome-TNF-α. (c) IgG titer was determined as the dilution factor of serum at the point when ELISA signal was still two folds more than the background average OD value. Each data point represents the IgG titer result of each individual mouse from immunization groups. Lines represents the mean of titers.
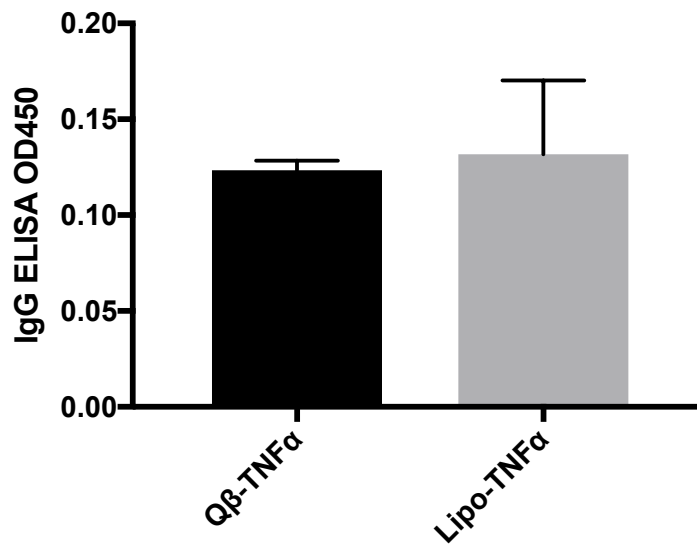
Figure 3.6. Comparison of ELISA OD values of specific IgG antibody using TNF-α-peptide or TNF-α-protein as coating substrate.

Mouse serum collected after 1st immunization of Qβ-TNF-α (0.5 µg TNF-α peptide) in 1:25600 dilution or 1st immunization of liposome$_{20\%-m}$-TNF- α-peptide (4.5 µg TNF-α peptide) in 1:100 dilution is used in ELISA with TNF-α protein (0.2 µg) coated in each well of ELISA plate.
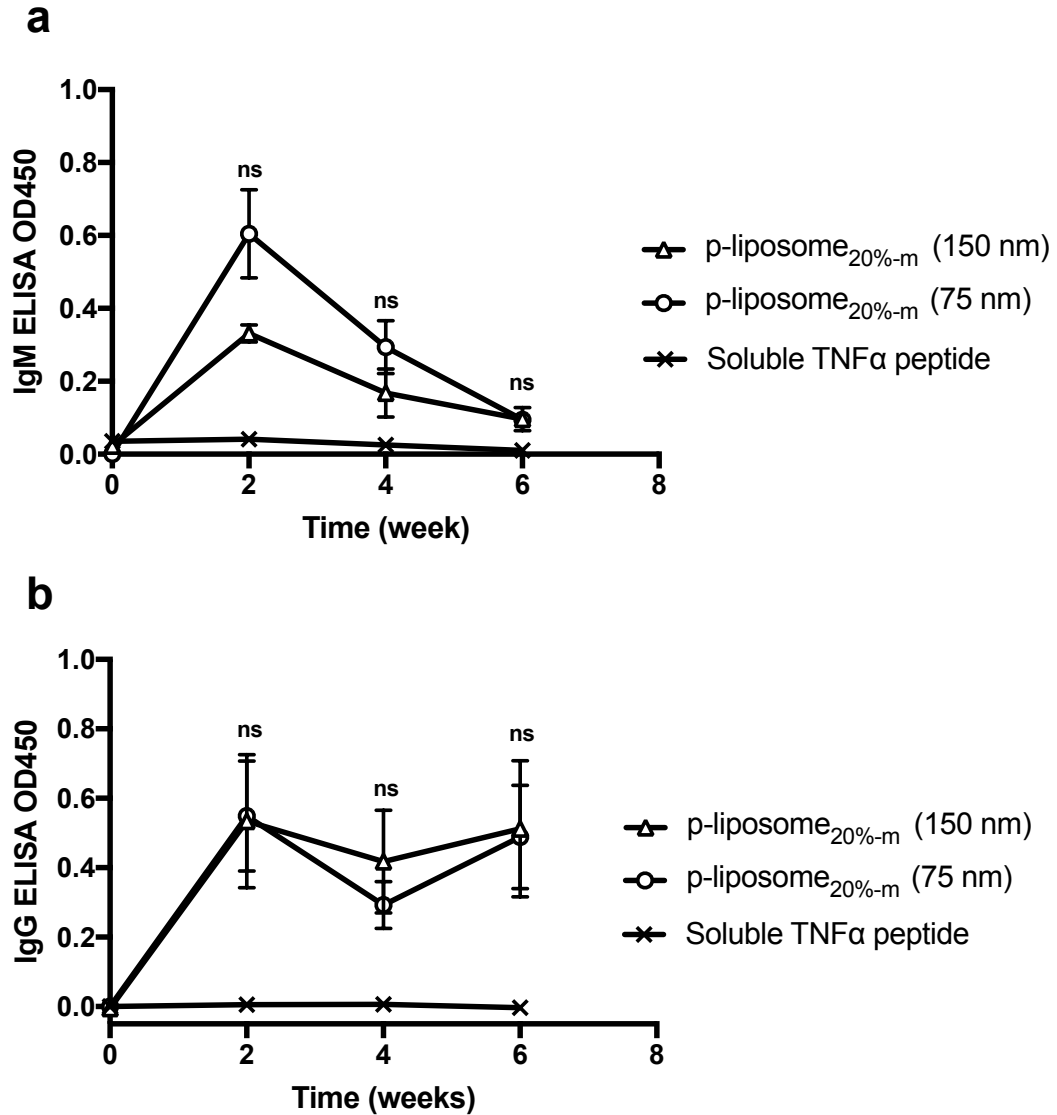
Figure 3.7. Anti-TNF-α-peptide antibody production in immunized mice.

ELISA OD values for anti- TNF-α-peptide antibodies IgM (a) and IgG (b) in mouse serum (1:100 dilution) during three inoculations using soluble TNF-α peptide, p-liposome$_{20\%-m}$ (D =75 nm) and p-liposome$_{20\%-m}$ (D= 150 nm). Blood serums were collected at week 2, week 4 and week 6, 11 days after each immunization.
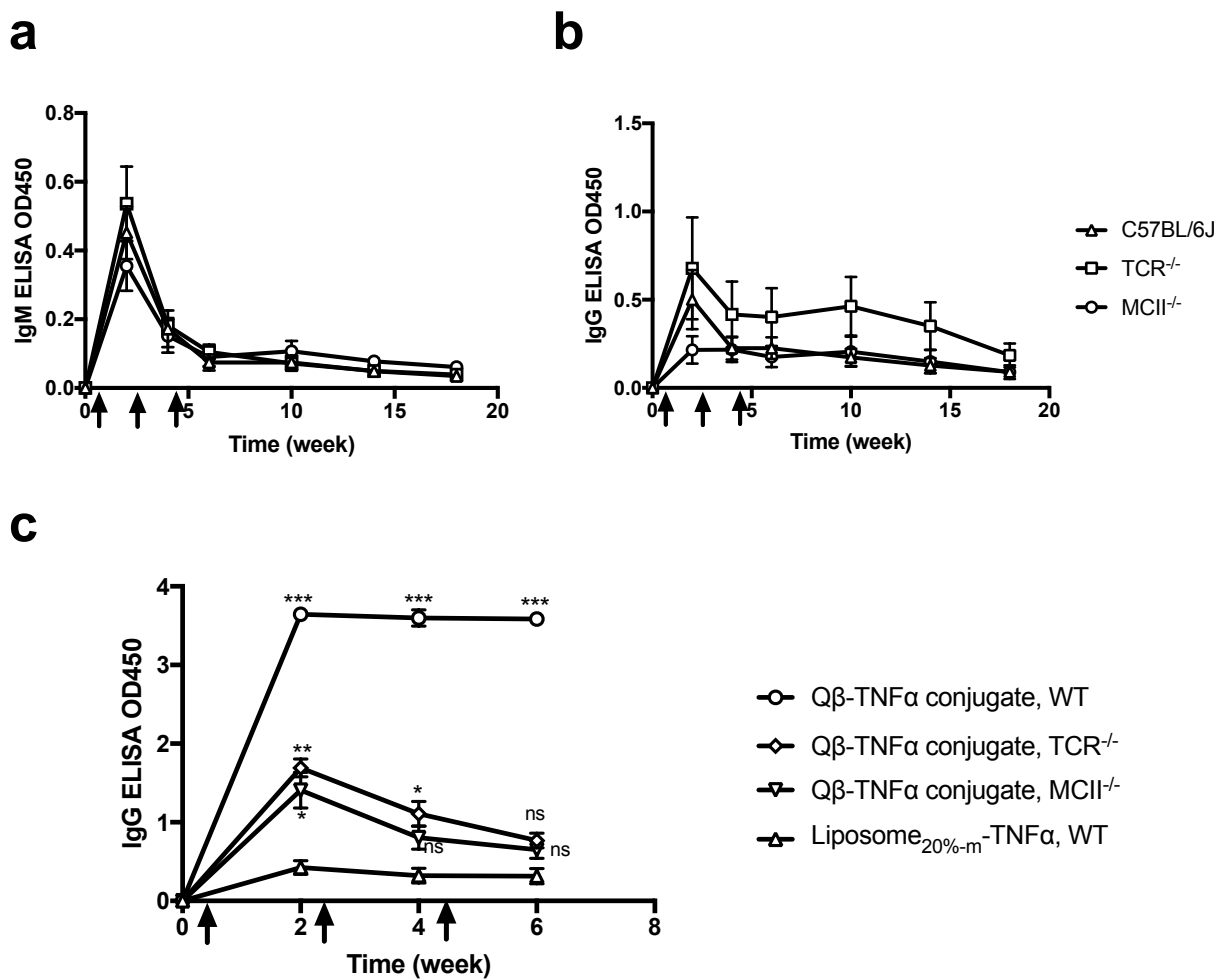
Figure 3.8. Anti-TNF-α-peptide antibody production in immunized T-deficient transgenic mice.

(a-b) Same dose (4.5 μg) of liposome-TNF-α peptide$_{20\%-m}$ was immunized to three groups of mice: wild-type mice (C57BL/6J), TCR deficient mice (TCR^{-/-}) and MHC Class II deficient mice (MCII^{-/-}). ELISA OD values for anti-TNF-α-peptide antibodies IgM (a) and IgG (b) in mouse serum (1:100 dilution), collected at week 2, 4, 6, 10, 14 and 18. (c) ELISA OD values for anti-TNF-α-peptide IgG antibody in mouse serum (1:100 dilution) after three repeated inoculations using liposome-TNF-α of 20% maleimide lipid (4.5 μg TNF-α peptide) and Qβ-TNF-α (0.5 μg TNF-α peptide) in WT mice, TCR^{-/-} mice, and MCII^{-/-} mice. Student's T-test was done for each group comparing to liposome-TNF-α in WT mice.
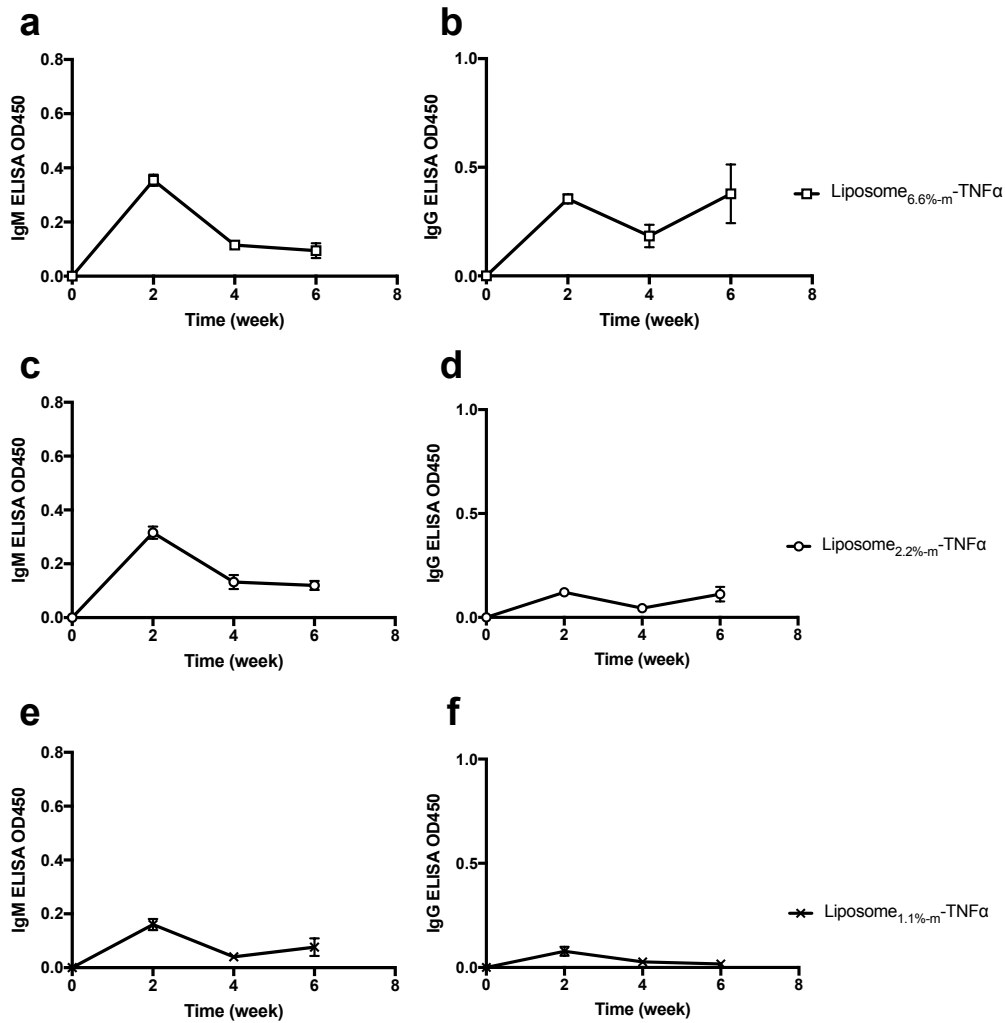
Figure 3.9. Anti-TNF-α-peptide antibody production in immunized mice by liposome-TNF-α peptide of different surface density from 6.6%-maleimide to 1.1%-maleimide.

(a-b) ELISA OD values for anti-TNF-α-peptide IgM (a) and IgG (b) antibody in mouse serum (1:100 dilution) after 3 immunization using liposome$_{6.6\%\text{-m}}$-TNF-α peptide (4.5 μg peptide). (c-d) ELISA OD values for anti-TNF-α-peptide IgM (c) and IgG (d) antibody in mouse serum (1:100 dilution) after 3 immunization using liposome$_{2.2\%\text{-m}}$-TNF-α peptide (4.5 μg peptide). (e-f) ELISA OD values for anti-TNF-α-peptide IgM (e) and IgG (f) antibody in mouse serum (1:100 dilution) after 3 immunization using liposome$_{1.1\%\text{-m}}$-TNF-α peptide (4.5 μg peptide).
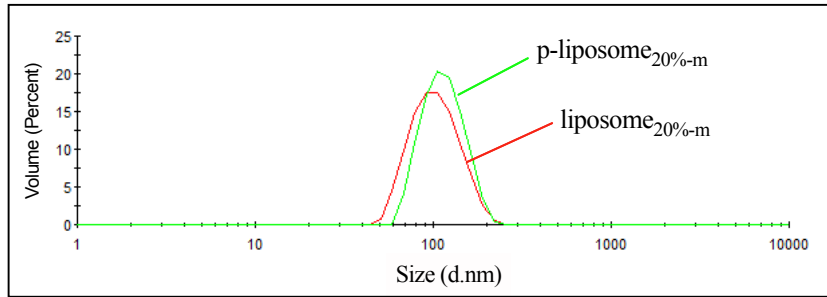
Figure 3.10. Characterization of liposome$_{20\%\text{-m}}$ and liposome$_{20\%\text{-m}}$-TNF-α of smaller size.

Dynamic light scattering size analysis of liposome$_{20\%\text{-m}}$ and liposome$_{20\%\text{-m}}$-TNF- α made with filter membrane of 50nm size.

3.7. References

1   Cheng, W. The Density Code for the Development of a Vaccine? *J Pharm Sci* **105**, 3223-3232, doi:10.1016/j.xphs.2016.07.020 (2016).

2   Bachmann, M. F. *et al.* The influence of antigen organization on B cell responsiveness. *Science* **262**, 1448-1451 (1993).

3   Chackerian, B., Lenz, P., Lowy, D. R. & Schiller, J. T. Determinants of autoantibody induction by conjugated papillomavirus virus-like particles. *J Immunol* **169**, 6120-6126 (2002).

4   Chackerian, B., Lowy, D. R. & Schiller, J. T. Induction of autoantibodies to mouse CCR5 with recombinant papillomavirus particles. *Proc Natl Acad Sci U S A* **96**, 2373-2378 (1999).

5   Chackerian, B., Lowy, D. R. & Schiller, J. T. Conjugation of a self-antigen to papillomavirus-like particles allows for efficient induction of protective autoantibodies. *J Clin Invest* **108**, 415-423, doi:10.1172/JCI11849 (2001).

6   Lechner, F. *et al.* Virus-like particles as a modular system for novel vaccines. *Intervirology* **45**, 212-217, doi:10.1159/000067912 (2002).

7   Chackerian, B. Virus-like particles: flexible platforms for vaccine development. *Expert Rev Vaccines* **6**, 381-390, doi:10.1586/14760584.6.3.381 (2007).

8   Cartwright, B., Smale, C. J., Brown, F. & Hull, R. Model for vesicular stomatitis virus. *J Virol* **10**, 256-260 (1972).

9   Baker, T. S. *et al.* Structures of bovine and human papillomaviruses. Analysis by cryoelectron microscopy and three-dimensional image reconstruction. *Biophys J* **60**, 1445-1456, doi:10.1016/S0006-3495(91)82181-6 (1991).

10   Desaymard, C. & Feldmann, M. Role of epitope density in the induction of immunity and tolerance with thymus-independent antigens. I. Studies with 2,4-dinitrophenyl conjugates *in vitro*. *Eur J Immunol* **5**, 537-541, doi:10.1002/eji.1830050806 (1975).

11   Desaymard, C. & Howard, J. G. Role of epitope density in the induction of immunity and tolerance with thymus-independent antigens. II. Studies with 2,4-dinitrophenyl conjugates *in vivo*. *Eur J Immunol* **5**, 541-545, doi:10.1002/eji.1830050807 (1975).

12   Turner, J. S., Marthi, M., Benet, Z. L. & Grigorova, I. Transiently antigen-primed B cells return to naive-like state in absence of T-cell help. *Nat Commun* **8**, 15072, doi:10.1038/ncomms15072 (2017).

13   Watson, D. S., Endsley, A. N. & Huang, L. Design considerations for liposomal vaccines: influence of formulation parameters on antibody and cell-mediated immune responses to liposome associated antigens. *Vaccine* **30**, 2256-2272, doi:10.1016/j.vaccine.2012.01.070 (2012).

14   Chen, Z., Moon, J. J. & Cheng, W. Quantitation and Stability of Protein Conjugation on Liposomes for Controlled Density of Surface Epitopes. *Bioconjug Chem* **29**, 1251-1260, doi:10.1021/acs.bioconjchem.8b00033 (2018).

15   Phelps, E. A. *et al.* Maleimide cross-linked bioactive PEG hydrogel exhibits improved reaction kinetics and cross-linking for cell encapsulation and in situ delivery. *Adv Mater* **24**, 64-70, 62, doi:10.1002/adma.201103574 (2012).

16   Stewart, J. C. Colorimetric determination of phospholipids with ammonium ferrothiocyanate. *Anal Biochem* **104**, 10-14 (1980).

17   Smith, P. K. *et al.* Measurement of protein using bicinchoninic acid. *Anal Biochem* **150**, 76-85 (1985).

18   Morton, R. E. & Evans, T. A. Modification of the bicinchoninic acid protein assay to eliminate lipid interference in determining lipoprotein protein content. *Anal Biochem* **204**, 332-334 (1992).

19   Mombaerts, P. *et al.* Mutations in T-cell antigen receptor genes alpha and beta block thymocyte development at different stages. *Nature* **360**, 225-231, doi:10.1038/360225a0 (1992).

20   Fikrig, E., Barthold, S. W., Chen, M., Chang, C. H. & Flavell, R. A. Protective antibodies develop, and murine Lyme arthritis regresses, in the absence of MHC class II and CD4+ T cells. *J Immunol* **159**, 5682-5686 (1997).

21   Taylor, K. M. G. & Morris, R. M. Thermal-Analysis of Phase-Transition Behavior in Liposomes. *Thermochim Acta* **248**, 289-301, doi:Doi 10.1016/0040-6031(94)01884-J (1995).

22   Banner, D. W. *et al.* Crystal structure of the soluble human 55 kd TNF receptor-human TNF beta complex: implications for TNF receptor activation. *Cell* **73**, 431-445 (1993).

23   Hu, S. *et al.* Comparison of the inhibition mechanisms of adalimumab and infliximab in treating tumor necrosis factor alpha-associated diseases from a molecular view. *J Biol Chem* **288**, 27059-27067, doi:10.1074/jbc.M113.491530 (2013).

24   Klibanov, A. L., Maruyama, K., Torchilin, V. P. & Huang, L. Amphipathic polyethyleneglycols effectively prolong the circulation time of liposomes. *FEBS Lett* **268**, 235-237 (1990).

25   Blume, G. & Cevc, G. Liposomes for the sustained drug release *in vivo*. *Biochim Biophys Acta* **1029**, 91-97 (1990).

26   Allen, T. M., Hansen, C., Martin, F., Redemann, C. & Yau-Young, A. Liposomes containing synthetic lipid derivatives of poly(ethylene glycol) show prolonged circulation half-lives *in vivo*. *Biochim Biophys Acta* **1066**, 29-36 (1991).

27   Maruyama, K. *et al.* Effect of molecular weight in amphipathic polyethyleneglycol on prolonging the circulation time of large unilamellar liposomes. *Chem Pharm Bull (Tokyo)* **39**, 1620-1622 (1991).

28   Senior, J., Delgado, C., Fisher, D., Tilcock, C. & Gregoriadis, G. Influence of surface hydrophilicity of liposomes on their interaction with plasma protein and clearance from the circulation: studies with poly(ethylene glycol)-coated vesicles. *Biochim Biophys Acta* **1062**, 77-82 (1991).

29   Sakaguchi, S., Yamaguchi, T., Nomura, T. & Ono, M. Regulatory T cells and immune tolerance. *Cell* **133**, 775-787, doi:S0092-8674(08)00624-7 [pii] 10.1016/j.cell.2008.05.009 (2008).

Chapter 4

Recombinant HIV-1 Gag Proteins Reversibly Assemble to Giant Spherical Particles Instead of Regular Virus-Like Particle

4.1. Abstract

HIV-1 Gag protein is the major structural protein for the assembly of virion particles, and it contains many CD4 T-cell epitopes. Although studies have been carried out using partially purified Gag proteins to build HIV virus-like particle, the outcomes of Gag assembly reaction remain controversial. Here we have developed an improved procedure for purification of several untagged retroviral Gag proteins from E. coli to more than 95% purity and characterized Gag assembly in solution. We found that HIV-1 Gag proteins can undergo nucleic acid-dependent aggregation with several unexpected features: (1) they form spherical particles that are as large as microns in diameter; (2) the size of the aggregates vary with the molar ratio between nucleic acids and proteins, with the average size of these particles reaching maximal at a molar ratio of 1:2 between nucleic acids and proteins; and (3) these particles can be efficiently disassembled

95

simply upon addition of excess nucleic acids into the solution, suggesting the presence of an ordered assembly. Single-stranded DNA oligos that are 10 nucleotides or shorter do not support the formation of these particles. Furthermore, the matrix domain of the Gag protein dramatically facilitates the formation of these aggregates. These studies uncover a previously uncharacterized pathway of HIV Gag assembly *in vitro* and have implications for HIV-1 Gag assembly and pathogenesis *in vivo*. However, the Gag assembly is not an ideal platform for construction of engineered nanoparticles with tailored densities, due to the size of aggregates and inclusion of nucleic acids during assembly.

4.2. Introduction

Our previous work demonstrated that VLPs can efficiently activate B cells and produce specific class-switched antibodies through a combination of high-density antigen display and strong T-cell epitope. Here, we aim to build HIV VLP with high-density display of HIV envelope protein for vaccine development. The HIV Gag protein is the major structural protein that is required for the assembly of HIV virions[1]. Moreover, it contains many CD4^{+} T cell epitopes in HIV[21,22], making it an ideal antigen carrier to elicit strong T-cell help.

The Gag protein, initially synthesized as a polyprotein precursor, is composed of four domains: the matrix (MA, or p17), the capsid (CA, or p24), the nucleocapsid (NC, or p7), and the C-terminal p6 domain[1, 2]. The overexpression of Gag protein alone in mammalian cells can produce VLPs that bud into the culture supernatant, even in the absence of cognate viral RNA genome, suggesting the promiscuity in the assembly process of HIV VLPs. Indeed, *in vitro*

studies using purified Gag proteins can initiate self-assembly of VLPs even with short DNA oligonucleotides[3].

Several investigators have carried out studies of VLP assembly using purified Gag proteins. Krausslich and coworkers showed that the N-terminal extension of the CA domain is critical for formation of spherical VLPs[4]. Absence of any N-terminal extension of CA promotes the formation of cylindrical particles. This result is consistent with the study by Vogt and coworkers, who showed that the purified recombinant protein containing the CA, NC and p6 domains of HIV-1 could form hollow, cylindrical particles in the presence of RNA, and the length of the particle depended on the type of RNA added[5]. Furthermore, the presence of SP1 peptide linker C-terminal to the CA domain may also act as a conformational switch, the presence of which promotes spherical particle formation[6]. However, the spherical particles formed by these purified Gag proteins, which were 90 nm in diameter, appeared to be in a dynamic equilibrium with aggregation, because all spheres were pelleted after centrifugation[6]. In an independent effort, Rein and coworkers reported that small spherical particles of 25-30 nm diameters can be assembled by purified Gag protein in the presence of nucleic acids[3]. Furthermore, addition of a second cofactor, inositol phosphates, is required for formation of VLPs that resemble authentic immature HIV-1 virions[7]. In contrast to these findings, Morikawa and coworkers showed that Gag protein can self-assemble in the absence of nucleic acids; VLPs that resembled authentic immature HIV-1 virions were formed at 37°C in the presence of Mg^{2+}, and addition of RNA facilitated this assembly process[8]. A detailed comparison of these assembly studies of HIV-1 Gag proteins is shown in Supplementary Table 1. Although there are clear differences in the quantitative features of these particles assembled, a common feature for most of these particles reported is their nanoscale, with diameters ranging from 20 to 100 nm.

These results suggest that the assembly of Gag proteins *in vitro* can achieve a point of cessation, at which the particles no longer 'grow' and have a well-defined size.

Here, using HIV Gag protein lacking only p6 domain (GagΔp6) and Gag protein lacking both p6 domain and a large portion of the MA domain (GagΔMAΔp6), we report that recombinant Gag proteins can form giant spherical particles (>1 μm in diameter) in the presence of nucleic acids, which is observed for both BH10 and NL4-3 Gag proteins. The assembly process required nucleic acids and the size of particles was dependent on the molar ratio between nucleic acids and proteins. Remarkably, this assembly process is reversible as addition of excess nucleic acids leads to the efficient disassembly of the already-formed spherical particles. When a large portion of the MA domain was deleted, the average size of the particles became smaller but micron-sized spherical particles were still observed, suggesting that the MA domain facilitates but is not required for the formation of these giant spherical particles. In contrast to the nanoscale particles reported previously in the literature, these studies thus reveal an unexpected feature of HIV Gag proteins assembly *in vitro* and support the presence of a dynamic equilibrium between particle assembly and disassembly.

4.3. Materials and Methods

DNA Constructs

Gag$_{BH10}$ full-length and GagΔp6 $_{BH10}$ DNA were amplified using HIV-1 BH10 genome (pBKBH10S DNA, NIH AIDS Reagent Program) as template and inserted into the prokaryotic expression vector pET21a by using restriction enzymes NdeI and XhoI. The 3' primer for

GagΔp6 DNA, with the following sequence

CGTACTCGAG**TTA**AAAATTCCCTGGCCTTCCCT, was designed to have a stop codon at the

end of SP2 domain so that the p6 domain is deleted upon expression. GagΔMAΔp6$_{BH10}$ DNA

was amplified by two-step PCR using pET21a- GagΔp6$_{BH10}$ as template, with two pairs of

primers designed to amplify the two portions of Gag DNA flanking the sequence that encodes

amino acids 16-99 in the matrix domain. After overlapping PCR extension, the product was cut

and ligated back to the same location in pET21a vector. NL4-3 GagΔp6 gene was amplified

using pGagMBPhis plasmid as template, a generous gift from Dr. James Hurley[1]. The same

strategy in using restriction enzymes and primers was employed to amplify GagΔp6$_{NL4-3}$ gene

and insert to pET21a expression vector. Rous sarcoma virus (RSV) Gag ΔMBDΔPR DNA in

pET3xc vector was generously provided by Dr. Volker Vogt[2]. All the DNA constructs were

sequenced and verified before protein expression and purification.

Gag Protein Expression and Purification

Purification of all Gag proteins were based on the published protocol from Rein et al[3] but

with important modifications. E. coli BL21DE3 competent cells (Invitrogen) were transfected

with expression vectors carrying the various Gag genes and cultured in LB media. Small scale

expression was first tested by inoculating a single colony from the plates of transfection to 5mL

LB media containing ampicillin overnight at 37°C with constant shaking at 250 rpm. The

overnight culture was used to inoculate 5mL fresh LB media at a ratio of 1:100, and the

inoculum was cultured for 2-3 hours until the optical density at 600 nm (OD$_{600nm}$) was at 0.6 -

0.8. The expression of the recombinant proteins was induced by the addition of isopropyl-beta-

D-thiogalactopyranoside (IPTG) to a final concentration of 0.5mM at 37°C. The expression of

the protein was quantitated at different time points after induction by running SDS-PAGE and Western blotting.

Large scale expression was conducted by inoculating a single colony into 50mL LB media and cultured overnight. 60mL of the overnight culture was then transferred to 3L fresh LB media and shaken until OD_{600} reached to 0.6-0.8. Protein expression was induced with addition of 0.5 mM IPTG, and the cells were grown for four more hours at 37°C. Bacteria were then harvested by centrifuge at 6,000 g for 7 minutes, and the pellet was stored at -80°C. For protein purification, the entire procedure was conducted at 4ºC unless otherwise noted. The cell pellet was first thawed and resuspended in 10-ml lysis buffer per gram of pellet (20mM Tris-HCl pH 7.4 at 21°C, 0.75M NaCl, 10% w/v glycerol, 10mM β-mercaptoethanol) that was supplemented with 1mM phenylmethyl sulfonyl fluoride (PMSF), and 0.5 mg/mL egg white lysozyme. The cell suspension was gently rocked for 1 hour at 4°C followed by sonication. The cell lysate was centrifuged at 12,000 g for 30 minutes to clear the supernatant. Polyethylenimine (PEI) was then added to the cleared cell lysate in a dropwise manner to a final concentration of 0.2% w/v, which was to precipitate the nucleic acids. The supernatant from PEI treatment was then treated with ammonium sulfate to 233 g/L to precipitate Gag protein. The protein pellet was resuspended using buffer D (20 mM Tris-HCl pH 7.4 at 21°C, 0.5M NaCl, 1 mM PMSF, 10 mM β-mercaptoethanol), and further centrifuged at 12,000 g for 15 mins to remove any undissolved pellet before the next step.

Cellulose phosphate resin (PC resin, fine mesh, Sigma) was treated with 0.5 M NaOH, 0.5 M HCl, 0.2 M Tris·HCl, pH7.4, and buffer A (20 mM Tris·HCl, pH7.4 at 21°C) sequentially before use. The supernatant from the re-dissolved protein solution was decanted to a 50-mL

polypropylene tube and 10 ml pre-treated PC resin was added. The tube was gently rocked at 4°C for 1 hr to allow the Gag protein binding to the PC resin. After binding, the PC resin was sequentially washed with buffer A containing 0.1 M, 0.2 M, and 0.5M NaCl respectively. The protein was then eluted with the same buffer containing 1M NaCl for three times, each time with gentle rocking for 1hr. The protein elution was combined, and anhydrous ammonium sulfate was added to reach to a final concentration of 423 g/L. The protein pellet was resuspended using buffer D followed by centrifugation to remove any particulates.

To improve the purity of Gag proteins, we added one more step of purification after the cation exchange using PC resin. An HiTrap heparin HP column (1 mL, GE) were mounted onto Bio-Rad DuoFlow system and equilibrated in buffer A containing 0.1M NaCl. The resuspended protein solution after the second ammonium sulfate precipitation was diluted with buffer A to lower the salt concentration to ~0.1 M, and then loaded onto the heparin column. After loading, the heparin column was first washed using buffer A containing 0.5 M NaCl. During this step, the majority of unwanted proteins as well as some GagΔp6 proteins were eluted. We then applied buffer A containing 0.75 M NaCl to the column, during which the majority of GagΔp6 proteins was eluted off the column. In contrast to either GagΔp6$_{BH10}$ or GagΔp6$_{NL4-3}$, HIV GagΔp6ΔMA and RSV Gag ΔMBDΔPR were both eluted off the heparin column in buffer A containing 0.35 M NaCl, suggesting their weaker affinities towards polyanions. The various Gag proteins eluted off the heparin column were all dialyzed into Buffer D containing 10% w/v glycerol, concentrated to about 5 mg/mL using protein concentrator (3kD molecular weight cutoff, Thermo Scientific), flash frozen and stored at -80°C. All protein concentrations were determined by UV spectrometry using extinction coefficient for each protein predicted at 280 nm based on amino acid sequence [20] (GagΔp6 62045 $M^{-1}cm^{-1}$, GagΔp6ΔMA 47940 $M^{-1}cm^{-1}$, and

RSV Gag ΔMBDΔPR 49680 $M^{-1}cm^{-1}$). Throughout, 12% SDS-PAGE gel with 0.1% SDS final concentration was used for assessment of protein purification. All protein samples were incubated with 2× Laemmlli sample buffer and heated to 95°C for 5 mins before loading onto gels. Protein bands were stained with Coomassie Brilliant Blue or silver nitrate[4]. The primary antibody used in Western blotting was mouse anti-p24 (cat#3537, NIH AIDS reagent) and the secondary antibody was anti-mouse alkaline phosphatase conjugated secondary antibody (Sigma) diluted at 1: 10,000.

In vitro Assembly Reaction

Protein stock solutions were thawed on ice and slowly diluted to 0.1 M NaCl with buffer F (20 mM Tris pH 8.0 at 21°C, 10 mM β-mercaptoethanol). Nucleic acids were added right after the dilution and the solution mixed thoroughly by gentle pipetting. The nucleic acids included in the study were yeast tRNA (phenylalanine specific from brewer's yeast, Sigma), 20mer-Cy3, a 20-mer DNA (GTGGTGTCAATTACGGTAGC) with a Cy3 fluorophore conjugated to its 3' end, oligo thymidylate of various lengths (IDT), and dNTP (NEB). The assembly reaction was incubated at room temperature for five minutes before examination by fluorescence microscopy or applied to grids for electron microscopy.

Electron Microscopic Examination

For the negative staining of the Gag assembly product, 5 μL of the assembly reaction was applied to carbon-coated grid (mesh size 50, Electron Microscopy Sciences), and drained with a filter paper after 5 minutes. 5 μL of 5% uranyl acetate was then applied to the grid and wiped off

with filter paper after 5 minutes. After air-drying for 5 mins, the grids containing assembly samples were ready to be imaged using a JEOL 1400-plus transmission electron microscope.

Flow Cytometry

The flow cytometry experiments were conducted using a Miltenyi MACSQuant VYB digital benchtop flow cytometer. After the assembly or disassembly reaction was initiated, at designated time as indicated in the figure legends, the suspensions of particles were directly loaded onto the flow cytometer without any additional treatment. Both forward and side scattered light at 561 nm were monitored using 561/10 nm band-pass filters.

4.4. Results and Discussion

Improvements in Purification of Retroviral Gag Proteins Expressed in E. coli.

Purification of recombinant HIV-1 Gag proteins that carry hexahistidine tags using Ni-NTA affinity column have been reported in literature[8, 9]. However, because hexhistidine tag influences the activity of nucleic acid binding proteins[10], we have started by preparing full-length HIV-1 Gag proteins without any affinity tags from both BH10 and NL4-3 strains, the two different isolates of HIV that have been studied in literature for Gag assembly *in vitro* (Table 4.1). Excluding the p6 domain, the sequence identity between these two versions of Gag protein is 96%. Consistent with literature report[3], the full-length Gag proteins showed significant degradation in *E. coli* upon their overexpression (Fig. 4.1A). To improve the yield of protein for the ease of purification, we have thus constructed overexpression plasmids for both strains in

which the p6 domain of Gag has been deleted (GagΔP6). The p6 domain of HIV-1 Gag protein

is not required for particle assembly in cultured cells but is required for budding of the assembled

particles from plasma membrane to extracellular milieu[1, 11, 12]. The GagΔp6 protein was reported

to have much less degradation issues when purified from E. coli[3]. Indeed, upon induction by

addition of IPTG, the GagΔp6 proteins accumulated to significant levels with less degradation

compared to that of the full-length Gag protein (Fig. 4.1A), which provided good starting

materials for subsequent protein purification. Rein and coworkers have published procedures for

purification of recombinant HIV-1 Gag proteins that do not carry any affinity tags[3, 13]. The

major purification steps in the published procedures involve fractionation through ammonium

sulfate precipitation of the cell lysate and cation exchange column using phosphate cellulose

resin. We have followed these steps, but with two major modifications for the purification

procedure described as follows.

First, we added a polyethylenimine (PEI) step before ammonium sulfate precipitation of

the cleared cell lysate. PEI has been frequently used in the fractionation and purification of

nucleic acids binding proteins [14], which can effectively remove nucleic acids that may present as

a contaminant in the final purified proteins. After we cleared the total cell lysate by

centrifugation, we added PEI to the supernatant at a final concentration of 0.2% w/v. Titration of

PEI concentration in the cell lysate indicated that this concentration was sufficient to precipitate

the bulk of nucleic acids in the cell lysate without precipitating the majority of the Gag proteins.

After centrifugation to remove the PEI-nucleic acids pellet, the supernatant was then subjected to

ammonium sulfate fractionation. This PEI step worked very well. As shown in Fig. 4.1B for the

purification of GagΔp6 from HIV isolate BH10 (GagΔp6$_{BH10}$), majority of the GagΔp6 protein

was retained in the supernatant after PEI precipitation (Lane 3). Moreover, majority of GagΔp6

protein was recovered back into the solution after precipitation using ammonium sulfate (Lane 4).

Second, we added a heparin column step after the phosphocellulose cation exchange column to further improve the purity of the protein. This step is necessary because we found that a major impurity was still present in the eluted protein from the cation exchanger using phosphocellulose. This impurity was a protein that was slightly smaller than the Gag protein. The Western blotting using anti-p24 monoclonal antibody revealed that the impurity also reacted positively with this antibody, suggesting that the impurity was a degradation product from the Gag protein. Heparin column was then utilized to separate the main protein from the degraded product. Gag protein of interest can be separated from the degradation product using concentration gradient of NaCl on the heparin column. As a result, the purity of the final GagΔp6 protein was over 95% as determined using SDS-PAGE and Coomassie brilliant blue staining (Fig. 4.1C). Using this modified purification protocol, we were able to purify additional Gag proteins studied in this work, all to greater than 95% purity (Materials and Methods). These include GagΔp6 protein from HIV isolate NL4-3, GagΔp6$_{NL4-3}$, GagΔMAΔp6$_{BH10}$ (Gag protein lacking both p6 domain and amino acid 16-99 of the matrix domain[6]) (Fig. 1 D,E), and a truncated version of the Rous sarcoma virus (RSV) Gag protein (AA85-577, RSV GagΔMBDΔPR) (Fig. 1F).

In vitro Assembly Properties of HIV-1 GagΔp6 Protein

To test the assembly of purified GagΔp6 $_{BH10}$ protein, we diluted the protein into the assembly buffer to reach 0.1 M NaCl at room temperature. Upon addition of yeast tRNA into

the diluted protein solution, the mixture immediately turned turbid. In contrast, control in the absence of nucleic acids remained clear (Fig. 4.2A upper right). To examine the assembly species formed upon addition of nucleic acids, we applied 5 µl of the turbid suspension on top of a clean coverslip and observed the sample under bright field in an optical microscope. Spherical particles of heterogeneous size, with diameters in the range of 1-10 µm were clearly observed, as shown for GagΔp6$_{BH10}$ in Fig. 4.2A. To better evaluate the properties of the assembled particles, we designed a short DNA oligomer of 20 nucleotides labeled with a single Cy3 fluorophore at its 3' end (20mer-Cy3). When this DNA oligo was added to the diluted GagΔP6 protein solution to initiate the assembly reaction, spherical particles of heterogeneous size, similar to those formed upon addition of yeast tRNA, were also observed under microscope (Fig. 4.2B). Moreover, these particles were fluorescent, as shown by a fluorescence image collected through Cy3 emission channel (Fig. 4.2C). The fluorescence image could be overlaid very well with its bright field image, indicating that all the particles formed under this condition contained 20mer-Cy3 inside (Fig. 4.2D). Throughout, the assembly experiments were done in parallel for GagΔp6 from BH10 and NL4-3, and no significant differences in the assembly behaviors were observed between the two GagΔp6 proteins.

To examine the spherical particles formed under these conditions more closely, we next employed transmission electron microscopy (TEM) to image these samples. As shown in Fig. 4.3A, large, spherical particles with diameter ranging from 1µm to 10 µm were easily identified on the grid with negatively stained samples. Interestingly, many particles showed additional features on their surfaces. These surface features are highlighted in Fig. 4.3B under a higher magnification. There were many needle-like thin structures about 100-200 nm in length that

106

protruded from the surface of these particles (Fig. 4.3B). Again, GagΔp6 proteins from NL4-3 and BH10 formed very similar particles under same assembly conditions.

The fact that no spherical particles were formed by the same protein upon dilution without adding nucleic acids indicates that the formation of these particles required nucleic acids. To gain more mechanistic information about formation of these giant spherical particles, we next analyzed the role of nucleic acids by systematically varying the molar ratio between nucleic acids and protein, and then examine the size and quantity of particles formed using fluorescence microscopy. In these experiments, the 20mer-Cy3 DNA and GagΔp6$_{NL4-3}$ was used throughout. We noticed that when the molar ratio of nucleic acids to protein was below certain threshold (1/32), no particles were observed, clearly indicating the requirement of nucleic acids for this assembly process to occur. As we further increased the amount of DNA included in the assembly reaction, particles started to form. Both the average number of particles formed per field of view and the average particle size increased with increasing nucleic acids. The average particle size reached a maximum at a molar ratio of 1:2 between the nucleic acid and the protein. Further increase in nucleic acids leads to less particles formed and also smaller size of spherical particles. The details of these results are summarized in Table 4.2A.

Limited by the stock concentration of the 20mer-Cy3 DNA, we were not able to increase the ratio of DNA/protein beyond 1:1 for the experiments in Table 4.2A. However, the decrease in particle assembly with increasing DNA upon a defined molar ratio between the DNA and the protein suggests that the self-assembly process may be reversible. To further examine this dependence quantitatively, we have used an oligo thymidylate, $(dT)_{30}$, to repeat the experiment. For this set of experiments, we were able to titrate nucleic acids well above the moles of proteins

so to examine a wider range of nucleic acids to protein ratios. As summarized in Table 4.2B, the threshold behavior of self-assembly was again observed. The particles started to form only when the molar ratio of nucleic acids to protein was at 1/45 or higher. Average size of the particles reached a maximum at a ratio of 1:2. As we further increased concentration of $(dT)_{30}$, to more than two folds of GagΔp6 protein, particle assembly disappeared. No visible particles were formed at even higher concentrations of $(dT)_{30}$ tested as examined under microscope. This quantitative dependence of self-assembly on nucleic acids, where a peak in the assembly reaction occurs at a certain ratio of nucleic acids to protein, indicates that the self-assembly process is reversible. To further test this phenomenon, we first added 20mer-Cy3 to diluted GagΔp6$_{BH10}$ at a molar ratio of 1:2, where the peak of assembly occurs (Table 4.2A). As expected, the sample quickly turned turbid after the addition of 20mer-Cy3. After 5 minutes, we then added additional $(dT)_{30}$ to a molar ratio of 8:1, and interestingly, the turbidity quickly disappeared after the addition of excess $(dT)_{30}$. As shown by both light microscopy and fluorescence microscopy, the majority of large particles formed by GagΔp6 and 20mer-Cy3 20mer disappeared after addition of $(dT)_{30}$ (Fig. 4.4 A, B). This process can also be monitored using flow cytometry. As shown in Fig. 4.4C, the addition of 20mer-Cy3 to the diluted GagΔp6$_{BH10}$ at a molar ratio of 1:2 yielded a large number of heterogeneous particles, indicated by the total forward scattered light (FSC-A). However, upon further addition of excess $(dT)_{30}$, majority of the large particles has disappeared (Fig. 4.4D). As a control, GagΔp6$_{BH10}$ diluted in buffer F in the absence of nucleic acids did not produce any significant particles. The fact that the particle assembly can be reversed by addition of excess nucleic acids suggests that the formation of these giant spherical particles is in a dynamic equilibrium with particle disassembly. This phenomenon is very different from what have been reported previously in literature for the assembly of Gag proteins *in vitro* (Table 4.1), where nanoscale particles with sizes ranging from 20 to 100 nm in diameters were observed.

There are three major differences: (1) these particles are microns in size, and have a regular spherical shape, which distinguish them from irregular or amorphous aggregates reported previously[4, 6, 15]; (2) the size of the particles varies with the molar ratio between nucleic acids and the proteins, and (3) the particles can be disassembled upon addition of excess nucleic acids. Neither (2) nor (3) has been reported previously. The peak assembly occurs at a molar ratio of 1:2 between nucleic acids and proteins, which further suggests an ordered assembly of Gag proteins in the presence of nucleic acids, in contrast to the formation of unstructured protein aggregates.

The threshold dependence of this self-assembly was also observed for yeast tRNA (Table 4.2C). Furthermore, the addition of dNTP instead of nucleic acids did not result in any assembly of the particles, despite the various concentrations we have tested. This result suggests that a nucleic acid molecule of a minimum length is required to initiate the assembly reaction. To further probe this potential dependence of the assembly reaction on the lengths of the nucleic acids molecules, we have tested oligo thymidylate of various lengths, ranging from $(dT)_5$ to $(dT)_{20}$. The results are summarized in Table 4.2D, for $(dT)_5$ and $(dT)_{10}$, no particles were formed regardless of their concentrations used, tested at three different ratios of nucleic acids to protein (1:25, 1:5, and 1:1). In contrast, particles of similar morphology could be observed for oligo thymidylates that are 12 nucleotides or longer. Early studies demonstrated that the minimum length of nucleic acids required to stably bind to the NC domain of HIV-1 Gag protein was 5 nucleotides[16]. The fact that $(dT)_5$ is inadequate to promote the self-assembly of GagΔp6 indicates that binding to nucleic acids by the NC domain is not sufficient to induce the assembly of these giant particles, additional nucleotides in the nucleic acid molecules are required.

In vitro Assembly of HIV-1 GagΔMAΔp6 Protein

Previously, the MA domain was also reported to recognize viral genome RNA although the affinity of the MA domain towards nucleic acids may be weaker than that of the NC domain[17] and this MA-RNA interaction could be abolished by the substitution of more than two basic residues[18]. To determine the role of MA domain in the formation of these giant spherical particles, we next constructed a mutant for BH10 Gag protein. In addition to the deletion of the p6 domain, a large portion of the MA domain, which corresponds to amino acids 16 to 99 in Gag, was also deleted, resulting in GagΔMAΔp6$_{BH10}$. Previously, it was reported that this large truncation in the MA domain changed the site of virus budding from plasma membrane to endoplasmic reticulum, but the morphology of resulting virions remains largely unchanged[19]. *In vitro* assembly of the purified mutant Gag protein that carries this truncation in the MA domain and the p6 deletion yielded both regular spherical particles with external diameter of 90 nm and amorphous protein aggregates[6]. Furthermore, these 90-nm particles did not appear to be stable, because all these particles were found in the pellet after centrifugation in a microcentrifuge, suggesting that these particles are in dynamic equilibria with protein aggregation, or alternatively, these particles can grow bigger with time.

Using the procedures that we have developed for GagΔp6, we were able to purify GagΔMAΔp6$_{BH10}$ to more than 95% purity (Fig. 4.1E, Materials and Methods). To induce the assembly of this mutant Gag protein, we followed the same procedures for GagΔp6. The stock protein solution was first diluted into buffer F, followed by addition of the 20mer-Cy3. As shown in Fig. 4.5 A-B, GagΔMAΔp6$_{BH10}$ assembled into particles that are visible under an optical microscope. However, these particles are visually two to three times smaller in size

compared to those particles formed with GagΔp6 (Fig. 4.4 A-B). Furthermore, after

centrifugation at 17,000 g for 5 minutes, majorities of the particles were centrifuged to form the

pellet but leaving submicron particles in the supernatant. These submicron particles left in the

supernatant could be clearly visualized under fluorescence microscope, although not by the

bright field microscope (Fig. 4.5 C-D). In contrast, all the giant particles formed by GagΔp6

protein were pelleted after centrifugation at 17,000 g for 5 minutes (data not shown). These

results suggest that the MA domain facilitates the formation of these giant particles. Deletion of

amino acids 16 to 99 of the MA domain does not prevent the formation of particles larger than 1

μm in diameter. However, the kinetics for formation of these particles is likely to be slowed

down significantly, given the presence of submicron particles that we could clearly observe

under a fluorescence microscope.

The smaller particles formed by GagΔMAΔp6$_{BH10}$, compared to GagΔp6$_{BH10}$, can also be

shown using agarose gel. As shown in Fig. 4.6A, after addition of 20mer-Cy3 to initiate the

assembly of both proteins, we loaded these protein-nucleic acid mixtures into a native 0.3%

agarose gel, and the migration of different species were visualized using a Typhoon imager for

Cy3 fluorescence. For GagΔp6$_{BH10}$, in addition to the band that corresponded to free DNA, there

was a major band that had slowly migrated into the gel, which likely correspond to the giant

spherical particles observed under optical microscope. In contrast, for GagΔMAΔp6$_{BH10}$, there

was a major band that migrated further down into the gel compared to that of GagΔp6$_{BH10}$,

suggesting that these particles were indeed smaller. Furthermore, the Cy3 bands were smearing

across the entire gel bed, consistent with even smaller particles that can be formed by these

proteins. Moreover, there were also stains upstream of the sample loading well, suggesting that

some of the protein-DNA complexes actually carried overall positive charges and thus migrated

towards opposite direction. Lastly, the particles formed by GagΔp6$_{BH10}$ and GagΔMAΔp6$_{BH10}$ can also be compared using flow cytometry (Fig. 4.6 B, C). The number of large particles formed by GagΔp6, with a FCS-A value of higher than 1k, was much more than that of GagΔMAΔp6, indicating that GagΔp6 formed bigger particles than GagΔMAΔp6 under the same assembly conditions. As a control, GagΔMAΔp6$_{BH10}$ diluted in buffer F in the absence of nucleic acids did not produce any significant particles.

A major difference between current and previous studies is our use of PEI for precipitation of nucleic acids before fractionation and purification of various Gag proteins. To assess whether the use of PEI may have caused the inadvertent formation of these giant spherical particles through yet unidentified mechanisms, we have purified RSV GagΔMBDΔPR using the very same procedure for HIV Gag and studied its assembly properties as a control. The RSV GagΔMBDΔPR shares similarities to HIV-1 GagΔMAΔp6 in domain structures but very low primary sequence identity. This protein was purified to greater than 95% purity (Fig. 4.1F), and we initiated the assembly reaction in the same manner as various HIV-1 Gag proteins. As shown in Fig. 4.7A, RSV GagΔMBDΔPR formed relatively homogenous virus-like particles as seen under TEM. The diameters of these particles ranged from 70 to 80 nm in general (Fig. 4.7B), consistent with previous literature report[25]. In contrast, those submicron particles formed by GagΔMAΔp6 (present in the supernatant after centrifugation) showed up as heterogeneous spherical particles, with size ranging from 50 nm to 1 μm in diameter (Fig. 4.7 C, D). These results demonstrate that the use of PEI is not the cause for the formation of giant spherical particles. Rather, the biochemical and biophysical properties of HIV-1 Gag protein give rise to the distinct features of the particles formed from this assembly process *in vitro*.

Our results for both GagΔp6 and GagΔMAΔp6 suggest that the self-assembly of GagΔp6 proteins *in vitro* can form giant spherical particles larger than 1 μm in diameter. These particles can be disassembled by addition of excess nucleic acids. The MA domain facilitates the assembly of these giant particles. None of these results have been reported previously. Moreover, the current results may also reconcile some observations in literature. First, our results on GagΔMAΔp6 are qualitatively consistent with Gross et al.[6]. They showed that the purified GagΔMAΔp6 proteins are capable of forming spherical particles of 90 nm in diameter, which are close to native HIV virions in size, but these particles are in dynamic equilibria with either protein aggregation or formation of even larger particles, so that they can be pelleted out of the solution. Second, Campbell and Rein showed previously that GagΔp6BH10 forms spherical particles of 25-30 nm diameter in the presence of nucleic acid[3]. As they pointed out in the paper, the GagΔp6BH10 solution quickly became turbid upon addition of nucleic acids, and "the turbidity settled to the bottom of the tube within a few hours". These biophysical features actually indicate that large particles already formed in their assembly reaction, because a suspension of proteinaceous particles of 25-30 nm diameter would not be visually turbid at 1 mg/ml concentration nor would it sediment just by gravity to the bottom of the tube within a few hours. Thus, current results might have been observed previously although left uncharacterized or quantitated. Our results uncover a novel aspect of HIV Gag protein assembly *in vitro*, which is the dynamic equilibrium between particle assembly and disassembly. Future studies remain necessary in order to identify the conditions for the formation of nanoscale particles in the range of 20 to 100 nm diameters, using purified HIV Gag proteins as the material. The structural studies on these giant spherical particles are also necessary in order to reveal the molecular mechanisms that give rise to these supermolecular assemblies.

4.5. Acknowledgements

4.6. Tables and Figures

Reference	HIV isolate	Domains included	Protein purity	Nucleic acids tested in assembly	Assembly condition	Properties of particles
Volker Vogt 1995	BH10	CA-NC and CA-NC-p6	~70%	Total *E. Coli* RNA	Protein (1mg/mL) dialyzed to buffer 0.1M NaCl, pH 8.0 at 4°C in presence of RNA	Rod-like particles of variable length but of constant 50 nm diameter
Alan Rein 1999	BH10	MA-CA-NC	85%-90%	Total *E. coli* RNA, yeast tRNA, *in vitro*-transcribed RNAs, and short DNA oligo-nucleotides	Protein diluted to 1mg/mL in 20mM Tris-HCl pH 8.0 with 0.1M NaCl, 10 mM DTT, at room temperature	Spherical particles 25-30 nm in diameter
Hans-Gorge Krausslich 1998	NL4-3	ΔMA-CA (AA16-99 of MA deleted), and various N-terminal extensions of CA	>95%, and all >90%	No nucleic acids required	Protein diluted and dialyzed overnight against assembly buffer (50mM Tris-HCl pH 8.0, 1M NaCl, at 4°C)	Spherical particles with diameters ranged from 20-100 nm, formation with various efficiencies
Hans-Gorge Krausslich 2000	Chimera*	ΔMA-CA-NC (AA16-99 of MA deleted)	>90%	Single-stranded DNA oligo-nucleotides	Protein dialyzed for 2 h against 50mM Tris–HCl pH 8.0, 0.1M NaCl, 1 mM EDTA, 1 mM DTT with nucleic acids at 4°C	Regular spherical particles with an external diameter of 90±5 nm as well as amorphous protein aggregates
Kouichi Sano 1999	Not reported	MA-CA-NC-6×His	95%	Calf liver RNA	protein incubated in the presence of 20 mM Tris pH8.6 at room temperature, 100 mM NaCl, 0.2 mM EDTA, 1 mM DTT, 5 mM MgCl$_2$ and/or calf liver RNA at 37 °C for 1- 3 h	Almost spherical, hollow particles surrounded by double-ring structure
Johnson Mak 2004	NL4-3	MA-CA-NC-p6-6×His	>95%	Yeast tRNA	Protein dialyzed overnight against buffer of 20mM Tris pH7.4, 150 mM NaCl, 10 mM DTT in presence of RNA at 4°C	Spherical particles with a diameter of 20 nm

Table 4.1. List of purified HIV-1 Gag proteins in previous publications.

(*: Obtained from both NL4-3 (ΔMA-CA *speI site*) and BH10 (CA *speI site*-NC))

A. Effect of molar ratio of 20mer-Cy3 to GagΔp6$_{NL4-3}$ protein on Gag self-assembly.

20mer-Cy3 final concentration (µg/mL)	0.83	1.83	3.67	7.33	14.67	29.17	58.33	116.7
GagΔp6$_{NL4-3}$ final concentration (mg/mL)				1.04				
Molar ratio of DNA vs protein	1:128	1:64	1:32	1:16	1:8	1:4	1:2	1:1
Average number of particles per field	-	-	79	86	109	135	119	88
Average particle size (diameter in µm)	-	-	1.54	1.88	2.31	3.01	3.03	2.03

B. Effect of molar ratio of (dT)$_{30}$ to GagΔp6$_{NL4-3}$ protein on Gag self-assembly.

(dT)30 final concentration (µg/mL)	1.13	2.08	4.17	8.33	16.67	53.33	108.3	215.0	430.0	858.3	1717
Molar ratio of DNA vs protein	1:180	1:90	1:45	1:22	1:11	1:4	1:2	1:1	2:1	5:1	9:1
Average number of particles per field	-	-	86	127	119	158	134	94	-	-	-
Average particle size (diameter in µm)	-	-	2.65	3.1	3.48	3.5	3.92	3.44	-	-	-

C. Effect of molar ratio of yeast tRNA to GagΔp6$_{NL4-3}$ protein on Gag self-assembly.

Yeast tRNA final concentration (µg/mL)	0.005	0.01	0.021	0.042	0.083	0.167
Molar ratio of DNA vs protein	1:80	1:40	1:20	1:10	1:5	1:2.5
Average number of particles per field	-	-	82	105	105	71
Average particle size (diameter in µm)	-	-	3.22	3.57	3.53	4.10

D. Self-assembly of GagΔp6$_{NL4-3}$ protein with different lengths of oligo thymidylate tested at three different ratios of DNA to protein.

	(dT)$_5$	(dT)$_{10}$	(dT)$_{12}$	(dT)$_{14}$	(dT)$_{16}$	(dT)$_{18}$	(dT)$_{20}$
1: 1	-	-	+	+	+	+	+
1: 5	-	-	+	+	+	+	+
1: 25	-	-	-	-	-	-	-

The experiments were conducted with GagΔp6 $_{NL4-3}$ protein; the assembled particles were observed directly under light microscope with a magnification of 400 times;
+: visible particles were formed with GagΔp6$_{NL4-3}$ protein
-: no visible particles were formed with GagΔp6$_{NL4-3}$ protein

Table 4.2. Effects of molar ratio of nucleic acids to GagΔp6NL4-3 protein on Gag self-assembly outcomes.
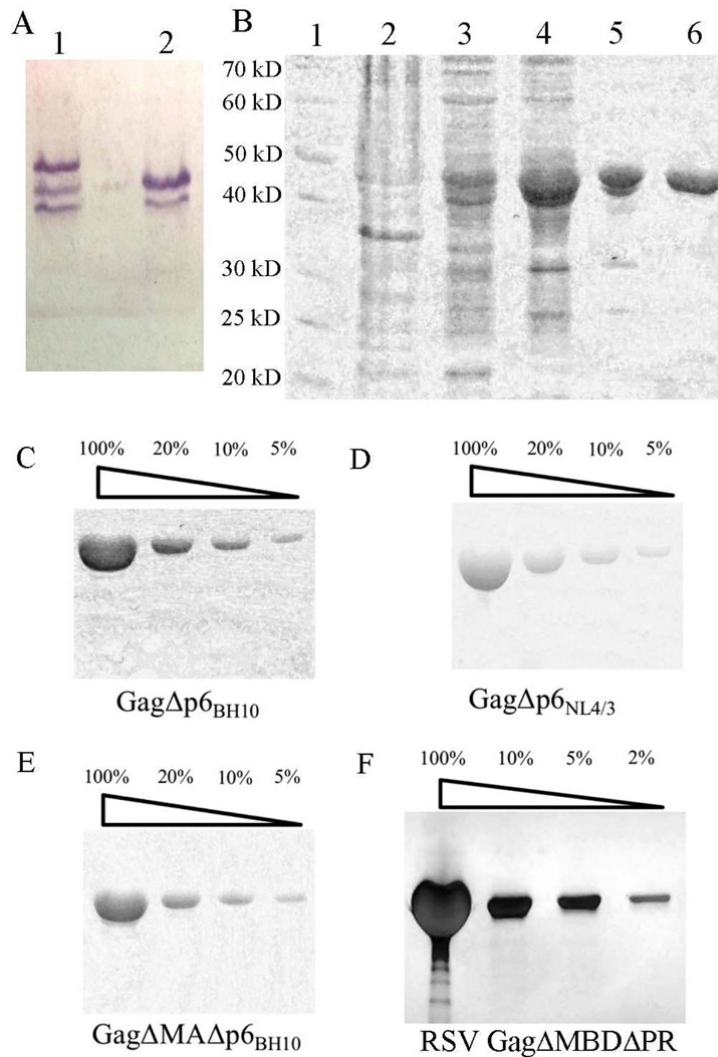
Figure 4.1. SDS-polyacrylamide gel images from purification of recombinant retroviral Gag proteins.

(A) Western blotting of the lysates from induced E. coli expressing full-length GagBH10 (Lane 1) and GagΔp6BH10 (Lane 2). (B) Products from major steps of protein purification for HIV-1 GagΔp6BH10. Lanes: 1: protein marker; 2: total lysate of cell pellet after 5-hour induction; 3: supernatant from cell lysate after 0.2% PEI treatment; 4: re-dissolution of protein pellet after 33% ammonium phosphate precipitation; 5: elution fraction after PC resin purification; 6: final product after heparin column chromatography. (C–F) Purity tests for various versions of recombinant retroviral Gag proteins: GagΔp6BH10 (C); GagΔp6NL4-3 (D); Gag ΔMA Δp6BH10 (E); and RSV Gag ΔMBDΔPR (F). The amounts of protein loaded in each lane were 30 µg, 6 µg, 3 µg, and 1.5 µg for (C), (D) and (E), corresponding to 100%, 20%, 10% and 5% respectively. The amounts of protein loaded in each lane for (F) were 25 µg, 2.5 µg, 1.25 µg, and 0.5 µg, corresponding to 100%, 10%, 5% and 2% respectively.
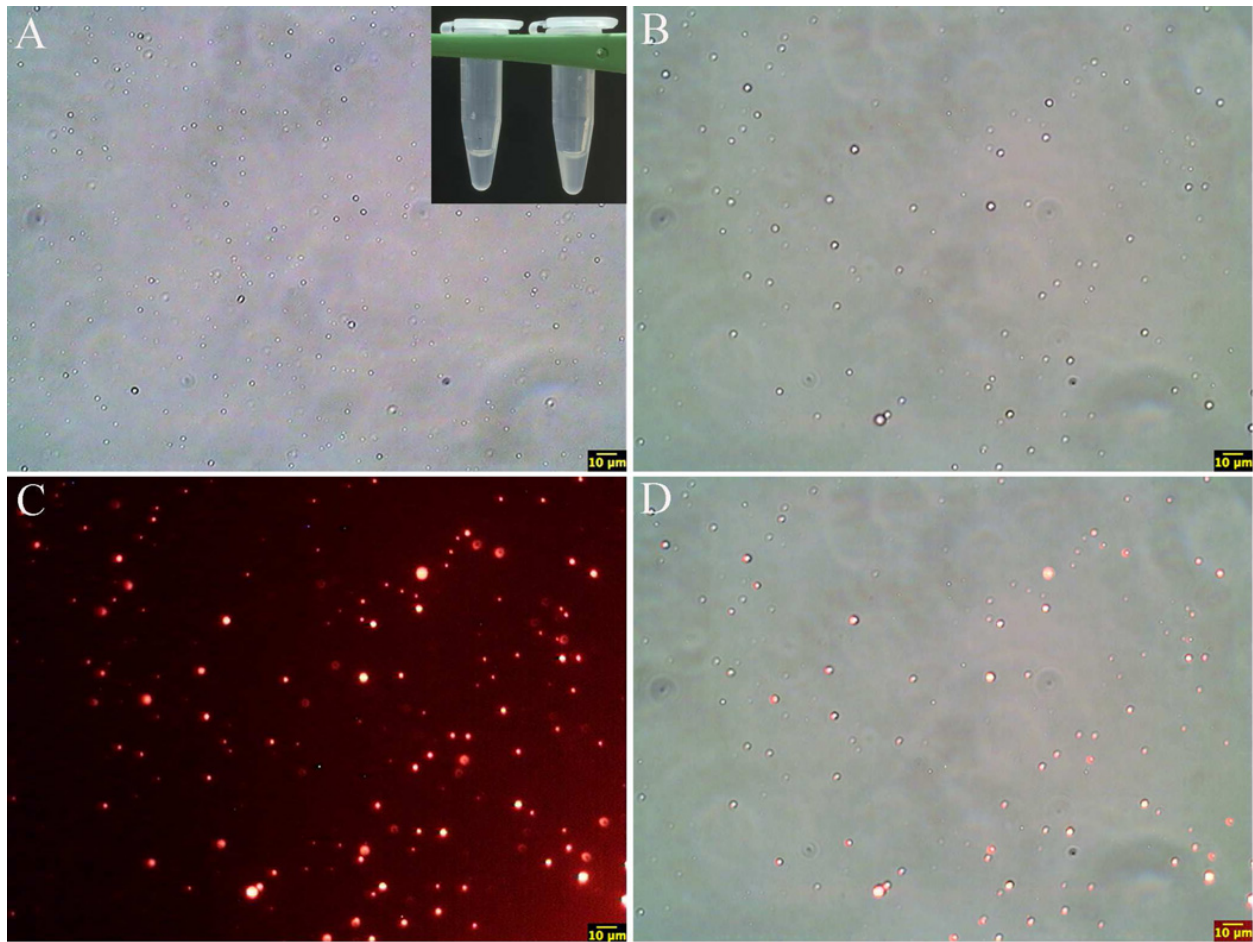
Figure 4.2. *In vitro* **assembly of HIV-1 GagΔp6$_{BH10}$ protein.**

(A) GagΔp6BH10 formed large heterogeneous particles of diameter around 1–5 µm, when 1µg yeast tRNA was added to 5 µg GagΔp6BH10 diluted with buffer F. Inset: GagΔp6BH10 solution became turbid upon addition of yeast tRNA (right), while it remained clear in absence of yeast tRNA (left); (B–C) GagΔp6BH10 formed similar particles with addition of 20mer-Cy3 compared to yeast tRNA, determined by microscope bright field figure (B) and fluorescence image (C). (D) Co-localization of the large particles in bright field with the red fluorescent particles in fluorescence image when overlapping two images of the same field from Panel C and D. All figures are taken under light microscope with a magnification of 400 times, and the scale bar indicates 10 µm.
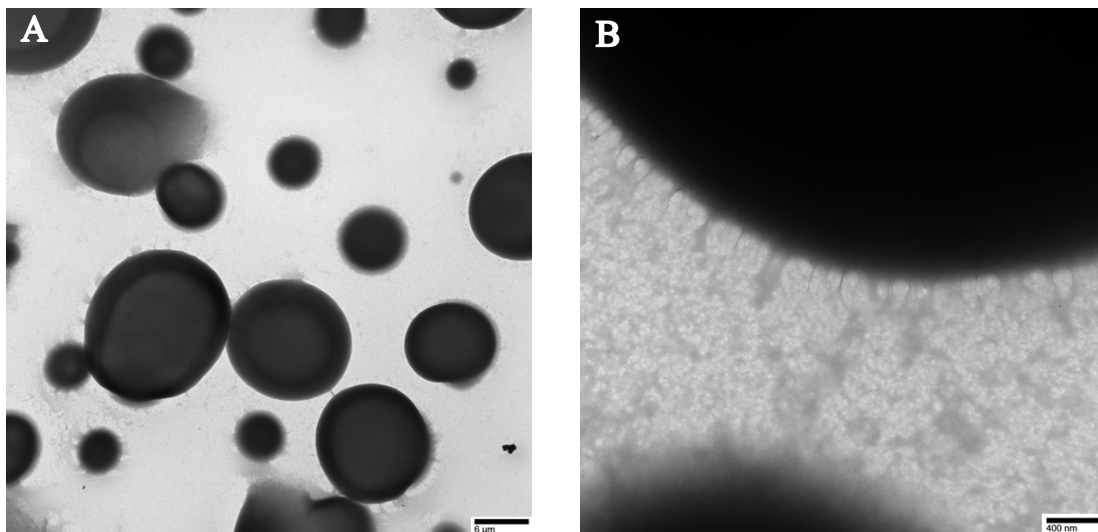
Figure 4.3. Electron microscopy of HIV-1 GagΔp6NL4-3 protein self-assembly in presence of 20mer-Cy3.

About 6μg GagΔp6NL4-3 protein stored in storage buffer (0.5M NaCl, 20nM Tris-HCl pH7.4) was added with four times volume of buffer F (20 mM Tris-HCl pH8.0), mixed well by gentle pipetting, and then added with 0.7μg 20mer-Cy3; The sample was placed at RT for 5 mins and then performed with negative staining. EM photos were taken at magnification of 2500 (A) and 40000 (B), respectively.
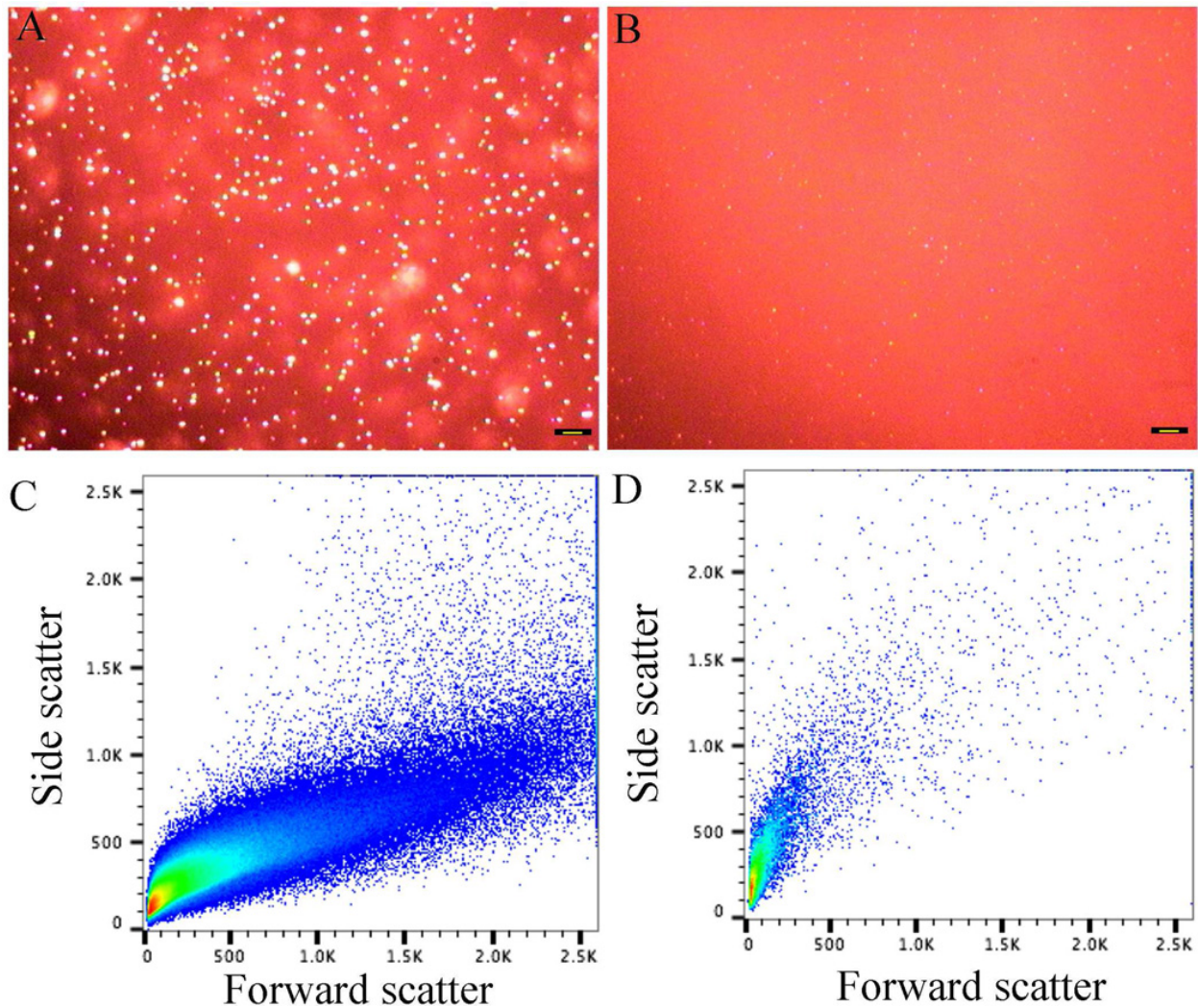
Figure 4.4. Microscopy photos and flow cytometry of *in vitro* assembly and disassembly of GagΔp6$_{BH10}$ protein.

(A) 5 µg GagΔp6$_{BH10}$ was diluted with buffer F, and then mixed with 20mer-Cy3 at a molar ratio of nucleic acids to protein as 1 to 2. (B) After the assembly of GagΔp6$_{BH10}$ with 20mer-Cy3 under the same conditions as in panel A, (dT)$_{30}$ was added to the sample to reach a molar ratio of nucleic acids to protein as 8:1. After incubation at 21°C for 10 min, it was sampled and observed under microscope in fluorescence mode. The yellow scale bars indicate 10 µm for both panels. (C) Flow cytometry of the assembly formed by GagΔp6$_{BH10}$incubated with 20mer-Cy3. The sample was prepared under same assembly conditions as in (A), and analyzed 5 min after the addition of nucleic acids. (D) Flow cytometry of the assembly formed by GagΔp6$_{BH10}$ first incubated with 20mer-Cy3 and then mixed with excessive (dT)$_{30}$. The sample was prepared under same assembly conditions as in (B). After addition of excess (dT)$_{30}$, the sample was incubated at 21°C for 10 min before flow cytometry analysis.

121
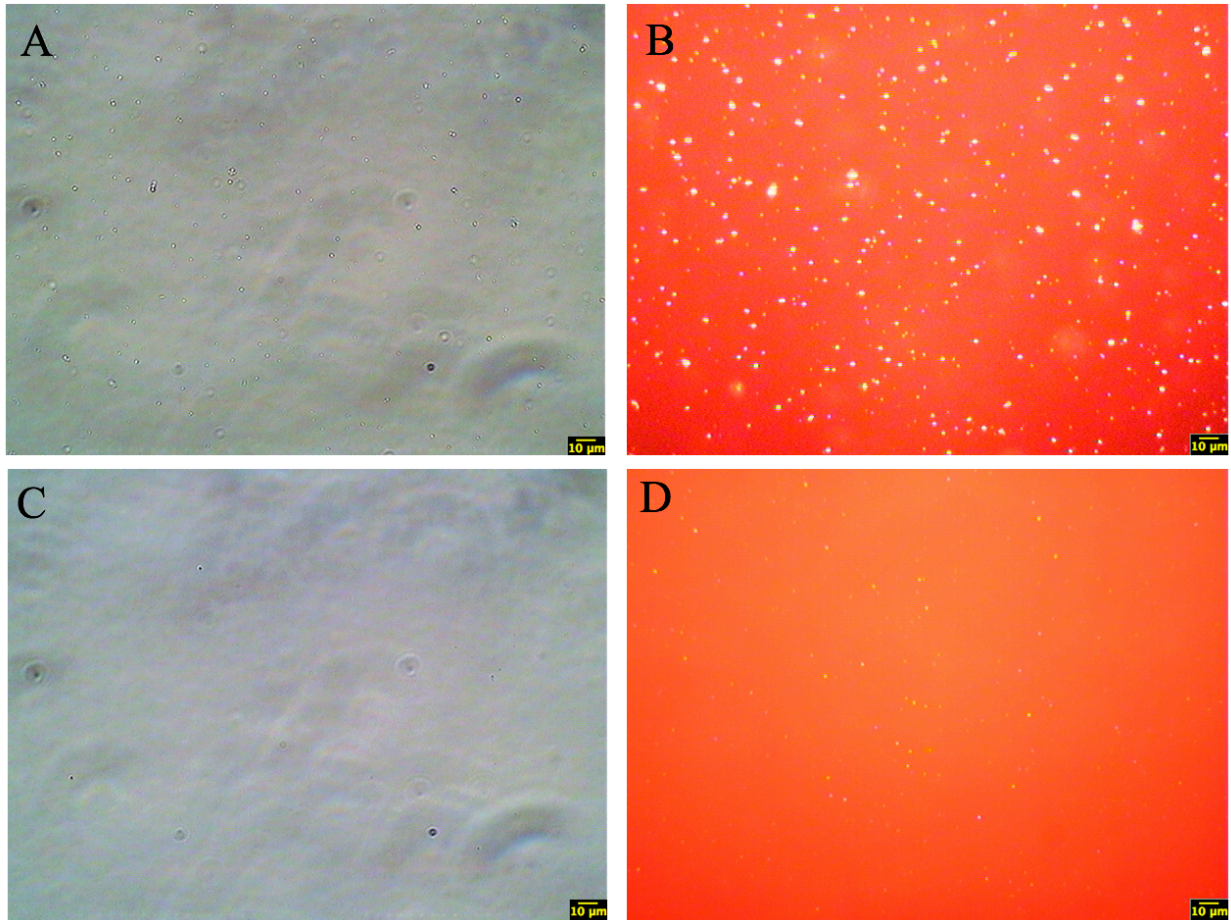
Figure 4.5. Microscopy photos of *in vitro* assembly of GagΔMAΔp6$_{BH10}$ protein.

(A-B) GagΔMAΔp6$_{BH10}$ was mixed with 20mer-Cy3 upon dilution with buffer F, placed at RT for 5 mins before observation under microscope at magnification of 400 times in both bright field (A) and fluorescence scope (B). (C-D) GagΔMAΔp6 $_{BH10}$ was mixed with Cy3DNA upon dilution with buffer F, and the tube was centrifuged at 17,000 g for 5 mins. Supernatant from the mixture was sampled and observed under microscope in bright field (C) and fluorescence mode (D).
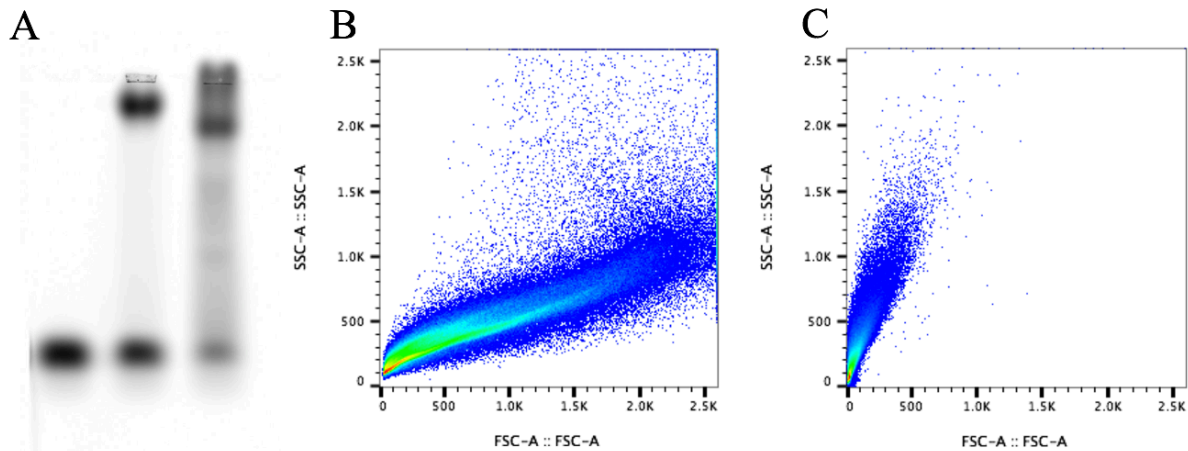
Figure 4.6. Comparison of the particles formed by GagΔp6 and GagΔMAΔp6 with addition of 20mer-Cy3.

(A) Gel electrophoresis of assembled particles of GagΔp6 and GagΔMAΔp6 proteins. 0.3% Agarose gel was run in TBE buffer at voltage of 100V for 1hr at 4°C and imaged by typhoon imager to detect Cy3 fluorophore. Lanes: 1. Control group containing only 0.7μg 20mer-Cy3; 2. 6μg GagΔp6$_{NL4-3}$ mixed with 0.7μg 20mer-Cy3 upon dilution with buffer F; 3. 5μg GagΔMAΔp6$_{BH10}$ mixed with 0.7μg 20mer-Cy3 upon dilution with buffer F. (B) Flow cytometry of the assembly formed by GagΔp6$_{BH10}$ incubated with 20mer-Cy3 at the ratio of 1:2, placed at RT for 1hr before flow cytometry analysis. (C) Flow cytometry of the assembly formed by GagΔMAΔp6$_{BH10}$ incubated with 20mer-Cy3 for 1hr, under same assembly conditions as Fig. 4.5A.
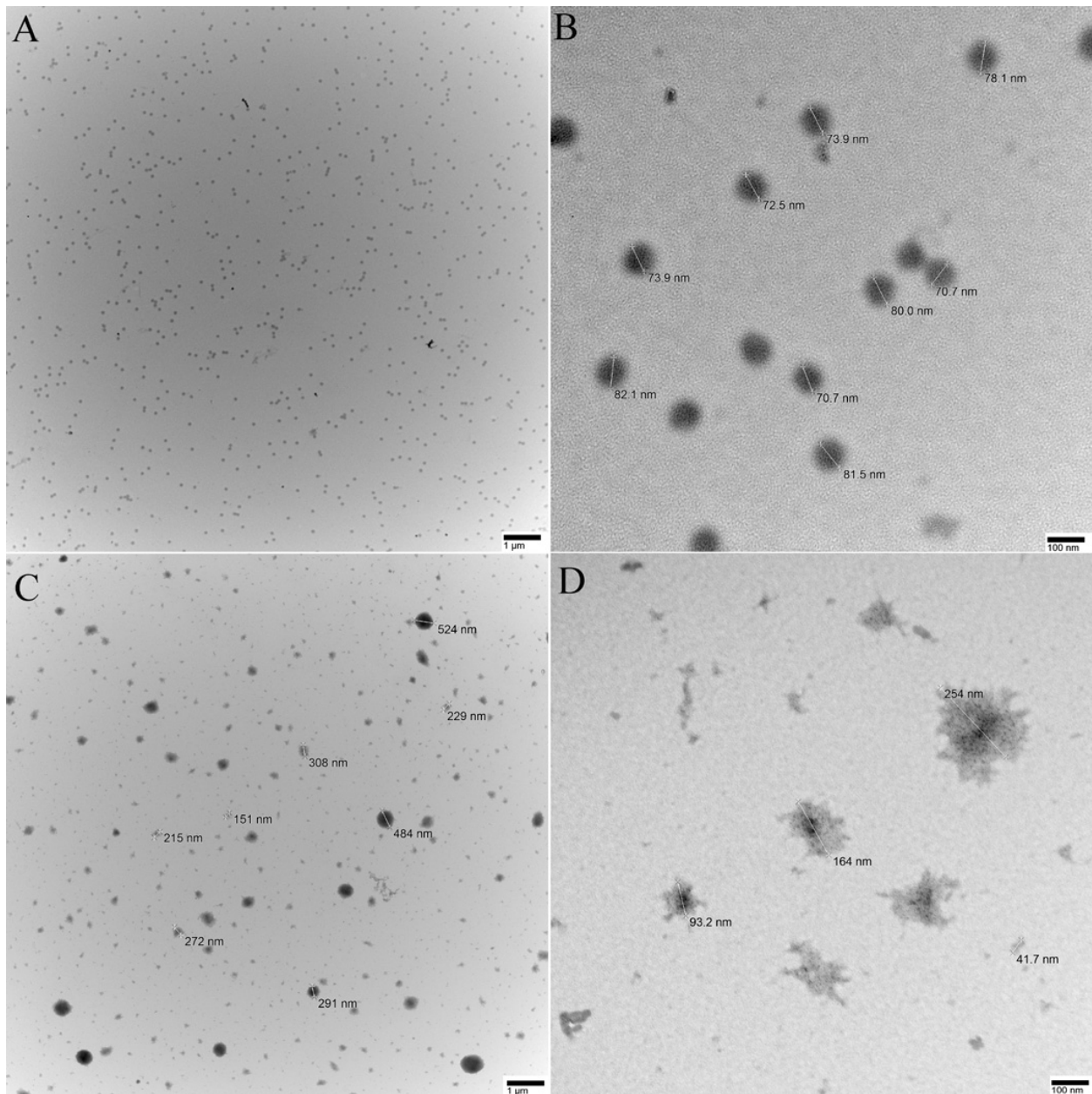
Figure 4.7. Particles assembled by RSV GagΔMAΔp6 and HIV-1 GagΔMAΔp6$_{BH10}$ in presence of yeast tRNA.

(A–B) 5.2 μg RSV GagΔMAΔp6 was mixed with 1μg yeast tRNA after dilution with buffer F, corresponding to a molar ratio of 1:2.5 between tRNA and protein. EM photos were taken at magnification of 13,000 (A) and 100,000 (B), respectively. (C–D) 5.4 μg HIV-1 GagΔMAΔp6$_{BH10}$ was mixed with 1μg yeast tRNA after dilution with buffer F, corresponding to a molar ratio of 1:3.3 between tRNA and protein. EM photos were taken at magnification of 13,000 (C) and 100,000 (D), respectively. The scale bars indicate 1 μm, 100 nm, 1 μm, and 100 nm for Panels A, B, C and D respectively.

124

4.7. References

1. Sundquist WI, Krausslich HG. HIV-1 assembly, budding, and maturation. Cold Spring Harb Perspect Med. 2012;2:a006924.

2. Mervis RJ, Ahmad N, Lillehoj EP, Raum MG, Salazar FH, Chan HW, et al. The gag gene products of human immunodeficiency virus type 1: alignment within the gag open reading frame, identification of posttranslational modifications, and evidence for alternative gag precursors. J Virol. 1988;62:3993-4002.

3. Campbell S, Rein A. *In vitro* assembly properties of human immunodeficiency virus type 1 Gag protein lacking the p6 domain. J Virol. 1999;73:2270-9.

4. Gross I, Hohenberg H, Huckhagel C, Krausslich HG. N-Terminal extension of human immunodeficiency virus capsid protein converts the *in vitro* assembly phenotype from tubular to spherical particles. J Virol. 1998;72:4798-810.

5. Campbell S, Vogt VM. Self-assembly *in vitro* of purified CA-NC proteins from Rous sarcoma virus and human immunodeficiency virus type 1. J Virol. 1995;69:6487-97.

6. Gross I, Hohenberg H, Wilk T, Wiegers K, Grattinger M, Muller B, et al. A conformational switch controlling HIV-1 morphogenesis. EMBO J. 2000;19:103-13.

7. Campbell S, Fisher RJ, Towler EM, Fox S, Issaq HJ, Wolfe T, et al. Modulation of HIV-like particle assembly *in vitro* by inositol phosphates. Proc Natl Acad Sci U S A. 2001;98:10875-9.

8. Morikawa Y, Goto T, Sano K. *In vitro* assembly of human immunodeficiency virus type 1 Gag protein. J Biol Chem. 1999;274:27997-8002.

9. McKinstry WJ, Hijnen M, Tanwar HS, Sparrow LG, Nagarajan S, Pham ST, et al. Expression and purification of soluble recombinant full length HIV-1 Pr55(Gag) protein in Escherichia coli. Protein Expr Purif. 2014;100:10-8.

10. Cheng W, Brendza KM, Gauss GH, Korolev S, Waksman G, Lohman TM. The 2B domain of the Escherichia coli Rep protein is not required for DNA helicase activity. Proc Natl Acad Sci U S A. 2002;99:16006-11.

11. Hockley DJ, Nermut MV, Grief C, Jowett JB, Jones IM. Comparative morphology of Gag protein structures produced by mutants of the gag gene of human immunodeficiency virus type 1. J Gen Virol. 1994;75 (Pt 11):2985-97.

12. Royer M, Cerutti M, Gay B, Hong SS, Devauchelle G, Boulanger P. Functional domains of HIV-1 gag-polyprotein expressed in baculovirus-infected cells. Virology. 1991;184:417-22.

13. Datta SA, Rein A. Preparation of recombinant HIV-1 gag protein and assembly of virus-like particles *in vitro*. Methods Mol Biol. 2009;485:197-208.

14. Lohman TM, Chao K, Green JM, Sage S, Runyon GT. Large-scale purification and characterization of the Escherichia coli rep gene product. J Biol Chem. 1989;264:10139-47.

15. Campbell S, Vogt VM. *In vitro* assembly of virus-like particles with Rous sarcoma virus Gag deletion mutants: identification of the p10 domain as a morphological determinant in the formation of spherical particles. J Virol. 1997;71:4425-35.

16. Fisher RJ, Rein A, Fivash M, Urbaneja MA, Casas-Finet JR, Medaglia M, et al. Sequence-specific binding of human immunodeficiency virus type 1 nucleocapsid protein to short oligonucleotides. J Virol. 1998;72:1902-9.

17. Chukkapalli V, Oh SJ, Ono A. Opposing mechanisms involving RNA and lipids regulate HIV-1 Gag membrane binding through the highly basic region of the matrix domain. Proc Natl Acad Sci U S A. 2010;107:1600-5.

18. Purohit P, Dupont S, Stevenson M, Green MR. Sequence-specific interaction between HIV-1 matrix protein and viral genomic RNA revealed by *in vitro* genetic selection. RNA. 2001;7:576-84.

19. Facke M, Janetzko A, Shoeman RL, Krausslich HG. A large deletion in the matrix domain of the human immunodeficiency virus gag gene redirects virus particle assembly from the plasma membrane to the endoplasmic reticulum. J Virol. 1993;67:4972-80.

20. Gill SC, von Hippel PH. Calculation of protein extinction coefficients from amino acid sequence data. Anal Biochem. 1989;182:319-26.

21. Addo MM, Yu XG, Rathod A, et al. Comprehensive epitope analysis of human immunodeficiency virus type 1 (HIV-1)-specific T-cell responses directed against the entire expressed HIV-1 genome demonstrate broadly directed responses, but no correlation to viral load. J Virol. 2003;77(3):2081-2092. doi:10.1128/JVI.77.3.2081-2092.2003

22. Ramduth D, Day CL, Thobakgale CF, et al. Immunodominant HIV-1 Cd4+ T Cell Epitopes in Chronic Untreated Clade C HIV-1 Infection. Unutmaz D, ed. PLoS One. 2009;4(4):e5013. doi:10.1371/journal.pone.0005013

Chapter 5

Discussion of Results and Future Directions

5.1. Overview of Results

The low density of envelope glycoprotein on HIV surface[1–3] suggest a potential mechanism for this virus to evade human immunity and delay the induction of neutralizing antibodies[4]. Surface antigen density has been recognized as an important factor in eliciting immune responses in various studies[5–8], but a systematic study to investigate its impact without the influence of additional antigens or adjuvants is yet to be done. In this thesis work, we hypothesize that antigen density itself serves as an independent signal in B-cell activation, especially for self-antigens that are tolerated by B cells. While foreign antigens may not require high epitope density for B cell activation, self-antigens may require a display of high surface density to elicit antibody responses[9].

To validate this hypothesis, a nanoparticle platform of well-controlled surface antigen density free of any additional immunogen or adjuvant is necessary. In Chapter 2, we designed a liposome nanoparticle conjugated with model proteins on the surface at a controlled density

through Ni-NTA-his-tag binding. Since previous literature has not established well-characterized methods to quantitatively measure antigen spatial densities, we developed both ensemble biochemical assay and single-molecule techniques to evaluate the protein density on the designed liposomes. The results showed that Ni-chelating liposomes can achieve well-controlled surface protein density, however, the protein molecules bound on liposomal surface decrease over time upon dilution due to the non-covalent binding between lipid Ni-NTA group and protein his-tag group. This apparently is not desired for *in vivo* application. An alternative approach to conjugate proteins on liposomal surface through maleimide-cysteine reaction was utilized, proving to be more stable in both PBS and serum buffer condition. Therefore, maleimide-liposome platform is selected to construct nanoparticles with various levels of surface density for study of B cell activation.

On the maleimide-liposome platform, we conjugated TNF-α peptide at different surface densities, which was a self-antigen associated with rheumatoid arthritis. Current antibody treatment for rheumatoid arthritis achieved clinical success by neutralizing excessive TNF-α cytokine in patients[10]. Here, we showed that a high-density liposomal display of TNF-α peptide can elicit antibody responses specific towards TNF-α protein in wild-type mice. This is the first study to demonstrate that high surface density of a self-antigen can break B-cell tolerance without any additional T-cell epitope or adjuvant. When lowering the surface density of TNF-α peptide, we identified a potential density threshold between liposome$_{1.1\%\text{-maleimide}}$ to liposome$_{2.2\%\text{-maleimide}}$, below which liposomes elicited much lower antibody response in mice suggesting insufficient breaking of B-cell tolerance. Moreover, we discovered that high-density display of TNF-α peptide breaks B-cell tolerance through T-independent pathways, because T-deficient

128

transgenic mice produced same level of specific anti-TNF-α antibody as wild-type mice upon immunization.

In order to evaluate the anti-TNF-α antibody production by liposomal display, we constructed Qβ bacteriophage virus-like particle conjugated with the same TNF-α peptide at high density level for same animal immunization experiment. Qβ-TNFα conjugate induced 1000 folds higher titer of specific IgG antibody than liposome-TNFα in wild-type mice, but only induced similar level of IgG as liposome- TNFα in T-deficient mice, suggesting Qβ VLPs can break B-cell tolerance of TNFα more efficiently with T-cell help. This result indicates that T cells are not required in recognition of high-density antigen display, but they can provide strong stimulation to B-cell activation and antibody production.

As VLPs demonstrated a better potency in recruiting T cell help to sustain B-cell activation, we intend to construct VLP platforms for development of HIV vaccine candidate. HIV Gag protein is an ideal candidate because HIV Gag protein is shown to self-assemble to VLP *in vitro*[11] and it contains multiple well-characterized human T-cell epitopes to boost immune responses. However, previous literature reported contradicting results in HIV Gag protein assembly to VLP[12–15]. In Chapter 4, we described our attempt in using HIV Gag protein to build virus-like particles. By developing an improved Gag protein purification method, we purified several untagged retroviral Gag proteins from E. coli to more than 95% purity. HIV-1 Gag proteins form large spherical particles of microns in size in the presence of nucleic acids. More interestingly, the large particles assembled can undergo disassembly upon addition of excess nucleic acids, suggesting the assembly is an ordered structure. This work uncovered a new characteristic of HIV Gag protein in assembly *in vitro* that may play a role in HIV

intracellular assembly and pathogenesis in T cells. But for this *in vitro* assembly to be useful for production of VLPs for vaccination purpose, more work remains to be completed for the construction of regular virus-like particles as antigen presentation platforms.

So far, we have successfully constructed liposome-based nanoparticles with controlled densities of antigens quantitated by both ensemble assay and single-molecule assay. Mouse immunization study revealed that high-density display of self-antigen by itself alone can break B-cell tolerance independent of T-cell help. Addition of T-cell help, although not required in B-cell activation, greatly boosts the specific antibody response proven by Qβ VLP conjugate. Inspired by the high immunogenicity of Qβ VLP, we studied HIV Gag protein assembly process *in vitro* for construction of HIV VLP and revealed the unexpected large micron-size particle formation by purified HIV Gag protein. More work remains to be carried out for the correct assembly of HIV VLP and conjugation of antigen on the surface.

5.2. Future Directions

***In vivo* and *In vitro* Study of B-cell Activation**

Immunization results in this thesis work focused on the evaluation of specific autoreactive antibody production elicited by liposome conjugated with antigens in mice, because antibody production is a key parameter in analysis of B-cell activation. To further investigate the B cell activation process *in vivo*, additional tests can be done in immunized mice: B cells isolated from lymph nodes and spleen can be evaluated by ELISPOT to determine the number of specific antibody secreting cells; lymph node B cells can be evaluated by flow cytometry to determine the number of activated B cells, formation of germinal centers, and the differentiation to memory B cells; cytokine level secreted by activated B cells can be evaluated by cytokine measurement assays. In summary, number of B cells activated as well as differentiation of B cells to germinal center or memory B cells can be evaluated to determine the immune effects of liposomes with different antigen densities *in vivo*.

In vitro study using primary B cells will further elucidate the process of B cell activation by antigen density signal. Because the number of specific B cells for a particular antigen is usually at a frequency of 0.05 to 0.005% in the normal repertoire[16] (even less if the antigen is self-antigen), it is not feasible to isolate sufficient antigen-specific B cells from wild-type mice for *in vitro* study. Here, we plan to use transgenic mice with all B cells genetically modified to recognize HEL (hen egg lysozyme). HEL-specific B cells will be isolated from mice and incubated with liposomes conjugated with HEL at different density levels. Afterwards, B cells will be evaluated by its surface activation signals, specific antibody production, cytokine release

and induced cell differentiation. Although, one potential challenge is the short life span of primary B cells *in vitro*. Our preliminary data showed that primary HEL-specific B cells start apoptosis process immediately after isolation and have only 20% viability in one day during *in vitro* culture, while it takes a few days for B cells to go through antigen-induced activation and antibody production process. Ways to increase primary B cell life span such as addition of pro-survival stimulus can be explored[17].

Mechanism of B-cell Recognition of Antigen Density

Our results revealed that high-density display of self-antigen TNFα can break B-cell tolerance and elicit autoreactive antibody production. However, the underlying mechanism of antigen density recognition by B cells remains to be clarified. It has been postulated that highly repetitive antigens can strongly crosslink B-cell receptors, forming receptor micro-clusters that set off a chain reaction of downstream events including initiation of calcium signaling and gene expression[18]. Upon encountering a particulate, B cells will first spread over antigen-bearing membrane and then contract, collecting bound antigens into a central aggregate[19]. In this case, a threshold of receptor molecule numbers is required, and low-density antigen display may fail to provide sufficient number of antigens for BCR binding in one encountering event. Nonetheless, this model fails to explain the scenario where too high of antigen density display leads to lower immune response[20].

In this thesis, we found the recognition threshold for self-antigen density is around 10,000 – 20,000 molecules/ μm^2, which was achieved through the use of 1-2% of maleimide lipids. To validate this result, we plan to build liposomes with lower antigen density than 10,000

molecules/ μm^2 to verify their inability to elicit autoreactive antibody response. Moreover, we can construct liposomes with defined antigen densities between 10,000 – 20,000 molecules/ μm^2 to determine the exact threshold for surface antigen density. However, since the antigen density on liposomes are only measured on average, it is inevitable to have a range of normal distribution in antigen density on liposomes, posing challenges to determine an accurate density threshold for B cell activation. Fluorescence labeling and optical tweezer technique can be used to solve this problem: a single B cell can be captured and tested for its activation signal upon contact with individual liposomes, antigen densities of which have been quantitatively measured through optical tweezers. This novel experiment design allows a precise control of a single cell-liposome contact, thus offering a clear vision in B cell's response toward different antigen densities.

Construction of HIV VLP for Vaccine Development

In the last chapter, we described our discovery of an unexpected assembly characteristic of HIV Gag protein forming large irregular particles instead of regular virus-like particles. Genetic modification to HIV Gag protein or change of assembly condition (buffer salt, pH, temperature…) can be further explored for efficient assembly of HIV VLP. Once HIV VLP can be formed, we aim to fuse antigen peptides from HIV envelope protein to Gag protein at the N-terminus without interference to VLP assembly. These engineered VLPs will carry B-cell epitope from HIV surface envelope protein at a defined density as well as T-cell epitopes from Gag protein. The combination of both high surface density of B-cell epitope and intrinsic T-cell epitope may trigger efficient B-cell activation with T-cell help. As previous HIV vaccine trials attempt to use recombinant subunit protein for immunization, this innovative approach in the

development of HIV vaccine may lead to better efficacy in eliciting immune responses in a clinically safe manner.

5.3. Concluding Remarks

Surface antigen density has been shown to be an important factor in eliciting immune responses since the work led by Zinkernagel on B cell responses to vesicular stomatitis virus glycoproteins in 1993[7]. 25 years later, we still have not completely understood the impact and underlying mechanisms of surface antigen density in activating B cells. One of the key issues is, how to quantitate and control the surface antigen density levels. In this thesis work, we successfully quantitated the antigen density on a synthetic liposome platform on a single-molecule level, offering an innovative way to accurately characterize liposomal surface antigen densities. Although the antigen density can be well controlled through lipid formulation, the distribution of antigen densities on liposomes tends to be wider than expected. Moreover, the fluidity of liposome membrane causes constant movement of surface antigen molecules, possibly leading to higher antigen density upon encountering B cell membrane. In comparison, virus-like particles assembled from fixed number of protein molecules may have a narrower distribution in their surface antigen densities, and the configuration of surface molecules is also rigid, perhaps making it more advantageous in building a well-controlled antigen presenting platform.

Another important question we have answered is, whether antigen density it alone can be an activation signal. Our results proved that liposomes of high-density antigen display without

any additional T cell epitope or adjuvant can effectively activate B cells *in vivo*. Liposome system free of other proteins and nucleic acids served as a simple, pure and non-immunogenic platform to showcase the effects of different antigen densities. Meanwhile, our results using Qβ VLP conjugate demonstrated the strong boosting effects of T-cell epitope, and addition of CpG demonstrated the boosting effect of TLR ligands. Further studies on how T-cell help and TLR signaling facilitated B cell activation, particularly for high-density antigen display on nanoparticles, will be carried out to complete our current understanding in the process of antigen density recognition.

5.4. References

1. Pang Y, Song H, Kim JH, Hou X, Cheng W. Optical trapping of individual human immunodeficiency viruses in culture fluid reveals heterogeneity with single-molecule resolution. *Nat Nanotechnol*. 2014;9(8):624-630. doi:10.1038/nnano.2014.140.
2. Desantis MC, Kim JH, Song H, Klasse J, Cheng W. Quantitative Correlation between Infectivity and Gp120 Density on HIV-1 Virions Revealed by Optical Trapping Virometry *. 2016. doi:10.1074/jbc.M116.729210.
3. Chertova E, Bess JW, Crise BJ, et al. Envelope glycoprotein incorporation, not shedding of surface envelope glycoprotein (gp120/SU), Is the primary determinant of SU content of purified human immunodeficiency virus type 1 and simian immunodeficiency virus. *J Virol*. 2002;76(11):5315-5325.
4. Schiller J, Chackerian B. Why HIV Virions Have Low Numbers of Envelope Spikes: Implications for Vaccine Development. *PLoS Pathog*. 2014;10(8):e1004254. doi:10.1371/journal.ppat.1004254.
5. Dintzis HM, Dintzis RZ, Vogelstein B. Molecular determinants of immunogenicity: the immunon model of immune response. *Proc Natl Acad Sci U S A*. 1976;73(10):3671-3675. doi:10.1073/pnas.73.10.3671.
6. Qin Q, Yin Z, Wu X, Haas KM, Huang X. Valency and density matter: Deciphering impacts of immunogen structures on immune responses against a tumor associated carbohydrate antigen using synthetic glycopolymers. 2016;101:189-198. doi:10.1016/j.biomaterials.2016.05.050.
7. Bachmann MF, Rohrer UH, Kündig TM, Bürki K, Hengartner H, Zinkernagel RM. The influence of antigen organization on B cell responsiveness. *Science*. 1993;262(5138):1448-1451. doi:10.1126/science.8248784.
8. Ingale J, Stano A, Guenaga J, et al. High-Density Array of Well-Ordered HIV-1 Spikes on Synthetic Liposomal Nanoparticles Efficiently Activate B Cells. *Cell Rep*. 2016;15(9):1986-1999. doi:10.1016/j.celrep.2016.04.078.
9. Cheng W. The Density Code for the Development of a Vaccine? *J Pharm Sci*. 2016;105(11):3223-3232. doi:10.1016/j.xphs.2016.07.020.
10. BETH WELCH. Adalimumab (Humira) for the Treatment of Rheumatoid Arthritis. *Am Fam Physician*. 1970;78(12):1406. https://www.aafp.org/afp/2008/1215/p1406.html. Accessed November 16, 2018.
11. Fäcke M, Janetzko A, Shoeman RL, Kräusslich HG. A large deletion in the matrix domain of the human immunodeficiency virus gag gene redirects virus particle assembly from the plasma membrane to the endoplasmic reticulum. *J Virol*. 1993;67(8):4972-4980. http://www.pubmedcentral.nih.gov/articlerender.fcgi?artid=237885&tool=pmcentrez&rendertype=abstract. Accessed January 30, 2016.
12. Campbell S, Rein A. *In vitro* Assembly Properties of Human Immunodeficiency Virus Type 1 Gag Protein Lacking the p6 Domain *In vitro* Assembly Properties of Human Immunodeficiency Virus Type 1 Gag Protein Lacking the p6 Domain. 1999;73(3).
13. Campbell S, Vogt VM. Self-Assembly *In vitro* of Purified CA-NC Proteins from Rous Sarcoma Virus and Human Immunodeficiency Virus Type 1. 1995;69(10):6487-6497.
14. Morikawa Y, Goto T, Sano K. *In vitro* assembly of human immunodeficiency virus type 1 Gag protein. *J Biol Chem*. 1999;274(39):27997-28002. http://www.ncbi.nlm.nih.gov/pubmed/10488150. Accessed January 22, 2016.
15. McKinstry WJ, Hijnen M, Tanwar HS, et al. Expression and purification of soluble

recombinant full length HIV-1 Pr55(Gag) protein in Escherichia coli. *Protein Expr Purif*. 2014;100:10-18. doi:10.1016/j.pep.2014.04.013.

16. Smith MJ, Packard TA, O'Neill SK, et al. Detection and Enrichment of Rare Antigen-specific B Cells for Analysis of Phenotype and Function. *J Vis Exp*. 2017;(120). doi:10.3791/55382.

17. Donahue AC, Fruman DA. Proliferation and survival of activated B cells requires sustained antigen receptor engagement and phosphoinositide 3-kinase activation. *J Immunol*. 2003;170(12):5851-5860. doi:10.4049/JIMMUNOL.170.12.5851.

18. Bachmann MF, Zinkernagel RM. The influence of virus structure on antibody responses and virus serotype formation. *Immunol Today*. 1996;17(12):553-558. doi:10.1016/S0167-5699(96)10066-9.

19. Fleire SJ, Goldman JP, Carrasco YR, Weber M, Bray D, Batista FD. B cell ligand discrimination through a spreading and contraction response. *Science*. 2006;312(5774):738-741. doi:10.1126/science.1123940.

20. Brewer MG, DiPiazza A, Acklin J, Feng C, Sant AJ, Dewhurst S. Nanoparticles decorated with viral antigens are more immunogenic at low surface density. *Vaccine*. 2017;35(5):774-781. doi:10.1016/j.vaccine.2016.12.049.